



The author(s) shown below used Federal funding provided by the U.S. Department of Justice to prepare the following resource:

Document Title: Development of Laser Ablation Direct Analysis in Real Time Imaging-Mass Spectrometry (LADI-MS)-Applications to Questions of Relevance to Forensic Science and Plant Biochemistry

Author(s): Kristen L. Fowble

Document Number: 304316

Date Received: March 2022

Award Number: 2017-R2-CX-0003

This resource has not been published by the U.S. Department of Justice. This resource is being made publicly available through the Office of Justice Programs' National Criminal Justice Reference Service.

Opinions or points of view expressed are those of the author(s) and do not necessarily reflect the official position or policies of the U.S. Department of Justice.

DEVELOPMENT OF LASER ABLATION DIRECT ANALYSIS IN REAL TIME IMAGING-MASS
SPECTROMETRY (LADI-MS)—APPLICATIONS TO QUESTIONS OF RELEVANCE TO FORENSIC
SCIENCE AND PLANT BIOCHEMISTRY

by

Kristen L. Fowble

A Dissertation

Submitted to the University at Albany, State University of New York

in Partial Fulfillment of

the Requirements for the Degree of

Doctor of Philosophy

College of Arts & Sciences

Department of Chemistry

2019

University at Albany, State University of New York

COLLEGE OF ARTS & SCIENCES

The dissertation submitted by

Kristen L. Fowble

under the title


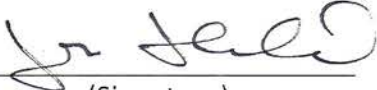
Development of Laser Ablation Direct Analysis in Real

Time Imaging-Mass Spectrometry (LADI-MS)—


Applications to Questions of Relevance to

Forensic Science and Plant Biochemistry

has been read by the undersigned. It is hereby recommended for acceptance to the Faculty of the University in partial fulfillment of the requirement for the degree of Doctor of Philosophy.

Chair:	<u>RABI ANN MUSAH</u> (Printed Name)	<u></u> (Signature)	<u>8/15/19</u> (Date)
Committee Member:	<u>I. Lednev</u> (Printed Name)	<u>I. Lednev</u> (Signature)	<u>8/15/19</u> (Date)
Committee Member:	<u>John Dane</u> (Printed Name)	<u>John Dane</u> (Signature)	<u>7/15/19</u> (Date)
Committee Member:	<u>J. XALANEK</u> (Printed Name)	<u></u> (Signature)	<u>8/15/19</u> (Date)

Recommended by the Department of Chemistry

, Chair,

(Signed)

Li Niu, Chair

(Printed Name)

Recommendation accepted on behalf of the Graduate Academic Council.

(Signed)

(Date)

DEVELOPMENT OF LASER ABLATION DIRECT ANALYSIS IN REAL TIME IMAGING-MASS
SPECTROMETRY (LADI-MS)—APPLICATIONS TO QUESTIONS OF RELEVANCE TO FORENSIC
SCIENCE AND PLANT BIOCHEMISTRY

by

Kristen L. Fowble

Copyright 2019

“Nothing in life is to be feared, it is only to be understood. Now is the time to understand more
so that we may fear less.”

-Marie Curie-

Acknowledgements

While there are many people to thank for their support over the course of my graduate career, first and foremost I must extend my gratitude to my mentor and thesis advisor, Professor Rabi Musah. If it were not for your unwavering support and mentorship, I would not have become the scientist, or woman I am today. I will forever be thankful for the opportunity to join your lab in my first few weeks here, and I want you to know that I have never second guessed my choice. You have afforded me so many opportunities to grow, and I appreciate each and every one of them.

I would like to thank the members of my doctoral thesis committee, Professor Igor Lednev, Professor Jan Halánek, and Dr. John Dane for their advice and support. I want to thank Professor Ting Wang as well for serving as a member of my proposal defense committee. I would also like to extend my gratitude to Dr. Robert Cody and Koji Okuda for their assistance in any and all things mass spec related. I will be eternally grateful to all members of the JEOL USA, Inc. staff for their hospitality and support during my extended visit to their facility. Additionally, I must thank Dr. Ciaran O'Connor from Elemental Scientific Lasers for sending us a demo laser unit. Without you, none of this would have been possible. I would also like to acknowledge and thank Dr. Edgard Espinoza for the provision of wood samples, and both he and his son Aiden for their preparation of the wood samples that were analyzed in this work. I must also extend a sincere thank you to Brian Gabriel for his help and unwavering guidance since day one of graduate school.

I want to thank the current and previous members of the ever growing Musah laboratory. Ashton Lesiak, Justine Giffen, and Denny He were there for my beginning years, and I appreciate

all of their assistance and training. It has been a pleasure working alongside Samira Beyramysoltan and Daman Arathala, and seeing their drive and productivity. I am eternally grateful to all the members in the lab: Cameron Longo, Meghan Fogerty, Allix Coon, Megan Chambers, Amy Osborne, Mónica Ventura, Jessica Hayes, Nana-Hawwa Abdul-Rahman, and Mark Katz, who have each helped me in their own way and knew instinctively how to support me on the tough days. It's been wonderful getting to know each of you in and outside of lab and becoming friends with all of you. Meghan, Cam, and Justine, I couldn't have asked for better conference buddies.

I am also grateful for all my friends outside of the lab, especially Dana, Cayman, Laura, Amanda and Leah. Dana, you have been one of my biggest supporters since college and I don't know if I'll ever be able to repay you for all you've done for me. Thank you for being there, be it over the phone or a quick road trip away. Leah, I'm so glad I met you, and thank you for always encouraging me to try new things. To Cayman, Laura, and Amanda, I couldn't have asked for better college roommates, and thank you for being there no matter the distance.

Finally, I would like to express my profound gratitude to my family. To Memaw, Pop Pop, Grandma, and Pop, I hope I have made all of you proud. Thank you to Mom, Dad and Donna for all of your encouragement, sacrifices, and love. I never would have accomplished so much without you. I love you all, and I hope you know how much you mean to me.

I must also acknowledge funding support from the National Institute of Justice (NIJ) [grant numbers 2017-R2-CX-0003 and 2015-DN-BX-K057] and the National Science Foundation [grant

number 1429329]. Furthermore, although this work was funded by the NIJ, the thoughts findings and conclusions presented here do not necessarily reflect those of the Department of Justice.

Copyright Permissions

A significant amount of the work presented in this dissertation has been published. Copyright permissions for the inclusion of the published work appearing in the abstract, appendices, and in Chapters 2-4 and 6, were acquired. The obtained permissions are reproduced below. All of the experimental work reported in this thesis, as well as in the referenced publications, was performed by Kristen Fowble. The published content is included because it encompasses a substantial segment of the research performed for the completion of the Ph.D. requirements. A list of the publications whose content is reproduced in this thesis in whole or in part is shown below followed by facsimiles of the permissions from the publishers.

1. The abstract and Chapters 2 and 3 adapted with permission from: Fowble, K. L., Teramoto, K., Cody, R. B., Edwards, D., Guarrera, D., and Musah, R. A. Development of “laser ablation direct analysis in real time imaging” mass spectrometry (LADI-MS): Application to spatial distribution mapping of metabolites along the biosynthetic cascade leading to synthesis of atropine and scopolamine in plant tissue. *Anal Chem.* **89**, 3421-3429 (2017), Copyright 2017 American Chemical Society.
2. Chapter 4 adapted with permission from: Fowble, K. L., Okuda, K., Cody, R. B., and Musah, R. A. “Spatial distributions of furan and 5-hydroxymethylfurfural in unroasted and roasted *Coffea arabica* beans.” *Food Res Int.* **119**, 725-732 (2019), Copyright 2019, Elsevier.
3. Chapter 6 adapted with permission from: Fowble, K. L., and Musah, R. A. “Simultaneous imaging of latent fingerprints and detection of analytes of forensic relevance by laser

ablation direct analysis in real time imaging-mass spectrometry (LADI-MS)." *Forensic Chem.* **15**, 100173 (2019), Copyright 2019, Elsevier.



RightsLink®

Home

Create Account

Help



ACS Publications
Most Trusted. Most Cited. Most Read.

Title: Development of "Laser Ablation Direct Analysis in Real Time Imaging" Mass Spectrometry: Application to Spatial Distribution Mapping of Metabolites Along the Biosynthetic Cascade Leading to Synthesis of Atropine and Scopolamine in Plant Tissue

Author: Kristen L. Fowble, Kanae Teramoto, Robert B. Cody, et al

Publication: Analytical Chemistry

Publisher: American Chemical Society

Date: Mar 1, 2017

Copyright © 2017, American Chemical Society

LOGIN

If you're a [copyright.com](#) user, you can login to RightsLink using your [copyright.com](#) credentials. Already a [RightsLink](#) user or want to [learn more?](#)

PERMISSION/LICENSE IS GRANTED FOR YOUR ORDER AT NO CHARGE

This type of permission/license, instead of the standard Terms & Conditions, is sent to you because no fee is being charged for your order. Please note the following:

- Permission is granted for your request in both print and electronic formats, and translations.
- If figures and/or tables were requested, they may be adapted or used in part.
- Please print this page for your records and send a copy of it to your publisher/graduate school.
- Appropriate credit for the requested material should be given as follows: "Reprinted (adapted) with permission from (COMPLETE REFERENCE CITATION). Copyright (YEAR) American Chemical Society." Insert appropriate information in place of the capitalized words.
- One-time permission is granted only for the use specified in your request. No additional uses are granted (such as derivative works or other editions). For any other uses, please submit a new request.



Title: Spatial distributions of furan and 5-hydroxymethylfurfural in unroasted and roasted Coffea arabica beans

Author: Kristen L. Fowble, Koji Okuda, Robert B. Cody, Rabi A. Musah

Publication: Food Research International

Publisher: Elsevier

Date: May 2019

© 2018 Elsevier Ltd. All rights reserved.

LOGIN

If you're a [copyright.com](#) user, you can login to RightsLink using your [copyright.com](#) credentials.

Already a [RightsLink](#) user or want to [learn more?](#)

Please note that, as the author of this Elsevier article, you retain the right to include it in a thesis or dissertation, provided it is not published commercially. Permission is not required, but please ensure that you reference the journal as the original source. For more information on this and on your other retained rights, please visit: <https://www.elsevier.com/about/our-business/policies/copyright#Author-rights>



ELSEVIER

Title: Simultaneous Imaging of Latent Fingermarks and Detection of Analytes of Forensic Relevance by Laser Ablation Direct Analysis in Real Time Imaging-Mass Spectrometry (LADI-MS)

Author: Kristen L. Fowble, Rabi A. Musah

Publication: Forensic Chemistry

Publisher: Elsevier

Date: Available online 22 July 2019

© 2019 Published by Elsevier B.V.

LOGIN

If you're a [copyright.com](#) user, you can login to RightsLink using your [copyright.com](#) credentials.

Already a [RightsLink](#) user or want to [learn more?](#)

Please note that, as the author of this Elsevier article, you retain the right to include it in a thesis or dissertation, provided it is not published commercially. Permission is not required, but please ensure that you reference the journal as the original source. For more information on this and on your other retained rights, please visit: <https://www.elsevier.com/about/our-business/policies/copyright#Author-rights>

Abstract

Methods for the accomplishment of small molecule imaging by mass spectrometry are challenged by the need for sample pre-treatment steps such as cryo-sectioning, dehydration, chemical fixation, or application of a matrix or solvent, that must be performed to obtain interpretable spatial distribution data. Furthermore, these steps along with requirements of the mass analyzer such as high vacuum, can severely limit the range of sample types that can be analyzed by this powerful method. Here, we report the development of a laser ablation-direct analysis in real time imaging-mass spectrometry (LADI-MS) approach which couples a 213 nm Nd:YAG solid state UV laser to a direct analysis in real time (DART) ion source and high-resolution time-of-flight mass spectrometer. This platform enables facile determination of the spatial distribution of small molecules spanning a range of polarities in a diversity of sample types, and requires no matrix, vacuum, solvent, or complicated sample pre-treatment steps. It furnishes high-resolution data, can be performed under ambient conditions on samples in their native form, and results in little to no fragmentation of analytes.

In this work, we demonstrate the applicability of LADI-MS to a variety of sample types to investigate questions of relevance to plant chemical ecology and forensic science. For example, the demonstration of the compartmentalization of small molecules can inform practices for the more efficient extraction of clinically relevant alkaloids from seed tissue or removal of potentially carcinogenic molecules in coffee beans. Additionally, the approach permits the analysis of large and irregularly shaped samples, like wood slices, and can permit the mapping of the locales of biologically active small molecules in endangered trees for the potential forensic identification of

their geographical origin, or assessment of the climactic and/or environmental conditions to which the tree was exposed over its lifetime. Additionally, the technique permits the collection of optical images and chemical information simultaneously, which can be helpful in those instances in which the amount of sample is limited (as may be the case in crime scene investigation applications).

Table of Contents

Acknowledgements	iv
Copyright Permissions	vii
Abstract	x
Table of Contents	xii
Abbreviations	xvii
List of Figures	xx
List of Tables	xxiii
List of Schemes	xxiv
List of Published Work Accomplished During Graduate Studies	xxv
Chapter 1: Introduction to Small Molecule Analysis in Complex Matrices by Mass Spectrometry	1
1.1. Small Molecules—Bulk Analysis	1
1.1.1. Mass spectrometry (MS).....	1
1.2. Small Molecules—Imaging Analysis	11
1.2.1. High-vacuum instrumentation.....	13
1.2.2. Ambient ionization imaging instrumentation.....	16
1.3. Statement of the Problem	20
Chapter 2: Development and Optimization of Laser Ablation Direct Analysis in Real Time Imaging-Mass Spectrometry (LADI-MS)	24
2.1. Introduction	24
2.2. Results	26
2.2.1. Laser ablation system	26
2.2.2. Ambient ionization mass spectrometry approach	30
2.2.3. Integration of the laser ablation and DART-HRMS platforms	33
2.2.4. Proof-of-principle imaging experiment-Blow fly wing.....	36
2.2.5. System assessment	38
2.3. Discussion	40

2.4. Conclusions	42
2.5. Materials and Methods	43
2.5.1. Chemicals	43
2.5.2. LADI-MS set-up	43
2.5.3. LADI-MS analysis of a blow fly wing	45
2.5.4. Spot size signal testing.....	46
2.5.5. Sensitivity testing.....	47
2.5.6. Ablation depth testing	48
Chapter 3: Application of LADI-MS to Spatial Distribution Mapping of Metabolites Along the Biosynthetic Cascade Leading to Synthesis of Atropine and Scopolamine in Plant Tissue	49
3.1. Introduction	49
3.2. Results	51
3.2.1. Microscopy of the imaged tissue.....	51
3.2.2. Tropane alkaloid biosynthesis	52
3.2.3. Ion images acquired by LADI-MS	54
3.3. Discussion	59
3.4. Conclusions	62
3.5. Materials and Methods	62
3.5.1. Seeds.....	62
3.5.2. Chemicals	63
3.5.3. Microscopy.....	63
3.5.4. Sample preparation for MALDI-MS/MS.....	63
3.5.5. MALDI-MS/MS analysis.....	64
3.5.6. Sample preparation for LADI-MS.....	64
3.5.7. LADI-MS analysis.....	64
3.5.8. LADI-MS seed analysis	65
Chapter 4: Application of LADI-MS to Determination of the Spatial Distributions of Furan and 5-Hydroxymethylfurfural in Unroasted and Roasted <i>Coffea arabica</i> Beans	66
4.1. Introduction	66

4.2. Results	69
4.2.1. Detection of furan and HMF in roasted coffee beans by dopant-assisted argon direct analysis in real time-high-resolution mass spectrometry (DART-HRMS).....	69
4.2.2. Independent confirmation of furan in unroasted and roasted coffee beans by GC-MS.....	71
4.2.3. Independent confirmation of HMF in unroasted and roasted coffee beans by GC-MS.....	73
4.2.4. Ion images acquired by LADI-MS	74
4.3. Discussion	77
4.4. Conclusions	79
4.5. Materials and Methods	79
4.5.1. Chemicals	79
4.5.2. Coffee beans	80
4.5.3. Argon DART-HRMS analysis	80
4.5.4. Coffee bean extract sample preparation.....	81
4.5.5. Standard samples preparation	82
4.5.6. GC-MS Analysis	82
4.5.7. LADI-MS coffee bean sample preparation.....	83
4.5.8. Light microscopy imaging of unroasted coffee beans	84
4.5.9. LADI-MS analysis.....	84
Chapter 5: Application of LADI-MS to the Forensic Determination of the Spatial Distributions of Small Molecules in Endangered Wood Samples	86
5.1. Introduction	86
5.2. Results	90
5.3. Discussion	97
5.4. Conclusions	99
5.5. Materials and Methods	100
5.5.1. Chemicals	100
5.5.2. Endangered wood samples.....	100

5.5.3. LADI-MS analysis	101
Chapter 6: Simultaneous Imaging of Latent Fingermarks and Detection of Analytes of Forensic Relevance.....	102
6.1. Introduction.....	102
6.2. Results.....	104
6.2.1. LADI-MS analysis of a cocaine-laden latent fingermark	104
6.2.2. LADI-MS analysis of a psychoactive plant-laden latent fingermark	106
6.2.3. LADI-MS analysis of a pseudoephedrine-laden latent fingermark.....	108
6.2.4. LADI-MS analysis of a developed and lifted latent fingermark	108
6.2.5. Micro-ablation of an explosive material located within a latent fingermark.....	110
6.2.6. Demonstration of the advantages of an ambient ionization mass spectrometric approach for latent fingermark analysis	111
6.3. Discussion	112
6.4. Conclusions.....	114
6.5. Materials and Methods.....	115
6.5.1. Chemicals	115
6.5.2. Fingerprint residues	115
6.5.3. LADI-MS analysis.....	117
Chapter 7: Other Forensic Applications of LADI-MS—Analysis of Inks on Paper and Gunshot Residue	120
7.1. Introduction.....	120
7.1.1. Analysis of inks on paper	121
7.1.2. Gunshot residue analysis (GSR)	123
7.2. Results.....	124
7.2.1. Application to inks on paper	124
7.2.2. Application to fired bullets and other inorganic materials.....	128
7.3. Discussion	130
7.4. Conclusions.....	131
7.5. Materials and Methods.....	132

7.5.1. Materials	132
7.5.2. Inks on paper sample preparation.....	132
7.5.3. Ammunition and lead plate	133
7.5.4. LADI-MS analysis.....	134
Concluding Remarks	136
References	137
Appendix	155

Abbreviations

AgNP	silver-nanoparticle
APCI	atmospheric pressure chemical ionization
API	atmospheric pressure interface
CI	chemical ionization
CID	collision-induced dissociation
CI-MS	chemical ionization-mass spectrometry
CITES	Convention on International Trade in Endangered Species
DAPCI-MS	desorption atmospheric pressure chemical ionization-mass spectrometry
DART	direct analysis in real time
DART-HRMS	direct analysis in real time-high-resolution mass spectrometry
DART-MS	direct analysis in real time-mass spectrometry
DART-SVP	direct analysis in real time-standardized voltage and pressure
DEFFI-IMS	desorption electro-flow focusing ionization-imaging mass spectrometry
DEFFI-MS	desorption electro-flow focusing ionization-mass spectrometry
DESI	desorption electrospray ionization
DESI-IMS	desorption electrospray ionization-imaging mass spectrometry
DESI-MS	desorption electrospray ionization-mass spectrometry
DHB	2,5-dihydroxybenzoic acid
DNA	deoxyribonucleic acid
EDX	energy-dispersive X-ray spectroscopy
EI	electron ionization
EI-MS	electron ionization-mass spectrometry
ESI	electrospray ionization
eV	electron volts
FWHM	full width at half maximum
G	atmospheric gases
GC	gas chromatography

GC-MS	gas chromatography-mass spectrometry
GC-TOF-MS	gas chromatography-time-of-flight-mass spectrometry
GSR	gunshot residue
HMF	5-hydroxymethylfurfural
HR	high-resolution
HRMS	high-resolution mass spectrometry
HR-TOF-MS	high-resolution-time-of-flight-mass spectrometry
IMS	imaging mass spectrometry
IR	infrared
IVA	infinitely variable aperture
LADI-MS	laser ablation direct analysis in real time imaging-mass spectrometry
LAESI	laser ablation electrospray ionization
LAESI-IMS	laser ablation electrospray ionization-imaging mass spectrometry
LAESI-MS	laser ablation electrospray ionization-mass spectrometry
LC	liquid chromatography
LC-MS	liquid chromatography-mass spectrometry
LC-MS/MS	liquid chromatography-tandem mass spectrometry
LC-QTOF	liquid chromatography-quadrupole time-of-flight
LDI	laser desorption ionization
LDI-MS	laser desorption ionization-mass spectrometry
LD-LTP-IMS	laser desorption-low temperature plasma-imaging mass spectrometry
LD-LTP-MS	laser desorption-low temperature plasma-mass spectrometry
LTP	low temperature plasma
<i>m/z</i>	mass to charge ratio
MALDI	matrix-assisted laser desorption ionization
MALDI-IMS	matrix-assisted laser desorption ionization-imaging mass spectrometry
MALDI-MS	matrix-assisted laser desorption ionization-mass spectrometry
MALDI-MS/MS	matrix-assisted laser desorption ionization-tandem mass spectrometry
MCP	microchannel plate

mmu	milli mass unit
MS	mass spectrometry
MS/MS	tandem mass spectrometry
N	neutral
<i>nano</i> -PALDI	nanoparticle-assisted laser desorption ionization
Nd:YAG	neodymium-doped yttrium aluminum garnet
Nd:YLF	neodymium-doped yttrium lithium fluoride
NMR	nuclear magnetic resonance
PEG	polyethylene glycol
RDX	1,3,5-trinitro-1,3,5-triazinane
RICs	reconstructed ion currents
SALDI-MS	surface-assisted laser desorption ionization-mass spectrometry
SEM	scanning electron microscopy
SEM/EDX	scanning electron microscopy-energy-dispersive X-ray spectroscopy
SIMS	secondary ion mass spectrometry
sp.	species
spp.	multiple species
TMP	turbo molecular pump
TOF	time-of-flight
TOF/TOF	time-of-flight/time-of-flight
TOF-MS	time-of-flight-mass spectrometry
UNODC	United Nations Office on Drugs and Crime
U.S.	United States
UV	ultraviolet
V	voltage
XYR	rotational XY shutter

List of Figures

Figure 1.1.	Depiction of a mass spectrum in which two charged species are detected.	1
Figure 1.2.	A depiction of a mass spectrum derived from an EI-MS experiment.	3
Figure 1.3.	A schematic of the DART ion source.	8
Figure 1.4.	A picture of DART-MS analysis of whole plant material.	10
Figure 1.5.	A mass spectrum derived from a soft ionization technique like DART-MS.	11
Figure 1.6.	A schematic describing IMS.	12
Figure 2.1.	A photograph of the NWR213 laser ablation system.	26
Figure 2.2.	Photographs of the NWR213 sample drawer.	27
Figure 2.3.	A photograph of the DART-SVP ion source, which is contained within the blue cylinder.	31
Figure 2.4.	A schematic diagram of the AccuTOF mass spectrometer that is utilized in LADI-MS.	32
Figure 2.5.	LADI mass spectrometry set-up.	34
Figure 2.6.	The LADI-MS system and the interface at the DART-MS sampling gap.	35
Figure 2.7.	A LADI-MS-derived mass spectrum (Panel A) and ion images of a blow fly wing.	37
Figure 2.8.	The RICs for quinine showing the counts detected for each spot size used to ablate one line scan.	39
Figure 2.9.	A plot featuring the concentration of quinine vs the integrated peak area from the RIC of quinine.	40
Figure 2.10.	A diagram illustrating the spot size testing.	46
Figure 2.11.	A diagram depicting the analysis of 5 μ L spots of varying concentrations of quinine in methanol.	47
Figure 3.1.	Light (A and C) and scanning electron microscopy (SEM) micrographs (B and D) of <i>Datura leichhardtii</i> seeds.	52
Figure 3.2.	Proposed pathway for the biosynthesis of atropine and scopolamine in Solanaceae family plants.	53
Figure 3.3.	Color-overlaid ion images acquired from analysis of a transverse section of a <i>D. leichhardtii</i> seed by LADI-MS.	55
Figure 3.4.	Illustration of differential distribution of detected ions as color overlays on the SEM micrograph of the transverse cross-section of the <i>D. leichhardtii</i> seed shown in Figure 3.1.	58

Figure 4.1.	A representative dopant-assisted argon DART-mass spectrum of a roasted coffee bean over a mass range of m/z 50-250.	70
Figure 4.2.	The standard curve for the quantification of furan (peak area vs concentration (ng g^{-1})) over a range of 0-100 ng g^{-1} .	72
Figure 4.3.	The GC extracted ion chromatograms (EIC) for furan in roasted and unroasted coffee bean headspace gases in the time range of 1-3 min are shown in Panels A and B, respectively.	73
Figure 4.4.	The GC extracted ion chromatograms (EIC) for HMF in the roasted and unroasted coffee bean 1:1 methanol:dichloromethane extracts in the time range of 14.5-15 min.	74
Figure 4.5.	A light microscopy image of a transverse cross-section of a green (unroasted) coffee bean.	75
Figure 4.6.	The color-overlaid ion images of the m/z values corresponding to furan and HMF in transverse cross-sections of unroasted (top) and roasted (bottom) coffee beans.	76
Figure 5.1.	A diagram depicting the morphology and anatomy of a tree trunk.	89
Figure 5.2.	A representative mass spectrum acquired from ablating the surface of a <i>D. nigra</i> sample using LADI-MS.	90
Figure 5.3.	Visible light optical images of the four samples of wood analyzed by LADI-MS.	91
Figure 5.4.	Ion images overlaid onto hyperspectral images acquired at 645 nm (Panel A) of the <i>D. nigra</i> sample.	92
Figure 5.5.	Ion images acquired using LADI-MS, overlaid onto hyperspectral images of a <i>D. maritima</i> sample.	93
Figure 5.6.	LADI-MS ion images overlaid onto a hyperspectral image of the <i>D. normandii</i> sample acquired at a wavelength of 725 nm (Panel A).	94
Figure 5.7.	Color-overlaid ion images of a mass consistent with 3,4-dimethoxydalbergione overlaid onto the corresponding hyperspectral images of the <i>Dalbergia</i> spp. tree samples analyzed.	95
Figure 5.8.	The hyperspectral and ion images for the <i>S. mahagoni</i> tree sample.	96
Figure 6.1.	A mass spectrum and LADI-MS ion images resulting from the analysis of a fingerprint deposited after exposure to cocaine.	105
Figure 6.2.	A LADI-MS-derived ion image and a representative LADI-mass spectrum obtained from the analysis of a fingerprint deposited after handling of <i>P. methysticum</i> plant material.	107
Figure 6.3.	A LADI-MS-derived mass spectrum and ion images showing the presence of endogenous and exogenous molecules in a pseudoephedrine-laden fingerprint.	109

Figure 6.4.	Ion image of dehydroxylated cholesterol in a lifted latent fingerprint, imaged on the adhesive side of packing tape by LADI-MS.	110
Figure 6.5.	Laser ablation DART-mass spectrum of an RDX particle located in a latent fingerprint and detected using methylene chloride as a dopant.	111
Figure 6.6.	LADI-mass spectra of a “fresh” blank fingerprint (top) and a blank latent fingerprint analyzed after 96 h (bottom).	112
Figure 7.1.	A peace sign image drawn with blue (outer circle) and orange (inner lines) Sharpie® markers (Panel A), and the corresponding DART-mass spectra and LADI-MS ion images.	125
Figure 7.2.	A peace sign image drawn with Bic® and Sharpie® black markers (Panel A), and the corresponding DART-mass spectra and LADI-MS ion images.	126
Figure 7.3.	The color-overlaid ion images for three compounds of interest detected in black pen inks.	127
Figure 7.4.	The color-overlaid ion images for three masses detected in black pen inks.	128
Figure 7.5.	The color-overlaid ion image of m/z 170.0970, a mass consistent with that of diphenylamine.	128
Figure 7.6.	Mass spectra showing the detection of copper (Panel A) and lead (Panel B) after the application of acac to the surface of the metal.	129

List of Tables

Table 2.1.	DART-HRMS parameters used for analyses.	46
Table 2.2.	Laser parameters used for analyses.	46
Table 6.1.	DART-HRMS parameters used for analyses.	118
Table 6.2.	Laser parameters used for analyses.	119
Table 7.1.	DART-HRMS parameters used for analyses.	134
Table 7.2.	Laser parameters used for analyses.	135

List of Schemes

Scheme 1.1.	The ionization mechanism of the DART ion source operated in positive ion mode.	9
Scheme 1.2.	The ionization mechanism of the DART ion source operated in negative ion mode.	10

List of Published Work Accomplished During Graduate Studies

1. **Fowble, K. L.**, and Musah, R. A. "Simultaneous imaging of latent fingerprints and detection of analytes of forensic relevance by laser ablation direct analysis in real time imaging-mass spectrometry (LADI-MS)." *Forensic Chem.* **15**, 100173 (2019).
2. **Fowble, K. L.**, and Musah, R. A. "A validated method for the quantification of mitragynine in sixteen commercially available Kratom (*Mitragyna speciosa*) products." *Forensic Sci Int.* **299**, 195-202 (2019).
3. **Fowble, K. L.**, Okuda, K., Cody, R. B., and Musah, R. A. "Spatial distributions of furan and 5-hydroxymethylfurfural in unroasted and roasted *Coffea arabica* beans." *Food Res Int.* **119**, 725-732 (2019).
4. **Fowble, K. L.**, and Musah, R. A. "Utilizing direct analysis in real time-high resolution mass spectrometry-derived dark matter spectra to classify and identify unknown synthetic cathinones." *Methods Mol Biol.* **1810**, 217-225 (2018).
5. Lesiak, A. D., **Fowble, K. L.**, and Musah, R. A. "A rapid, high-throughput validated method for the quantification of atropine in *Datura stramonium* seeds using direct analysis in real time-high resolution mass spectrometry (DART-HRMS)." *Methods Mol Biol.* **1810**, 207-215 (2018).
6. **Fowble, K. L.**, Shepard, J. R. E., and Musah, R. A. "Identification and classification of cathinone unknowns by statistical analysis processing of direct analysis in real time-high resolution mass spectrometry-derived "neutral loss" spectra." *Talanta.* **179**, 546-553 (2018).
7. **Fowble, K. L.**, Teramoto, K., Cody, R. B., Edwards, D., Guarrera, D., and Musah, R. A. Development of "laser ablation direct analysis in real time imaging" mass spectrometry (LADI-MS): Application to spatial distribution mapping of metabolites along the biosynthetic

cascade leading to synthesis of atropine and scopolamine in plant tissue. *Anal Chem.* **89**, 3421-3429 (2017).

8. Musah, R. A., Lesiak, A. D., Maron, M., Cody, R. B., Edwards, D., **Fowble, K. L.**, Dane, A. J., and Long, M., "Mechanosensitivity below ground: Touch-sensitive smell-producing roots in the 'shy plant', *Mimosa pudica* L." *Plant Physiol.* **170**, 1075-1089 (2016).

Chapter 1: Introduction to Small Molecule Analysis in Complex

Matrices by Mass Spectrometry

1.1. Small Molecules—Bulk Analysis

1.1.1. Mass spectrometry (MS)

Mass spectrometry is an analytical technique used to determine the molecular weight of a molecule. It is one of the most sensitive chemical characterization methods available for the determination of molecular composition and structure. Mass spectrometers are typically comprised of three major components: 1) the ion source which converts analytes to charged particles; 2) the mass analyzer which separates the combination of ions generated by the ion source; and 3) the detector which detects and registers the number of ions as they reach it.

A mass spectrometer is used to measure the mass-to-charge ratio (m/z) of charged molecular species, and results in a mass spectrum (Figure 1.1).¹ The mass-to-charge ratio appears on the x-axis. Detected molecules appear as “peaks” in the mass spectrum and are defined by their position on the x-axis (i.e. their m/z). For example, for a molecule of mass 100 Daltons with a charge of +1, the m/z is $100/1 = 100$, and it would be positioned on the x-axis at m/z 100 (Figure 1.1).

Figure 1.1 also shows a peak at m/z 50, which represents the presence of a second charged species

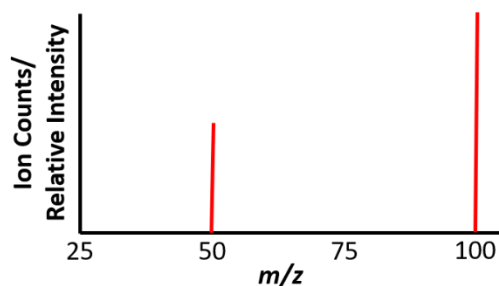


Figure 1.1. Depiction of a mass spectrum in which two charged species are detected.

with a molecular mass of 50 Daltons (assuming the charge of +1). Thus, for molecules with a charge of ± 1 , the observed m/z value represents its nominal mass/molecular weight.

A second attribute of peaks detected in a mass spectrum is the peak height, which is registered on the y-axis either as “ion counts” or “relative intensity”. Ion counts refer to how many ions of the same m/z value are detected at the same time. Typically, in a mass spectrometer detector, the ions themselves are not counted; the electrons which are emitted from the interaction of the ions in an electric field will be registered, and this is correlated to an ion current. The ion current is directly proportional to the number of ions that reach the detector. Relative intensity is an arbitrary depiction of the ion current of every detected ion, compared to the most intense (tallest) peak. The tallest peak in a mass spectrum, which by convention represents 100% “relative intensity” (m/z 100 in Figure 1.1) is known as the “base peak” and the intensities of all of the other observed ions will be described relative to this 100% value. For example, in Figure 1.1, the peak at m/z 50 has a 50% relative intensity because it is half as tall/intense as the base peak (i.e. it is half as abundant as the charged molecule at m/z 100).

Instruments that utilize a high-resolution mass analyzer can provide the chemical formula of a detected ion based on its exact mass and the presence of isotope peaks and their relative intensities, as these are correlated to the combination and number of atoms in the molecule.¹ Additionally, mass spectrometry experiments resulting in molecule fragmentation can reveal a tremendous amount of structural information because molecule fragmentation in the gas phase follows well understood mechanisms.

To be detected by a mass spectrometer, a molecule or atom must be charged. Therefore, an essential part of the MS platform is the component that converts the sample into charged particles (i.e. the ion source). There are various types of sources that can be used in MS. These can be categorized as hard or soft depending on the extent to which the molecules detected are subjected to fragmentation. Soft ionization mass spectrometric analysis of a mixture of two compounds would result in a mass spectrum similar to that depicted in Figure 1.1. The only masses detected are those of the intact charged molecules (if the charges on the molecules are ± 1). In comparison, a hard ionization technique would result in a mass spectrum like that depicted in Figure 1.2 for the analysis of a single compound. Multiple peaks at different m/z values are detected at various relative intensities. The green star indicates the charged unfragmented molecule, and the additional peaks are those corresponding to fragment ions that are derived from it.

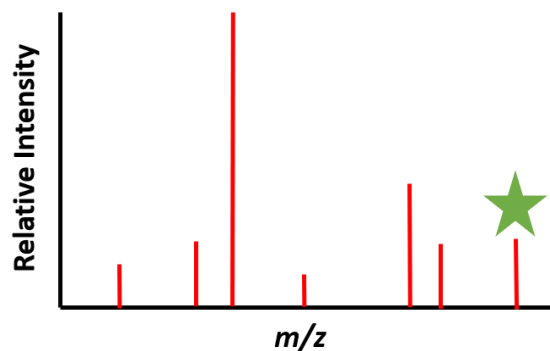


Figure 1.2. A depiction of a mass spectrum derived from an EI-MS experiment. The green star denotes the charged unfragmented molecule detected by the MS, and the other peaks are fragment ions derived from it.

Different ionization sources have their own advantages and disadvantages that are dependent on the class of compound. Major ionization types utilized in mass spectrometry include (but are not limited to) electron ionization, chemical ionization, and ambient ionization, and are described in more detail below.

Electron ionization (EI)

EI is a hard ionization technique that involves subjection of a sample in the gas phase to bombardment by high-energy electrons (~70 eV). The sample molecules thus exposed eject an electron, yielding a cation radical termed the “molecular ion”, and denoted by M^+ . In addition, because the energy of the bombarding electrons usually far exceeds the ionization potential of the sample molecules, the excess energy within the newly created M^+ results in fragmentation of the chemical species.¹ Any fragments that are formed will be registered in the mass spectrum (Figure 1.2), and the composite of these with their relative intensities is referred to as the “fragmentation pattern” of the molecule. The fragmentation patterns that are obtained in EI-MS experiments are considered to be a unique “fingerprint” for the compound analyzed. This is because fragmentation occurs following a set of pathways that can be predicted depending on the structural features of the analyzed compound, and thus multiple EI analyses of the same compound generally result in identical spectra. These pathways include sigma-bond cleavage, homolytic cleavage, heterolytic cleavage, and rearrangements.¹ Massive databases of the EI fragmentation patterns of small molecules have been compiled and are used as structure identification tools. For example, to identify an analyte, its EI mass spectral fragmentation pattern can be screened against the EI spectra in a library to find a match. Potential matches are often reported with a percent certainty, with high matches revealing the identity of the compound.

It is extremely common to couple mass spectrometers with a type of chromatographic instrument which results in the so called “hyphenated” MS techniques such as gas

chromatography (GC)-MS and liquid chromatography (LC)-MS. In such cases, the chromatographic interface precedes the mass spectrometer, such that samples to be analyzed are first introduced to the chromatograph where they are separated into purified components which are transferred sequentially to the mass spectrometer as they are eluted from the chromatography column. This approach to analyzing samples is particularly important for mixtures and enables two techniques to be combined to yield results in a single experiment. This, in addition to the exquisite reproducibility of EI fragmentation patterns for small molecules, regardless of instrument brand, makes GC-MS in particular the workhorse of many laboratories, including crime labs.

Although EI-MS can provide diagnostic fragmentation patterns for different chemical classes and specific compounds, one of its disadvantages is that the molecular ion is sometimes absent in the collected mass spectrum, making identification of an unknown difficult.¹ Additionally, some molecule types undergo such extensive fragmentation²⁻³ that structurally similar compounds can result in identical fragmentation patterns, making their definitive identification by MS alone difficult.

Chemical ionization (CI)

CI was developed by Munson and Field in 1966⁴ as a supplementary ionization approach in an EI-MS instrument.¹ It is a soft ionization technique that is sometimes employed when the molecular ion is not observed by EI. Although some fragmentation of analytes occurs, more fragments tend to be observed at higher intensities compared to EI, because much less energy is

applied to induce ionization. The ionization mechanism involves gas-phase reactions between analytes and atoms or small molecules, rather than ionization via loss or gain of electrons to yield molecular ions. The reactions occurring can be referred to as *molecule/ion* reactions, meaning that the gas-phase molecule of interest is reacted with a gas-phase reagent ion, which is used to transfer a proton or adduct to the analyte.¹ The gas-phase reactions occurring within the instrument are dependent on the reagent gas (a source of reagent ions) being used.¹ The most commonly used reagent gases include helium, hydrogen, methane, water, isobutane, methanol, and ammonia. The reagent gas molecules are subjected to EI to produce the reagent gas ions needed for the ionization of the sample. Most involve the transfer of a proton to the analytes (resulting in $(M+H)^+$), providing that the proton affinity of the analyte exceeds that of the reagent ion. Some reagent gases result in adducts rather than protonation of the molecule. For example, tetramethylsilane can be used as a reagent gas and typically results in charged adducts of the form $(M+Si(CH_3)_3)^+$.¹

With the multitude of reagent gases and resulting reactant ions of varying proton affinities, different gases can be used for the optimal detection of small molecules in a complex matrix. The reagent gas can be chosen to avoid potential interferences from the sample matrix and for this reason, CI-MS can be made to achieve lower limits of detection than EI-MS. Additionally, the extent to which the molecules of interest are fragmented (if at all) can be optimized by choosing a reagent gas with a particular proton affinity. The use of reactant gas ions with much lower proton affinities relative to those of the analytes, will result in greater analyte fragmentation.¹

Although EI- and CI-MS were some of the earliest mass spectrometric techniques developed, they still remain two of the most commonly used MS approaches today. Nevertheless, there are several challenges that plague their routine use for small molecule analysis, especially when complex matrices are involved. First, to be ionized and detected, molecules must be in the gas phase. This condition is most often accomplished by using a high vacuum to reduce the boiling point temperature of the molecule, but even so, it is sometimes not possible to achieve low enough vacuums to vaporize all molecules. Additionally, the sample preparation steps that are often required prior to analysis in order to accommodate the chromatographic separation step can be quite elaborate, and time and resource intensive, particularly for complex sample types, such as plant materials. For the analysis of unknowns in mixtures, the tedious method development and sample pretreatment steps required to achieve molecule identity confirmation can preclude the rapid analysis of samples.

Ambient ionization

One of the major developments that is responsive to the challenges of MS analysis of molecules that are not amenable to detection by GC/EI-MS by virtue of the difficulties inherent in ionizing them, or the problematic sample preparation steps required, is atmospheric pressure ionization.⁵⁻⁸ The vast number of these techniques and related derivatives that have been developed,⁵⁻¹¹ are split between those based on electrospray ionization (ESI) and atmospheric pressure chemical ionization (APCI) approaches. The advantage of these techniques is that they enable the analysis of samples in their native state without pretreatment steps. These ionization

sources use solvent, heat, or gas streams to desorb small amounts of material from the native sample for introduction to the mass analyzer. Since there is no high-vacuum requirement, the samples often do not have to undergo sample pretreatment steps such as solubilization, for introduction into a high-vacuum system. The two most commonly used ambient ionization sources are desorption electrospray ionization (DESI)- and direct analysis in real time (DART)-MS. DESI-MS, described by Takáts et al. in 2004,¹¹ utilizes a charged solvent spray for the ionization of molecules from a sample surface.^{5-7, 11} DART, first introduced by Cody, Laramée, and Durst in 2005,⁹ is a plasma-based ionization source. The work presented here demonstrates novel applications of DART, and thus a more detailed description of this APCI technique is described below.

Direct analysis in real time—high-resolution mass spectrometry (DART-HRMS)

First described in 2005, DART is a relatively new soft ionization source that can be coupled to any mass analyzer equipped with an ambient pressure interface.⁹ The source and its component parts are described in detail by Cody et al., and a schematic of it is shown in Figure 1.3.^{9, 12} DART can be used with helium, nitrogen, or argon as the carrier gas, with helium-DART

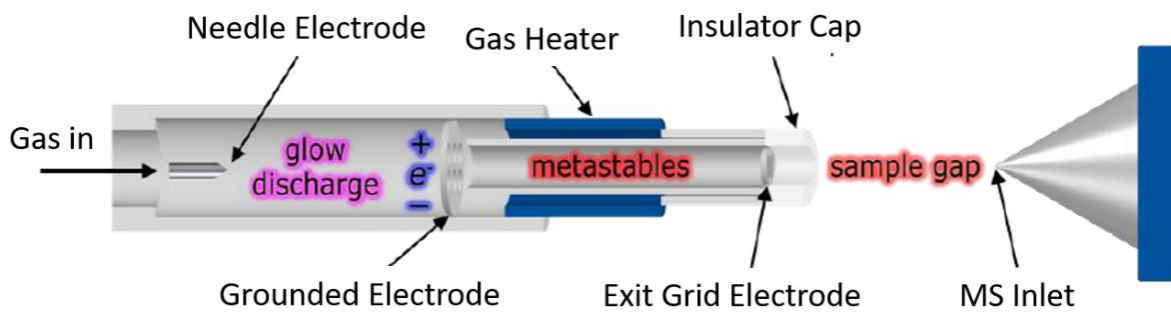
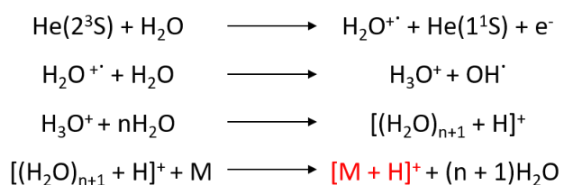


Figure 1.3. A schematic of the DART ion source.^{9,12}

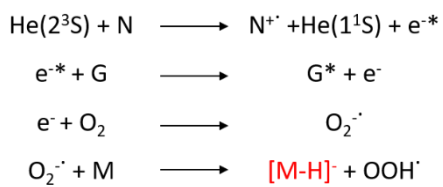
being the most common. It also can be operated in positive or negative ion modes. The ionization mechanisms of DART using helium gas are described in Schemes 1.1 and 1.2. Briefly, the ionization mechanism in positive ion mode involves the creation of metastable helium atoms that interact with atmospheric water to generate protonated water clusters. These then interact with the analytes in the open-air sampling gap where proton transfer from the protonated water clusters to the sample can occur depending on the proton affinity of the molecules in the sample. This interaction results in the detection of the intact protonated molecule $[M+H]^+$ (labelled in red in Scheme 1.1).⁹



Scheme 1.1. The ionization mechanism of the DART ion source operated in positive ion mode.^{9,12}

Since DART ionization is heavily dependent on the proton affinity of the analytes, the relative intensities of peaks in the resulting mass spectrum do not necessarily represent the relative amounts of the molecules in a mixture. Coffee can be used as a case in point. A coffee brew contains both caffeine and chlorogenic acid. Caffeine, an amine, has a relatively high proton affinity of $\sim 218 \text{ kcal mol}^{-1}$, while chlorogenic acid has a proton affinity of only $\sim 30 \text{ kcal mol}^{-1}$ in water.¹³⁻¹⁴ Thus, even if the caffeine content is much lower than that of chlorogenic acid, the DART mass spectrum of coffee will most likely still be dominated by a peak for caffeine due to its much higher proton affinity, because it is protonated more readily than chlorogenic acid. As such, the limits of detection and sensitivity of DART-MS are analyte-dependent.

In negative ion mode, electrons interact with a neutral (denoted as “N”), such as the exit grid electrode, resulting in the formation of electrons through Penning ionization.⁹ These electrons will then react and thermalize by collisions with atmospheric gases (G), which then



Scheme 1.2. The ionization mechanism of the DART ion source operated in negative ion mode.^{9,12}

interact with atmospheric oxygen. This results in the creation of ionized oxygen which subsequently abstracts protons from the compounds in the sample. Typically, DART-MS experiments conducted in negative ion mode will result in a deprotonated analyte [M-H]⁻ (shown in red in Scheme 1.2).⁹ Changing the carrier gas to argon or nitrogen has an effect on the dominant ionization mechanism and has been described previously.¹⁵⁻¹⁷

The development of the DART ion source permits the direct analysis of various sample types in their native form.¹⁰ Sampling occurs in the open-air gap between the ion source and MS inlet, thus permitting the analysis of large solid objects such as plant parts, animal tissues or food, in addition to powders and liquids.¹⁰ Figure 1.4 shows the analysis of a plant leaf; sampling occurs by holding the intact leaf between the DART ion source (encased in the blue cylinder) and the MS inlet. As a soft ionization technique, the analysis of complex matrices

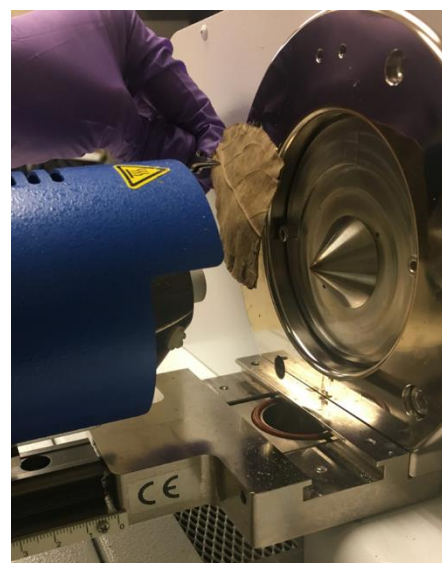


Figure 1.4. A picture of DART-MS analysis of whole plant material. The leaf is placed directly between the ion source and MS inlet in the open-air sampling gap.

results in mass spectra that contain peaks for all components in a mixture. This is illustrated in Figure 1.5. Each peak is representative of an intact molecule, denoted by a different colored star, and not a fragment ion. Thus, DART ion sources are typically coupled with high-resolution mass analyzers that can provide exact masses and detection of isotope peaks. The high-resolution masses permit the determination of candidate molecular formulas and can result in tentative

identifications of the analytes in a mixture. As such, the technique has been utilized in a variety of studies of the small molecule composition of very complex matrices such as plant materials, food stuffs, human urine and saliva, condom lubricants, and rhinoceros' horn, among many others.^{10, 18-30} Often, even when the identities of the detected compounds are not known, the entire mass spectral profile for these sample types can be used as “chemical fingerprints” for identification of whole materials.^{18-26, 28, 30}

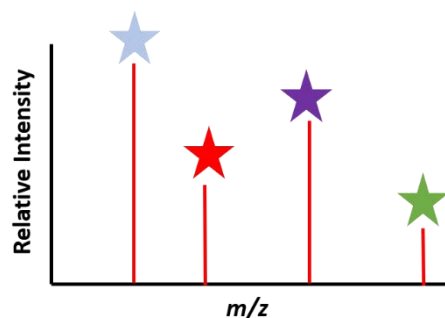


Figure 1.5. A mass spectrum derived from a soft ionization technique like DART-MS. Each peak represented by a colored star corresponds to an intact molecule.

1.2. Small Molecules—Imaging Analysis

One of the most powerful recent developments in mass spectrometry is its use in imaging the spatial distributions of detected molecules within a sample. Imaging mass spectrometry (IMS), as it is commonly called, provides a means whereby spatial distribution maps of molecules within plant, animal and human tissues can be accomplished. The ability to achieve this has profound implications for advancements in numerous fields including medicinal chemistry, point of care diagnostics, forensic science, plant biochemistry, and food science, among many others.³¹⁻³⁵ In 2D IMS experiments, mass spectra are collected at every x,y-coordinate within a selected area of the surface of a sample. Once these are compiled, the relative intensity over the entire area of the scanned sample of an m/z value of interest can then be assessed. This interrogation furnishes a visual representation of the spatially resolved distribution of that ion over the entire

area. This is illustrated in Figure 1.6. A sample, in this case a plant leaf, is surveyed at every x,y-coordinate over the entire surface. This results in a mass spectrum at each of those x,y-coordinates (center image). If a soft ionization source is utilized, the mass spectrum will detect the presence of multiple molecules in the sample, each denoted by a different colored star. The user can then choose any analyte of interest and view its spatial distribution in the plant leaf. In Figure 1.6, each analyte detected in the mass spectrum is differentially distributed within the plant leaf. Any analyte detected during the experiment can be mapped in this way.

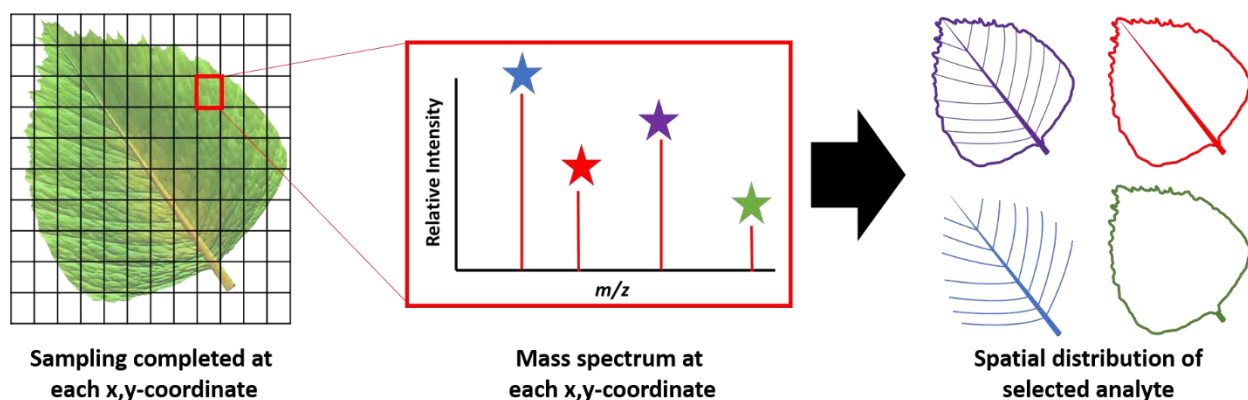


Figure 1.6. A schematic describing IMS. A sample (plant leaf) is analyzed at every x,y-coordinate on its surface. This results in mass spectra being collected at each of those discrete areas. The user can then choose an analyte of interest, such as those denoted by the different colored stars, and map their spatial distributions in the plant leaf. In this illustration, each of the four different analytes are localized to different areas of the leaf (as indicated in the color-coded spatial distribution maps).

There are a variety of IMS techniques that are described in the literature,³¹⁻⁵⁶ including matrix-assisted laser desorption ionization (MALDI)-IMS, DESI-IMS, secondary ion-MS (SIMS), laser ablation electrospray ionization (LAESI)-IMS, and their derivatives (i.e. *nano*-DESI), among others. The techniques vary in terms of ionization mechanisms, sample preparation steps, high-vacuum requirements, and the need for solvents. Until recently, many of the IMS approaches were optimized for the detection and mapping of large molecules or polymeric materials such as proteins in biological samples. However, there have been an increasing number of developments

directed towards small molecule imaging analysis.⁵⁷ Brief descriptions of some of the most commonly utilized IMS techniques are presented below.

1.2.1. High-vacuum instrumentation

Laser desorption ionization (LDI)-IMS

As suggested by the name, LDI-MS utilizes a laser for the desorption and ionization of the analytes in the sample. This technique has been applied to the imaging of pheromones and other compounds localized within different insect parts.^{43, 58} However, the utilization of the laser alone for the desorption and ionization of molecules results in low signal intensities and limited ability to analyze some classes of molecules.¹ To improve upon LDI-MS, multiple derivatives of the approach were developed. These include matrix-assisted LDI and surface-assisted LDI, which utilize small organic molecules, inorganic substrates, and other compounds for ionization enhancement.⁵⁹⁻⁶¹

Matrix-assisted LDI (MALDI)-IMS

The most common of the mainstream IMS approaches uses matrix-assisted LDI as the ionization source. MALDI-MS, first developed by Tanaka in 1988,⁶¹ utilizes a matrix to facilitate ionization upon the firing of a laser at the sample.⁵⁹ MALDI-IMS is a soft ionization technique. The addition of the matrix permits reduction of the laser energy needed for ionization in LDI-MS experiments. This results in less fragmentation of analytes and promotes higher signal

intensities.⁵⁰ MALDI is especially useful for high mass range measurements (~100,000 Daltons), because multiply-charged ions are possible. The technique has been fully optimized for the detection of large biomolecules such as proteins, oligosaccharides, and polymers in biological sample types. Its application to the detection of lower masses is complicated by the presence of the matrix which can interfere with detection of ions and interpretation of the data in the low mass region of the spectrum. However, with recent advancements in high-resolution mass analyzer technology, this issue is not as problematic.

In MALDI-IMS, a matrix is applied to the entire surface of the sample to be analyzed. It is most often a small organic molecule, whose purpose is to absorb the laser's energy while facilitating ionization of the compounds.¹ The analytes within a sample desorb into the matrix crystals. When the laser beam hits the surface of the matrix-covered sample, the matrix ionizes the desorbed compounds which are subsequently detected by the mass spectrometer.¹ Another role of the matrix is to dilute the analyte, thereby reducing the potential for the occurrence of analyte-analyte molecular interactions when the laser is fired.¹ The matrix crystal's properties, particularly its size, are dependent on a number of factors including the solvent used and the manner of its application. The more homogenous the layer of matrix that is applied to the surface of the sample, the more uniform its crystal formation, resulting in more intense signals and better imaging results. The spatial resolutions attainable with MALDI-IMS instruments are now at ~20 μm , although currently, values of 50-250 μm are more typical.³¹

MALDI imaging has been applied to a variety of samples including hair strands, latent fingerprints, and plant, human and animal tissue.^{46, 51, 53, 56, 62-64} In most cases, the most critical aspect of the MALDI-MS experiment is sample preparation which, in addition to matrix

application, may have special sample dependent requirements.^{49, 65} For example, in the case of detecting arginine in plant seeds, there was careful consideration given to the matrix used in order to prevent adverse effects on the tissue.⁵⁶ In the case of tissue analysis, cross-sections often have to be flash frozen and sliced with a cryostat.^{46, 51} Furthermore, samples need to be completely flat in order to achieve uniform matrix deposition and sampling.

Surface-assisted LDI (SALDI)-IMS

Unlike MALDI-MS, SALDI-MS does not use a small organic molecule matrix. In its place, an “active surface” is utilized to assist in the ionization of the molecules of interest.⁶⁰ Derivatives of SALDI-MS that include nanoparticle-assisted LDI (*nano*-PALDI) and silver-nanoparticle (AgNP)-assisted LDI, employ nanoparticles as the active surface.⁶⁰ The nanoparticles can be comprised of silver, gold, silicon or other metal oxides.⁵⁵ Although the nanoparticles assist in the ionization of the molecules within the samples, the mechanism by which this occurs is not well understood.⁶⁰ The use of inorganic materials, instead of a small organic molecule, eliminates the low molecular weight interferences that occur with the utilization of MALDI-MS.⁶⁰

In *nano*-PALDI experiments, the nanoparticles must first be prepared.⁵⁵ The development of nanoparticles for application to the surface of the sample requires many steps that vary depending on the nanoparticles used.⁵⁵ Once prepared, they must be applied to the sample surface. In this regard, SALDI-MS is similar to MALDI-MS.⁵⁵ However, since the nanoparticles are already of a fixed size and shape, the spatial resolution is less affected than in MALDI-MS experiments in which the resolution is dependent on the size of the matrix crystals formed.⁶⁰

Since SALDI-MS does not require a small molecule be used as the matrix, the detection and mapping of small molecules is not typically hindered.

Secondary ion mass spectrometry (SIMS)

SIMS is a mass spectrometric technique that utilizes the collision of energetic primary ions on a sample's surface to create secondary ions.⁶⁶ A major advantage of this approach is that nanometer level spatial resolution can routinely be achieved.^{32, 47, 67} It can also be used to observe both organic and inorganic ions. In imaging SIMS, the primary ion beam is rastered across the surface of the sample to create a 2D image based on its constituents.⁶⁶ SIMS is not a soft ionization technique and it induces significant fragmentation. However, with the development of new ion beams, it has been successfully applied to the imaging of small molecules. Applications have included determination of alterations made to artwork,⁵⁴ mapping of exogenous and endogenous compounds in latent fingerprints,^{63, 68} and detection of dyes in hair samples.⁴⁴

1.2.2. Ambient ionization imaging instrumentation

Use of high-vacuum techniques can preclude the ability to detect volatile small molecules, as they can evaporate or sublime under these conditions. Additionally, some sample types are not amenable to sampling by high-vacuum approaches, such as living tissues, or porous samples that may require prolonged instrument depressurization time. In response to these difficulties,

ambient ionization imaging techniques were developed more recently.⁵² These approaches permit the analysis of living tissues and other samples that are not as readily analyzed by high-vacuum methods.⁵² Some of these approaches are described below.

Desorption electrospray ionization (DESI)-IMS

DESI-MS is an ambient and soft ionization technique that utilizes an electrospray emitter to cause charging of solvent droplets as they are sprayed from the source.¹¹ The charged droplets then come into contact with the sample to be ionized. Analytes are desorbed into the charged solvent droplets deposited onto the surface.¹¹ As more solvent is sprayed onto the surface, it collides with the solvent containing the desorbed analytes to create secondary ion droplets which are then forced into the mass spectrometer inlet.¹¹ Like MALDI-MS, DESI-MS is a soft ionization technique that causes little to no fragmentation of the molecules within the sample. A variety of solvents can be used to form the electrospray that desorbs analytes from the sample's surface.

In imaging DESI-MS, the solvent spray is directed at the sample's surface as it is scanned beneath the ion source.⁴⁵ The technique usually achieves a spatial resolution of ~100-200 μm .⁵² DESI-MS requires that the geometry and orientation of the ion source and the mass spectrometer inlet be exact in order to allow ions to reach the inlet successfully. This geometry must be maintained throughout the movement of the sample stage during imaging. The DESI-IMS method has also been used for indirect sampling, as was done for the imaging of the anti-cancer alkaloid rohitukine in *Dysoxylum binectariferum* seeds during their development.⁵⁰ Instead of sampling the seeds directly, cross-sections were hand pressed against TLC plates to acquire an imprint of

the compounds within the seed. A spatial resolution of $250 \times 250 \mu\text{m}^2$ was attained in these experiments.⁵⁰ DESI-MS imaging can be accomplished with few sample pre-treatment steps, although the choice in solvent can limit the range of ions detected in an untargeted analysis. The advantage of using solvent for targeted applications is the potential to optimize solvent selection for the particular analyte of interest. The spatial distribution maps of chlorogenic acids in a coffee bean were observed using imaging DESI-MS with a spatial resolution of $100 \mu\text{m}$.⁴⁸ Although the coffee bean samples used in these experiments were sliced using a microtome, the sample surface was not uniform.⁴⁸ This caused irregular sampling of ions, leading to variations in ion intensities across an image.⁴⁸ This was also observed in the analysis of grapevine stems; the variations to the surface of the sample distorted the ion images compared to those obtained by MALDI-IMS.⁶⁹

nano-DESI-IMS

To improve upon the poor spatial resolution observed in typical DESI-IMS experiments, *nano-DESI-IMS* was developed.⁷⁰ The principle of the technique is the same, with improvements being made to the probes used to emit the spray of solvent to the surface of the sample. In *nano-DESI-IMS* experiments, the probes are much narrower and are placed directly above the sample. One probe is used to introduce a solvent droplet to the sample's surface, and a second is used to absorb the droplet containing the desorbed analytes and transfer the solvent to the mass spectrometer's inlet.⁷⁰ This results in improved spatial resolutions, averaging $50\text{-}100 \mu\text{m}$.^{52, 70}

Desorption electro-flow focusing ionization (DEFFI)-IMS

DEFFI-MS was developed as an improvement to DESI-MS and works in a similar manner. First characterized and described by Forbes et al. in 2013,⁷¹ DEFFI-MS has shown improved signal-to-noise ratios in both positive and negative ion mode for detection of narcotics and explosives when compared to DESI-MS.⁷¹ The approach involves the use of a carrier gas to focus the flow of the liquid emanating from a small capillary to produce a steady stream of fluid.⁷¹ This flow of liquid is charged by an electric field which produces a high-velocity spray of droplets that interact with the surface of the sample.⁷¹ The development of DEFFI-MS has resulted in an ion source with improved signal compared to DESI-MS and also requires less gas pressure and lower applied potentials, leading to other possible benefits.⁷¹ Imaging experiments can also be performed while maintaining the correct positioning of the ion source in relation to the moving stage and have been applied to mapping of the spatial distributions of explosives and narcotics in artificial fingerprints.³⁶⁻³⁷

Laser ablation electrospray ionization (LAESI)-IMS

LAESI-MS is an example of laser ablation being coupled to a soft ionization source used for post-ablation ionization. In LAESI-MS experiments, the laser is used to ablate small areas that are on the surface of the sample, followed by ionization using an ESI source.⁴¹ In this regard, the laser ablation aspect is only used to supply the spatial distribution information by indicating the discrete areas of the sample surface that were interrogated. Typically, the laser utilized operates in the mid-IR range⁴¹ and it can be limited in its ability to ablate hard surfaces. However, LAESI is

particularly useful in the analysis of biological tissues because their high water content permits absorption of the laser energy resulting in ablation of analytes.^{38, 40-42} This approach can result in multiply charged ions, permitting the analysis of large biomolecules.³⁴ Typical spatial resolutions are limited by the size of the laser beam, and range from 300-350 μm .^{34, 40}

Laser desorption low-temperature plasma (LD-LTP)-IMS

One of the most recent developments in the area of ambient ionization IMS is a technique known as LD-LTP-MS.³⁹ Similar to LAESI, the approach involves a two-step process with ionization occurring after a laser is used for ablation. In this case, a continuous wave UV laser was coupled to a LTP ion source for detection of metabolites in different plant tissues including cacti and seeds.³⁹ The use of a UV laser provides more energy at the surface of a sample than an IR laser can permit. Additionally, UV light can be absorbed by a broader range of plant metabolites and pigments, whereas IR lasers are limited to samples that contain a high water content for the vaporization of molecules in the matrix.³⁹ A spatial resolution range of 50-300 μm was reported.³⁹

1.3. Statement of the Problem

Although a number of recent advancements have been reported for the application of IMS techniques to the detection of small molecules, each of the aforementioned approaches presents challenges, particularly when it comes to the routine analysis of small molecules in complex matrices. The requirement of operating under high vacuum can preclude the ability to

map the spatial distributions of some volatile small molecules. Additionally, it can cause evaporation of the matrix over the long analysis times of MALDI-MS imaging experiments, resulting in gradually reduced ionization and a correspondingly reduced signal over the course of the analysis. Another challenge associated with high-vacuum techniques is their inability to image some sample types because of their physical properties. For example, wood and other plant materials like seeds can be quite porous. Hard, porous samples may crack under high-vacuum conditions, and often require hours of depressurization time to reach the requisite operating parameters while the sample chamber is evacuated. In addition to its operation under high-vacuum conditions, SIMS induces fragmentation of the analytes detected and is thus better suited for the analysis of large biomolecules. Since this technique induces extensive fragmentation, the detection of small molecules and interpretation of the experimental results can be complicated by the difficulty in distinguishing between the sources of fragment ions.

Techniques that incorporate ESI, such as DESI-IMS and LAESI-IMS, have limitations associated with the requirement to use a solvent. Depending on the solvent used for the desorption of ions, the range of the molecules detected will be limited based on their polarity and compatibility with the solvent chosen for the experiment. Also, the requirement in DESI-IMS for solvent to be applied to the surface of the sample can result in surface wetting, which can distort the spatial distributions of the molecules present in the sample.⁷²

To circumvent some of these challenges, we propose to develop a new ambient ionization IMS technique to permit the types of analyses that are difficult or impossible to conduct by the techniques currently commercially available. Possible applications include mapping small molecules in biosynthetic cascades to help elucidate the steps and potential trafficking of

molecules in different tissue areas, determining the outer boundaries of diseased biological tissues by distinguishing between healthy and unhealthy areas based on their small molecule profiles, and mapping the distribution of banned pesticides or herbicides in crops, among many other uses. Our goal is to develop a technique that permits the analysis of such samples under ambient conditions. Without the requirement of high vacuum, the approach would permit the detection of small volatile compounds that would otherwise evaporate or sublime. Additionally, the technique would provide a means to investigate, without tedious sample preparation steps, the spatial distributions of small molecules in large and irregularly shaped sample types that remain unamenable to sampling under high-vacuum conditions due to their porosity. These sample types can include woody seeds or wood pieces that are not easily sectioned using a cryostat or microtome and thus are difficult to image. The technique would ideally operate without the use of solvent, thereby permitting untargeted analyses that would result in the detection of a wide range of molecules with varying polarities. The absence of a matrix requirement would allow for the collection of high-resolution images without the prerequisite method development of matrix selection and application, reducing some of the tedious sample pretreatment steps required for typical IMS analyses.

Presented here is the progress that has been made to date in the development of such a system, and the ways in which it was applied to answer important questions of relevance to several sub-disciplines of forensic science. The technique also has applications to food science, plant natural products, environmental chemistry, and other areas. The approach to creating an IMS instrument optimized for the routine detection of the spatial distribution of small molecules was to combine a laser ablation platform and a DART ion source that was interfaced with a high-

resolution mass analyzer. A detailed description of how this was done to create a new technique termed laser ablation direct analysis in real time imaging-mass spectrometry (LADI-MS) is described in Chapter 2. The chapter discusses each component part of the new system and provides an overview of its capabilities and functions. In the subsequent chapters, the application of LADI-MS to a wide variety of sample types including food products, plant seeds, wood tissues, and samples of forensics relevance is illustrated. Specifically, compartmentalization of small molecules related to one another by their involvement in the biosynthetic cascade leading to the synthesis of the clinically relevant drugs atropine and scopolamine in different areas of a *Datura* sp. seed is demonstrated in Chapter 3.⁷³ Chapter 4 shows the advantages of working under ambient conditions by demonstrating the localizations of two potentially carcinogenic volatile molecules in coffee beans before and after roasting, to help inform approaches for their removal.⁷⁴ Chapter 5 focuses on the application of the technique to the determination of the spatial distributions of small biologically active molecules in wood tissue and discusses its potential utility in helping track the illegal trade in endangered timber. Finally, Chapters 6 and 7 show the application of the technique to samples of high forensics relevance, including latent fingerprints,⁷⁵ inks on paper, and fired ammunition.

Our findings establish LADI-MS as a useful new IMS technique optimized for the analysis of small molecules in complex matrices, and which holds promise as a tool that can be directed towards answering questions of import in several disciplines including food chemistry, medicinal chemistry, forensic science, and plant biochemistry.

Chapter 2: Development and Optimization of Laser Ablation Direct Analysis in Real Time Imaging-Mass Spectrometry (LADI-MS)

2.1. Introduction

As described in the previous chapter, recent significant advancements in imaging mass spectrometry (IMS) have provided a means whereby spatial distribution mapping of molecules within plant, animal and human tissues can be accomplished.³¹ In this regard, much of the progress has been made in detecting macromolecules such as proteins, nucleic acids and other polymers, rather than small-molecules. The most well-established methods utilize a MALDI source, although others such as SIMS, DESI, *nano*-DESI, LAESI,⁷⁶ and their derivatives have also been used for IMS. In these approaches, successful experiments usually involve significant and often time-consuming methods development, and this in turn defines the sample types that can be analyzed.⁷⁷

Until recently, the mapping of *small molecule* distributions in biological matrices was not amenable to accomplishment by these methods for a variety of reasons.⁷⁸ Imaging by MALDI was initially challenged by high background contributions from the matrix. In DESI analysis, the size of the charged droplet beam was too large relative to the area analyzed, and the data were poorly resolved. Some of these deficiencies have been overcome through advances in matrix deposition methods, mass analyzer enhancements, and charged droplet beam size reductions, among other developments.⁷⁸ Nevertheless, significant concerns remain, including the continued need for high vacuum (SIMS, MALDI), the requirement of a matrix (MALDI), the need for a solvent (DESI,

LAESI) which can be problematic in cases where the sample is sensitive to surface wetting, the optimization of multiple experimental parameters associated with ion source operation, ion suppression effects, limitations in the dielectric constant range for the compounds detected in a single experiment, and the requirement for sophisticated sample preparation steps such as dehydration, chemical fixation and cryo-sectioning, among others. Even in cases such as matrix-free LDI or SIMS, the significant fragmentation of the analytes that occurs limits their application.^{76, 79}

Given the aforementioned issues, a technique that permits the following abilities would be advantageous and extend the scope of sample types that could be more readily and routinely analyzed: (1) analysis of samples under ambient conditions with minimal to no sample pretreatment or need for solvent; (2) imaging of irregular surfaces; (3) obtaining high spatial resolution; (4) routinely detecting a range of molecules of varying polarities in a single experiment; and (5) ease of setup. In the case of certain types of materials such as plant tissue, the ability of the technique to penetrate barriers such as the cell wall and cuticle or waxy surfaces, as well as to analyze both fresh and dried samples, would also be highly desirable. Furthermore, many mass spectrometric techniques permit the routine detection of organic molecules or metallic species but not necessarily both. Thus, another desirable feature would be the ability to use the same platform to detect both.

In this chapter, we describe combining an ambient ionization direct analysis in real time (DART) source coupled to a high-resolution mass spectrometer (JEOL AccuTOF) with a laser ablation system (NWR213) to create a new technique termed “laser ablation direct analysis in real time imaging-mass spectrometry” (LADI-MS). Some features of the developed system are

demonstrated through the imaging of the small molecules detected in a blow fly wing, and testing of the spot-size limit of detection, the concentration of analyte limit of detection, and laser ablation depth.

2.2. Results

LADI-MS was developed by combining three components: (1) a laser ablation system; (2) an ambient ionization source; and (3) a high-resolution time-of-flight mass spectrometer (HR-TOF-MS) with an atmospheric pressure interface (API). The individual components are described below.

2.2.1. Laser ablation system

The laser ablation system used is an Elemental Scientific Lasers NWR213 unit (ESL, Bozeman, MT) (Figure 2.1) which utilizes a UV 213 nm neodymium-doped yttrium aluminum garnet (Nd:YAG) laser with a maximum repetition rate of 20 Hz. The maximum fluence, or energy density of the laser, is 30 J cm^{-2} . Nd:YAG lasers typically have a wavelength of 1064 nm and must pass through a 2nd, 3rd and 5th harmonic to reach a final wavelength of 213 nm. The laser beam is aperture imaged, using an IVA or XYR device, which permits



Figure 2.1. A photograph of the NWR213 laser ablation system.

ablation craters of both circular and rectangular shapes, respectively. The IVA device will make circular spots from 4 to 110 μm in diameter in 1 μm increments. With the XYR device, rectangles can be made at 1 μm increments with a maximum diagonal of 110 μm , and they can be rotated in 1° increments.

The sample chamber of the ablation system rests upon an x,y-moveable stage which allows the sample to be rastered beneath the stationary laser as it fires at the surface, creating an ablation plume. Although the sample chamber itself has a volume of 800 mL, within the chamber is a small 1 mL volume cup that is suspended directly above the ablated area. This

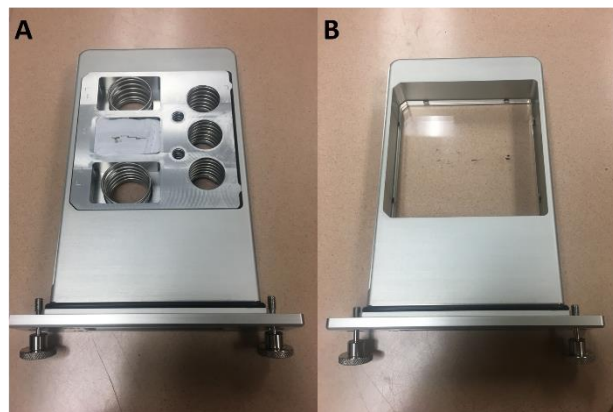


Figure 2.2. Photographs of the NWR213 sample drawer. Panel A shows the sample drawer with an insert that can accommodate SEM stubs or glass slides. Panel B show the drawer with a plexiglass insert that can accommodate samples of irregular shape and thickness.

provides a smaller volume within which the created ablation plume is contained. The unique sample drawer can accommodate samples of up to 10 cm in length and width, and up to 2 cm in depth, permitting the analysis of irregularly shaped and large samples. Figure 2.2 shows the sample drawer with an insert for analysis of scanning electron microscopy (SEM) stubs or glass slides (Panel A) and with a plexiglass plate for samples of irregular shape (Panel B).

Laser parameters

The laser ablation system parameters that can be varied include the laser fluence, laser frequency, spot size and shape, helium flow rate, scan speed, and warm-up and washout delay times. All laser parameters can be set using the ActiveView software that accompanies the system and can be changed to accommodate variations in the MS signal strength and sample type. Each of these is described below.

Laser frequency

The maximum laser frequency for the NWR213 laser ablation system is 20 Hz. All of the samples imaged required the maximum frequency. This allowed the laser to fire as rapidly as possible as the sample was rastered beneath it.

Fluence

The maximum laser fluence, or energy density, is 30 J cm^{-2} . This parameter must be varied as a function of sample type. Fragile tissues require a lower fluence in order to prevent destruction of areas that extend beyond the specified spot size. Other samples require a higher fluence in order to permeate the sample surface and obtain an optimal MS signal. This was especially true for detection of inorganic species.

Laser spot size

The laser spot shape can be set to square or circular, and the spot size can be varied from $4\text{-}250 \mu\text{m}^2$ or $110 \mu\text{m}$ in diameter. This setting plays a crucial role in the calculation of the spatial resolution of an experiment. Although smaller spot sizes result in higher spatial resolution, larger

spot sizes provide higher MS signal, because of the greater volume of ablated sample that reaches the mass analyzer.

Laser scan speed

Along with spot size, the scan speed is used to define the amount of sample to be ablated, which is a function of how long the laser is held on one area before moving to the next position along the line scan (described below). The scan speed must be optimized so that the laser does not remain at the same spot for too long, causing oversampling of one area on the one hand, or move too quickly to the next spot, preventing sufficient ablation on the other.

Line scans

The laser ablation system is equipped with an integrated ActiveView software-controlled microscope by which the surface being ablated can be viewed. The width of the line scans is determined by the spot size, as each horizontal line is created through the firing of a series of successive square- or circle-shaped laser beams as the sample is rastered. When the line scans are created with no overlap between them, there is a gap that appears between the line scans where no data was collected. This appears as a white line in the resulting ion images. It was determined that by overlapping the line scans by 5-15 μm , this gap can be eliminated.

Helium flow rate

The flow rate of helium into the sample chamber can be varied from 0-1 L min^{-1} . The rate is modified from sample to sample in order to attain the best signal, although it usually remains in the range of 500-700 mL min^{-1} . When a glass tee (discussed below) is used in the open-air gap

between the ion source and MS inlet, the helium flow rate required is significantly lower than without it.

Warm-up and washout delays

At the beginning of each line scan the laser takes 5-10 s to warm-up to the desired user defined fluence. This warm-up delay can be longer if the laser does not reach the set fluence within the specified time frame, which can occur when operating at higher fluences. At the end of each line scan, the laser turns off and does not move to the next line for another few s. This time frame is known as a “washout delay”, and it prevents carry over of ions from one line scan to the next. The time it takes for an ablation plume to be cleared from the sample chamber (as defined by the manufacturer) is 0.7 s. Thus, the washout delay time set by the user is arbitrary, as it far exceeds the time needed to evacuate the ablation plume from the sample chamber.

2.2.2. Ambient ionization mass spectrometry approach

The ambient ionization mass spectrometry technique utilized here is DART-HRMS, and involves the coupling of an ambient ionization DART source to a high-resolution TOF mass spectrometer. The individual components are discussed in more detail below.

Ion source

The ionization source utilized is a DART-standardized voltage and pressure (SVP) ion source, pictured as the blue cylinder in Figure 2.3. Typical DART-HRMS analyses are completed

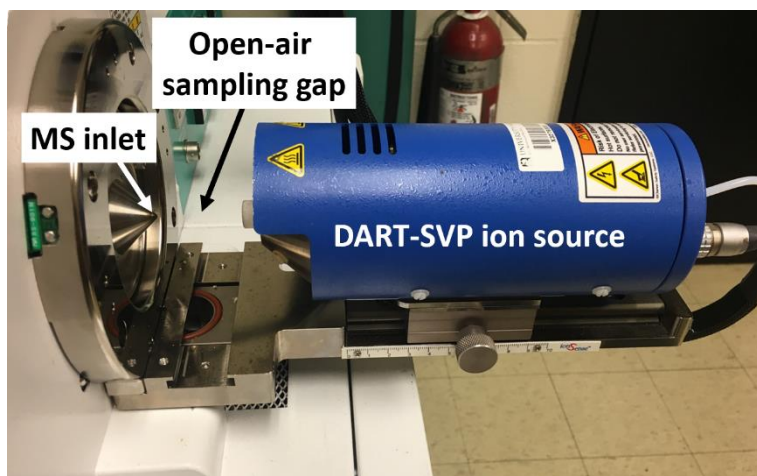


Figure 2.3. A photograph of the DART-SVP ion source, which is contained within the blue cylinder. The MS inlet is shown at the left of the image. The space between the ion source and MS inlet is the open-air sampling gap.

by suspending the sample in the open-air gap between the ion source and MS inlet. The DART ion source operates in positive and negative ion modes thus permitting the detection of a number of different classes of molecules, and can be operated with helium, nitrogen, or argon

gases, each resulting in different ionization mechanisms. A detailed description of its component parts and the mechanisms of ionization is provided by Cody, Laramée, and Durst.⁹ Briefly, in the case of positive mode helium DART, which is used most frequently, the flow of metastable helium exiting the ion source will interact with and ionize the sample plume via proton transfer from protonated water clusters (described in Chapter 1).

High-resolution time-of-flight mass spectrometer

The high-resolution mass spectrometer used in all experiments was either a JEOL AccuTOF LC-plus JMS-T100LP HRMS, or a JEOL AccuTOF-LP 4G HRMS (JEOL USA, Inc., Peabody, MA, USA). The TOF mass analyzer, depicted in Figure 2.4, is comprised of an API, ion guide, mass analyzer, and detector.⁸⁰

Atmospheric pressure interface (API)

The ions generated by the ion source are directed into the mass spectrometer by way of an API with ion transport guide and focusing lenses. There are two off-axis skimmers, or orifices, with a ring lens between them leading to the ion guide, as depicted in Figure 2.4.⁸⁰ The orifices are misaligned intentionally to allow the neutral particles and droplets to be diverted from

entering the ion guide, thereby permitting only the charged ions. The voltages of the two orifices and ring lens can be changed to function under soft conditions (orifice 1 at 20 V) or conditions that induce fragmentation (e.g. orifice 1 at 90 V).

Ion guide

The high frequency ion guide is a quadrupole and is represented by the two bent horizontal lines in the ion transport section of Figure 2.4.⁸⁰ The quadrupole is used to focus the ions entering orifice 2 to the central axis for transportation to the TOF analyzer. It is evacuated by a single split flow turbo molecular pump (TMP). The TMP allows for successive pumping for transport from the high-pressure region to the TOF high-vacuum region.⁸⁰ High frequency and DC voltages are applied to all electrodes of the quadrupole for focusing of the ions. The ions pass through another orifice after which a focusing lens, represented by the six rectangles within the

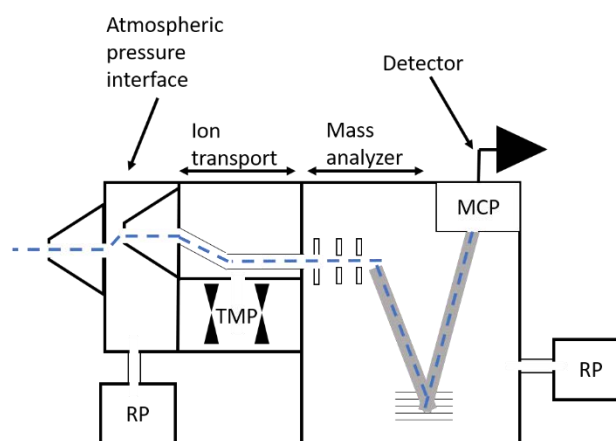


Figure 2.4. A schematic diagram of the AccuTOF-mass spectrometer that is utilized in LADI-MS. The system is comprised of an atmospheric pressure interface, ion transport, mass analyzer, and detector.⁸⁰

mass analyzer section of Figure 2.4,⁸⁰ directs the ion beam into the orthogonal-extraction reflectron time-of-flight mass analyzer.

Analyzer

The mass spectrometer incorporates a single stage reflectron mass analyzer flight tube with a vacuum system. The orthogonal ion extraction allows for efficient analysis of a continuous ion beam. The TOF-MS uses a 2-stage acceleration and single-stage reflectron (five horizontal lines in the mass analyzer section of Figure 2.4). The advantages of using a reflectron TOF mass spectrometer are its ability to collect spectra rapidly with good peak definition, high resolving power with accurate mass determinations, and good sensitivity which is important for imaging experiments. The resolving power of the two mass spectrometers utilized in the applications described in the subsequent chapters are 6,000 and 10,000 (FWHM definition) with accurate mass determinations within 5 mmu.

Detector

The detector is comprised of a “Chevron” dual-microchannel plate (MCP) and an anode.⁸⁰ The “Chevron” dual-MCP is comprised of two MCPs arranged in the shape of a V.

2.2.3. Integration of the laser ablation and DART-HRMS platforms

The laser ablation system was coupled to the DART-HRMS by way of a transfer line extending from the NWR213 unit to the open-air sampling gap (Figure 2.3). A diagram depicting the LADI-MS instrumentation is shown in Figure 2.5. The black box represents the sample

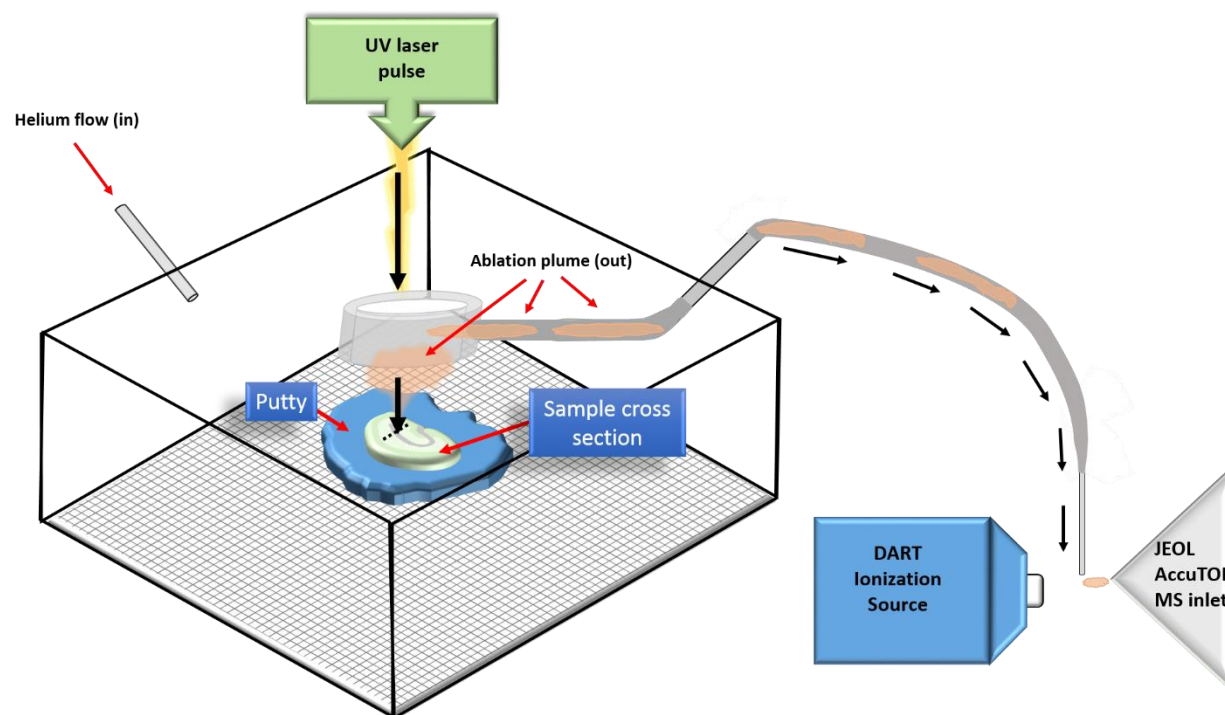


Figure 2.5. LADI mass spectrometry set-up. A sample suspended in silicone putty is placed within the sample chamber of an ESL NWR213 laser imaging platform. The chamber rests on an automated computer-controlled x,y-stage. Rastering the sample at constant speed beneath the laser pulse results in an ablation plume which is transported via helium gas through tubing, and directed to the open air space between the DART ion source and the inlet of the mass spectrometer. Adapted with permission from: Fowble, K. L., Teramoto, K., Cody, R. B., Edwards, D., Guarrera, D., and Musah, R. A. Development of “laser ablation direct analysis in real time imaging” mass spectrometry (LADI-MS): Application to spatial distribution mapping of metabolites along the biosynthetic cascade leading to synthesis of atropine and scopolamine in plant tissue. *Anal Chem.* **89**, 3421-3429 (2017), Copyright 2017 American Chemical Society.⁷³

chamber that rests on the x,y-moveable stage. The stage rasters beneath the UV laser from left to right allowing the laser to ablate the surface of the sample (embedded on silicone putty), from right to left. The ablation plume is contained in the ablation cup after its formation. High-purity helium is constantly flowing into the back of the laser ablation system, indicated by “Helium flow (in)” (in Figure 2.5), and forces the ablation plume, by positive pressure, out of the laser ablation system through the transfer line. The transfer line was comprised of tygon or stainless-steel tubing and could be heated to facilitate transfer of the ablated material to the MS inlet. A photograph of the LADI-MS system set-up with a heated stainless-steel transfer line is shown in

Figure 2.6 Panel A. The transfer line originates at the ablation cup, extends out the right side of the sample chamber (Panel A), and terminates at the open-air gap between the DART ion source and MS inlet (Panel B). A glass tee can be utilized at the DART-MS interface to help direct the flow of the ablation plume from the transfer line to the MS inlet after ionization by the DART ion source. An image of the interface between the transfer line, DART ion source, and MS inlet is shown in Figure 2.6 Panel B.

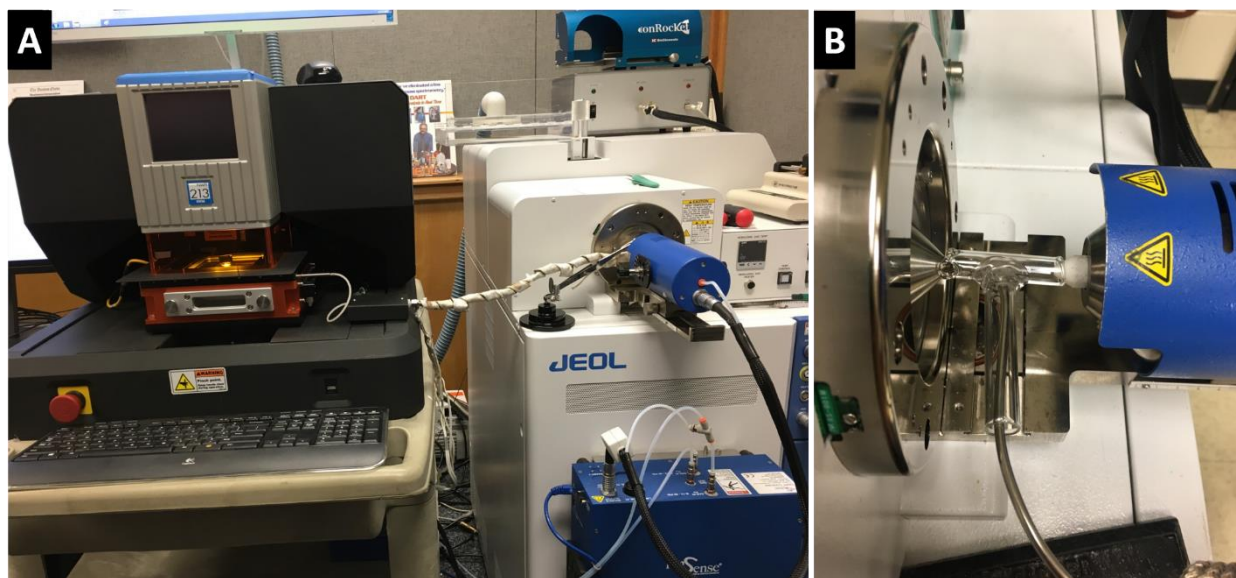


Figure 2.6. The LADI-MS system and the interface at the DART-MS sampling gap. In Panel A, a photograph of the laser ablation system (left) connected to the DART-HRMS (right) by a heated stainless-steel transfer line is shown. The transfer line originates from the right side of the laser and ends at the glass-tee (Panel B) between the ion source and MS inlet.

During an imaging experiment, the laser beam is stationary as the sample is rastered beneath, causing ablation of the surface of the sample. The depth of ablation can vary depending on the sample type being analyzed and the fluence of the laser. Harder surfaces such as metals, will have a shallower ablation depth than samples such as animal or plant tissues. Since LADI-MS utilizes DART-HRMS, the experiments are completed under ambient conditions with no need for high-vacuum, solvent, matrix, or tedious sample preparation steps.

2.2.4. Proof-of-principle imaging experiment-Blow fly wing

To determine if the coupling of an ambient ionization mass spectrometry technique (DART-HRMS) to a laser ablation imaging system (NWR213) would permit the detection and mapping of small molecule spatial distributions in different sample types, a proof-of-concept imaging experiment was completed. The sample used was that of a blow fly wing (Family: Calliphoridae), which was placed within the sample chamber after being affixed to double-sided adhesive carbon tape. The entire surface of the fly wing was ablated by the NWR213 unit, while coupled to a DART-HRMS instrument. During the experiment, the MS signal was monitored in real time, and the appearance of the signal confirmed that ions derived from the blow fly wing were being detected. A representative mass spectrum obtained from this experiment is displayed in Figure 2.7 Panel A. It features prominent peaks at nominal m/z 194 and m/z 371, and a peak of lower intensity at m/z 204. The ion at m/z 371 corresponds to a plasticizer that originated from the tygon tubing and/or capillary used in the open-air sampling gap. The compositions of the compounds detected at m/z values 194.0771 and 204.0872 are unknown, but m/z 204.0872 could correspond to protonated *N*-acetylglucosamine- H_2O , which is a monomer unit of chitin, an important polymeric component of blow fly wings.⁸¹ The ability to observe a mass spectrum indicated that it might be possible to map the spatial distributions of detected ions in the entire wing. To obtain information about possible localization of ions of interest in the blow fly wing, the following data processing steps were performed.

Data processing for imaging analyses

At the conclusion of an imaging analysis, the NWR213 laser ablation system produces an excel file that contains pertinent experimental information including a log of laser on/off times that are correlated to laser fluence and position. This information is coupled to the mass spectrometer's output files. Reconstructed ion currents (RICs) are created for each of the ions of interest in TssPro 3.0, TssUnity, or msAxel data processing software. These RICs are then exported to excel files. The headings of the exported files are modified to correspond to the Agilent file

format. Specifically, the scan numbers are removed and the time labels are converted from min to s. The updated excel files are then imported into lolite imaging software.

This software permits the coupling of the data file from the mass spectrometer to the text file created by the NWR213 based on the time stamps, to create ion images for each of the analytes. The lolite software creates the ion images based on the raw counts of each selected analyte. In Figure 2.7, the ion

images for the m/z values 204.0872 and 194.0771 are shown in Panels B and C, respectively. The relative intensities of the analytes are represented visually by the

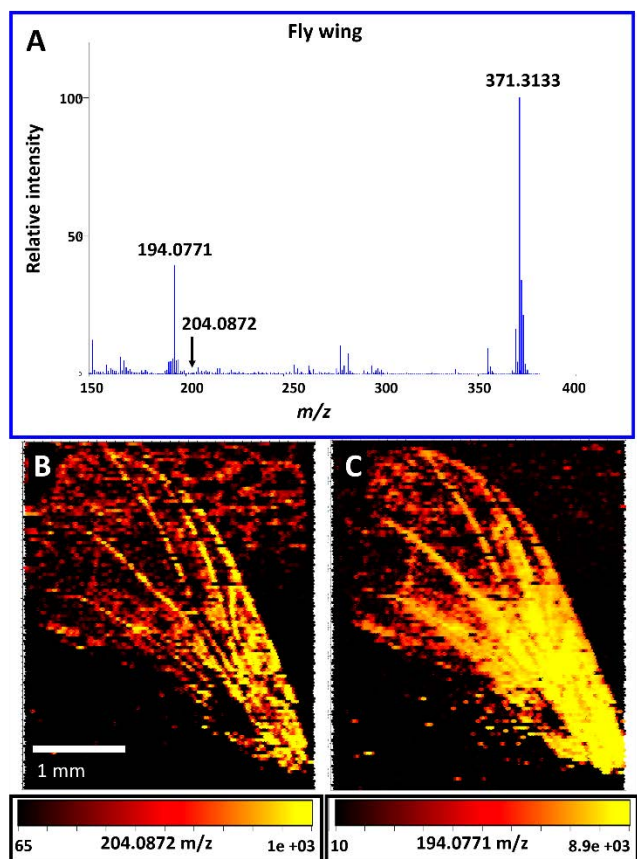


Figure 2.7. A LADI-MS-derived mass spectrum (Panel A) and ion images of a blow fly wing. In Panels B and C, the ion images of two unknown compounds (m/z 204 and m/z 194, respectively) detected within a blow fly wing are shown. The compounds are confined mainly to the veins of the fly wing.

variations in the color in these images. In the color scheme used here, yellow indicates a very high intensity and black a very low or zero intensity. Both ions mapped in Figure 2.7 are localized with high intensity in the veins of the fly wing. This experiment in particular shows the potential use of the technique for analysis of delicate tissue types.

2.2.5. System assessment

The successful detection and imaging of the spatial distributions of compounds localized to the veins in a blow fly wing (Figure 2.7) established that LADI-MS could be utilized as an IMS technique optimized for the detection of small molecules. The proof-of-concept experiment demonstrated that the imaging of small molecules in a complex matrix could be accomplished without many of the challenges associated with other IMS techniques (discussed in Chapter 1), and their required sample preparation steps, including the application of a matrix, solvent or use of high-vacuum conditions. To further investigate the scope and capabilities of the LADI-MS technique, such as analyte sensitivity, spot size limit of detection, and ablation depth, a number of additional experiments were performed.

Spot size signal testing

To investigate the limit of detection associated with a representative laser spot size, a series of line scans were acquired across the surface of a 5 μL deposit of 1000 ppm quinine in methanol on chromatography paper. The corresponding extracted RICs are shown in Figure 2.8.

The first RIC (Panel A) covers circular spot sizes with diameters of 110, 100, 90, 80, 70, 60, 50, 40, and 30 μm . Panel B includes the laser spot sizes, 50, 20, 10, 5, and 4 μm . The quinine spot was ablated twice at the 4 μm spot size. Panel C shows the RIC resulting from ablation with the following spot sizes: 30, 25, 20, 15, 10, and 5 μm . The results show that for all laser spot sizes, quinine was readily observed, and that detection occurs at spot sizes as low as 4 μm , the smallest spot size achievable with the NWR213 system.

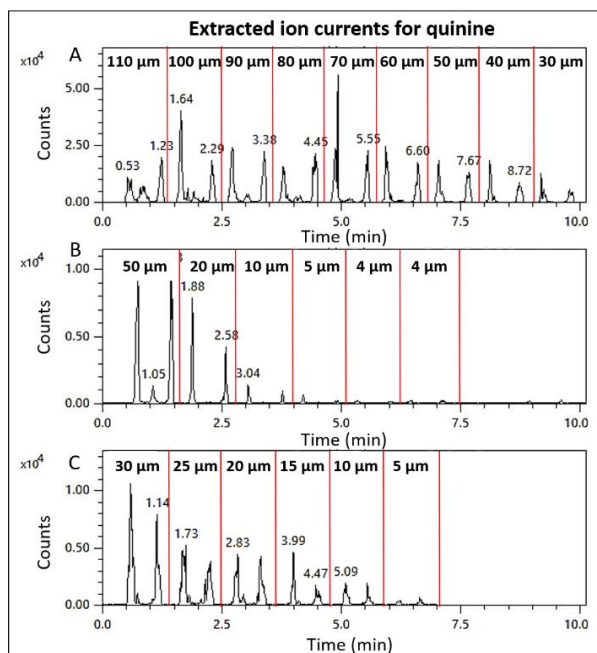


Figure 2.8. The RICs for quinine showing the counts detected for each spot size used to ablate one line scan. Panel A is comprised of spot sizes ranging from 110-30 μm ; Panel B covers spot sizes of 50, 20, 10, 5 and 4 μm ; and Panel C is comprised of spot sizes from 30-5 μm .

Sensitivity testing

A preliminary assessment of the sensitivity of the LADI-MS technique was conducted using 5 μL aliquots of varying concentrations of quinine in methanol that were deposited on chromatography paper. Ablation in the form of a single line scan, at a laser spot size of 110 μm , was performed on samples representing each of the concentrations used (i.e. 100 ppb, 1 ppm, 10 ppm, 100 ppm, and 1000 pm) to determine the limit of detection of quinine. A plot of the integrated peak areas of the RICs for each concentration versus the concentration in each case revealed a linear relationship between the two (Figure 2.9). Quinine remained detectable at the 100 ppb level.

Laser ablation depth testing

Although the laser ablation depth will vary greatly depending on the attributes of the substrate and the laser fluence used, it would be beneficial to know the ablation depth on a standard substrate. To assess the

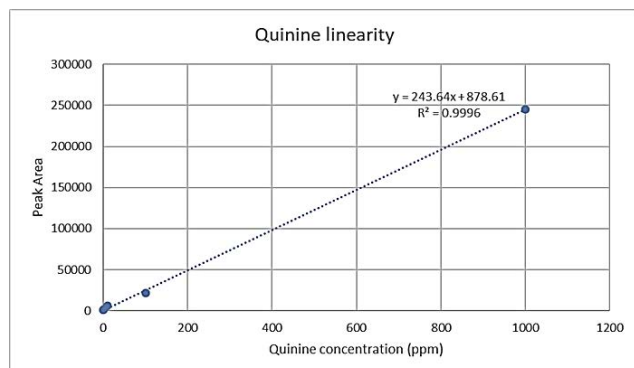


Figure 2.9. A plot featuring the concentration of quinine vs the integrated peak area from the RIC of quinine. The calculated R^2 value is 0.9996.

ablation depth on a hard surface, a thin sheet of copper alloy 110 (minimum of 99.9% Cu and 0.04% O) was sampled. The laser was set to the highest energy density ($\sim 30 \text{ J cm}^{-2}$) and the frequency reduced to 1 Hz. The laser was fired at the surface for one pulse resulting in a crater. The ablation depth was calculated from the difference in the z-axis focus prior to and following the ablation. The average measured ablation depth at 30 J cm^{-2} was $17.6 \mu\text{m}$. The laser energy was reduced to 50% of its total energy density and the ablation depth was measured again. The average ablation depth at 50% energy fluence was $11.2 \mu\text{m}$.

2.3. Discussion

LADI-MS is the integration of two standalone instruments. The coupling of a laser ablation unit and DART-HRMS permits the acquisition of spatial distribution information (laser ablation) and mass spectral information (DART-HRMS) as demonstrated by the ion images of compounds found in a blow fly wing (Figure 2.7). Furthermore, the analysis is done in open air, so there is no

need to perform sample pre-treatment steps such as cryo-sectioning or sample fixation in various media such as gelatin. No matrix is required because ionization by DART is accomplished using metastable helium. In principle, this approach could be successfully applied to many different disciplines such as medicine, biology, environmental science and forensics. Additionally, because no solvent is required, another advantage is the ability to simultaneously detect small molecules that span a range of polarities.

Although the development of LADI-MS as described here is novel, it is not the first instance of the coupling of a laser to a DART or other plasma ionization source. IMS has also been accomplished under ambient conditions using an IR laser coupled to a DART source.⁸² However, in contrast to the approach described here, the laser was limited in power and wavelength (which reduced the range of compounds detected), the laser spot size was large (thereby limiting resolution), and the samples analyzed did not exhibit differential distribution of analytes. Another IMS ambient ionization method that features a low-temperature plasma probe has been reported, but the spatial resolution that can be achieved is limited by the size of the capillary of the probe.⁸³ Zhang et al.⁸⁴ have demonstrated that a platform comprised of a multiwavelength laser and a DART source, coupled to a mass spectrometer can be used to detect dye and drug samples directly from TLC plates. However, potential imaging capabilities of this system were not presented. Since the development of LADI-MS,⁷³ a similar approach has been published utilizing continuous wave UV LD-LTP-MS for the mapping of the spatial distributions of small molecules in plant tissues.³⁹ In this technique, a UV laser with a wavelength of 405 nm was used to desorb molecules from the surface of plant tissue followed by their ionization using an LTP ion source.³⁹

The interrogation of the LADI-MS system revealed that the approach is capable of detecting MS signal at spot sizes as low as 4 μm (Figure 2.8). Using quinine as the analyte, the counts observed increased as the laser spot size was enlarged. This was expected; as the spot size increases, the ablation plume becomes larger and more sample is transferred from the laser ablation chamber to the DART-HRMS. The RIC peak shape (two strong peaks with a valley between) shown for each spot size in Figure 2.8 is a result of the coffee ring effect which caused the quinine in solution to localize to the outer edge of the deposited 5 μL spot. Although the system can detect quinine at a concentration of 100 ppb in methanol, it is anticipated that detection limits will vary as a function of the analyte. Ionization by DART is heavily reliant on the proton affinities of the compounds found within the sample (as described in Chapter 1), and thus, analytes with high proton affinities are anticipated to yield strong signals relative to those that have low proton affinities, for analyses using the same laser spot size and sample concentrations.

2.4. Conclusions

The development of LADI-MS is described. The system is comprised of a laser ablation unit coupled to a DART-HRMS instrument. The parameters for the laser ablation system were described in detail and include the laser fluence, spot size, frequency, helium flow rate and scan speed. Signal was acquired for quinine in methanol at a spot size as low as 4 μm . The limit of detection for quinine spotted on chromatography paper was 100 ppb, although this will vary depending on the analyte. The system was applied to the imaging of the spatial distributions of small molecules in a fragile tissue type (blow fly wing) demonstrating its utility as an IMS

technique. Numerous other imaging applications of LADI-MS to samples of interest to forensic science and plant chemical ecology will be discussed in subsequent chapters.

2.5. Materials and Methods

2.5.1. Chemicals

Quinine and Whatman™ brand chromatography paper (Cat. No. 3001-851) were purchased from Sigma Aldrich (St. Louis, MO). High-purity helium and nitrogen gases were purchased from Airgas (Albany, NY) or Matheson (Manchester, NH). A thin sheet (~ 2mm) of copper alloy 110 (minimum of 99.9% Cu and 0.04% O) was provided by the University at Albany machine shop (Albany, NY).

2.5.2. LADI-MS set-up

An ESL NWR213 computer-controlled solid state laser ablation system (Elemental Scientific Lasers, Bozeman, MT), which includes a 213 nm Nd:YAG laser with a spot size range of 4-250 μm^2 or 110 μm diameter, and a 10 cm x 10 cm x 2 cm (length x width x depth) high performance TwoVol ablation chamber was used. The high-resolution mass spectrometers coupled to the NWR213 system and used for the imaging of the blow fly wing and system assessment experiments were a JEOL AccuTOF LC-plus JMS-T100LP HRMS (6,000 FWHM) and a JEOL AccuTOF-LP 4G HRMS (10,000 FWHM) (JEOL USA, Inc., Peabody, MA, USA), respectively. In all experiments, the mass spectrometers were coupled to a DART-SVP ion source operated in

positive ion mode. The rate of the DART ion source helium flow was 2.0 L min^{-1} . The mass spectrometer orifice 1 voltage was set to 20 V and the orifice 2 and ring lens voltages were both set to 5 V each.

The samples were placed in the system's airtight 800 mL sample chamber which is mounted on a motorized, computer-controlled x,y-moveable stage. The window of the sample chamber is made of glass with an optical coating to minimize energy loss before the laser beam reaches the surface of the sample. The NWR213 ablation system is equipped with a 1 mL ablation cup into which the ablation plume is directed from the sample chamber. Transport of the plume to the open-air gap between the DART ion source and JEOL AccuTOF mass spectrometer inlet was accomplished using ultra-high purity helium flowing at a constant rate into the sample chamber and out through tygon (blow fly wing imaging) or heated stainless-steel (quinine sensitivity, spot size, and ablation depth testing) tubing positioned at the mass spectrometer inlet (Figure 2.6 Panel B). Polyethylene glycol (PEG) was used as a reference standard for the calibration of the collected spectra. TssPro 3.0 (Shrader Analytical Software Solutions, Grosse Pointe, MI, USA) and the msAxel Data Processing software package (JEOL USA, Inc., Peabody, MA, USA) were used for peak calibration and peak centroiding. Mass spectral analysis, elemental composition determination and isotope analysis were performed using Mass Mountaineer software (Massmountaineer.com, Portsmouth, NH, USA). Creation of ion images from the coupling of MS and laser output data was performed using Lolite imaging software (University of Melbourne, AUS). Equation 2.1 was used to calculate the spatial resolution obtained for a given experiment, where x is the spot size in the x-dimension (μm), a is the scan speed of the sample

chamber ($\mu\text{m s}^{-1}$), b is the MS acquisition rate (s scan^{-1}), and y is the spot size in the y -direction (μm). In Equation 2.1, 0.7 is representative of the sample cell washout time (s).

$$\text{Spatial Resolution} = (x + 0.7a + ab) \times y \quad (\text{Eq. 2.1})$$

2.5.3. LADI-MS analysis of a blow fly wing

A wing was removed from a dehydrated carrion fly of unknown species using tweezers. The wing was placed on double-sided adhesive carbon tape that was affixed to a glass slide for analysis. Tweezers were used to ensure that the fly wing was securely attached. The DART-HRMS and laser parameters utilized for the analysis are listed in Tables 2.1 and 2.2, respectively.

For the creation of ion images (Figure 2.7 Panels B and C), the laser and MS output files were combined in Iolite imaging software. After calibration using TssPro or msAxel software packages, RICs were created for each of the ions of interest. The RICs consist of raw counts for the chosen mass at each scan number in the analysis. This output is then converted to an Excel spreadsheet containing the raw counts for all ions of interest at each s in an experiment. The NWR213 system produces a laser output file that contains the x,y -coordinate information for each s in the experiment. The MS and laser output data are then imported into Iolite software which constructs the ion images based on the shared time scale in both files. The color scale (black to yellow) correlates to the relative intensity (counts) of the indicated ion at any time point (s) or x,y -coordinate. Black or dark red is indicative of a low or zero intensity and yellow is reflective of a high intensity of the given ion.

Sample	Gas heater	Ion guide voltage**	MS acquisition rate
Blow fly wing	350 °C	400 V	0.5 s scan ⁻¹
Spot size test	500 °C	1000 V	0.5 s scan ⁻¹
Sensitivity test	550 °C	1000 V	0.5 s scan ⁻¹

*All analyses were performed in positive ion mode.

**The ion guide voltage is also referred to as the “peaks voltage” of a JMS-T100LP instrument.

Sample	Fluence	Scan speed	Spot size*	Spatial resolution
Blow fly wing	1.5 J cm ⁻²	60 μm s ⁻¹	60 x 60 μm ²	132 x 60 μm ²
Spot size test	3 J cm ⁻²	70 μm s ⁻¹	-	-
Sensitivity test	3 J cm ⁻²	70 μm s ⁻¹	110 μm	-

*The laser ablation system was operated with a square spot shape for the imaging analysis of the blow fly wing. A circular spot shape, with the indicated diameter, was used in the spot size and sensitivity tests.

2.5.4. Spot size signal testing

A 1000 ppm solution of quinine in methanol was created. A 5 μL aliquot of the quinine solution was deposited onto a piece of chromatography paper, represented by the blue circle in Figure 2.10, and allowed to dry in air. The paper was subsequently affixed to double-sided adhesive tape and inserted into the sample chamber for analysis. The laser was used to ablate the chromatography paper in a straight line, depicted by the dashed lines in Figure 2.10, across the deposited quinine spot at the following circular laser spot sizes: 110, 100, 90, 80, 70, 60, 50, 40, 30, 25, 20, 15, 10, 5 and 4 μm in diameter. Ablation of one line scan was performed for each spot size; this was

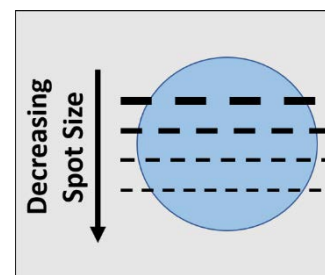


Figure 2.10. A diagram illustrating the spot size testing. A single spot of quinine in methanol was deposited (represented by the blue circle). The laser was then used to ablate line scans (dashed lines) across the deposited spot using decreasing spot sizes.

repeated until all spot sizes were complete. The other laser parameters used are listed in Table 2.2. The DART-HRMS parameters used are listed in Table 2.1. Using the msAxel software package, RICs were created for quinine (Figure 2.8).

2.5.5. Sensitivity testing

Multiple solutions of quinine in methanol were prepared by serial dilutions from a 1000 ppm stock solution. The resulting concentrations were 100 ppb, 1 ppm, 10 ppm, 100 ppm, and 1000 ppm of quinine in methanol. Aliquots of these solutions (5 μ L)

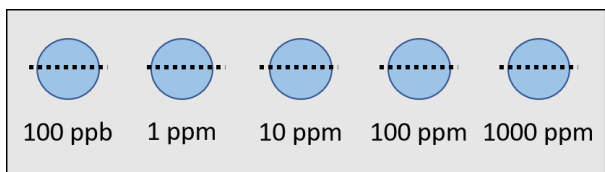


Figure 2.11. A diagram depicting the analysis of 5 μ L spots of varying concentrations of quinine in methanol. The blue circles represent the deposited spots of 100 ppb, 1 ppm, 10 ppm, 100 ppm, and 1000 ppm quinine in methanol. The dashed line represents the single line ablated by the laser across each spot.

were deposited in a row on chromatography paper as shown in Figure 2.11, and allowed to dry in air. The blue circles represent the deposited 5 μ L spots of quinine in methanol. The laser was used to ablate a small line scan, represented by a dashed line in Figure 2.11, at the largest circular laser spot size (110 μ m in diameter), across each of the deposited spots of varying concentrations of quinine in methanol. The DART-HRMS and laser parameters used are listed in Tables 2.1 and 2.2, respectively. Again, RICs were created for quinine using msAxel software. Following the extraction of the quinine ion current, the areas under the “peaks” in the RIC were integrated. The integrated peak areas were then plotted in Excel versus the corresponding concentration of quinine (Figure 2.9).

2.5.6. Ablation depth testing

A thin sheet (~2 mm) of copper alloy 110 was affixed to the plexiglass insert of the sample drawer (Figure 2.2 Panel B) using adhesive tape and then placed within the sample chamber. The laser frequency was reduced to 1 Hz. The laser was fired, with the largest circular spot size (110 μm diameter), at the surface of the copper and the shutter was closed after one laser pulse. The z-axis camera was focused on the surface of the copper sheet before ablation. The z-axis position at this point was recorded. After ablation, the objective lens of the NWR213 unit was focused at the bottom of the ablation crater. The new z-axis position was recorded. The difference between these two positions was calculated and determined to be the ablation depth. The first pulse was completed at a laser fluence of 30 J cm^{-2} and the second occurred at 15 J cm^{-2} . No other laser parameters were required and the DART-HRMS was not utilized in this experiment.

Chapter 3: Application of LADI-MS to Spatial Distribution Mapping of Metabolites Along the Biosynthetic Cascade Leading to Synthesis of Atropine and Scopolamine in Plant Tissue

3.1. Introduction

Many different plants and the molecules synthesized by them have been utilized for centuries for their applications to medicine and/or ceremonial and religious practices.⁸⁵⁻⁸⁹ Whole plants, extracts, and even isolated purified plant-derived compounds are used in herbal, homeopathic and modern medicine, and it is estimated that approximately 50% of drugs approved for medicinal use are derived in part from plants.⁹⁰ Many of these phytochemicals exhibit structures of sufficient enough complexity that they remain challenging to synthesize in lab settings, both in terms of the skills and technology necessary to construct the scaffolds, and the expense required. Because of this, a variety of molecules that are currently utilized in medicine or other areas, are still being extracted from plant tissues.⁸⁹ Two of these molecules are the tropane alkaloids scopolamine and atropine, which have antimuscarinic and anticholinergic effects and are produced by plants within the *Atropa*, *Brugmansia*, *Hyoscyamus*, *Datura* and *Mandragora* genera of the Solanaceae family.^{89, 91-93}

In those instances in which natural products of commercial importance are derived from natural sources such as plants, the methods that are used to track their presence and locations within plant tissues are exceedingly important, as such knowledge can inform the development of isolation protocols, and advancements in understanding of where and how they are

synthesized. While mass spectrometry and various types of chromatography are heavily utilized techniques for the accomplishment of this task, the process of detecting and isolating such compounds remains difficult. Due to the complexity of the plant tissue itself, it is necessary to perform various pre-treatment steps prior to sample analysis. These can include extractions, followed in some cases by solvent and plant oil removal steps, and derivatization for some analytes of interest.⁹⁴⁻⁹⁵ This is particularly true for GC- and LC-MS techniques. In contrast to this, DART-HRMS has been used to detect the biomarkers through direct analysis of bulk plant material without the need for any prior sample preparation.^{18, 22-25, 28} However, for DART-MS and other routinely used techniques, the spatial distribution information that is associated with each of the analytes detected remains inaccessible unless individual tissue sections are analyzed independently so that the locales of molecules of interest can be revealed. The advantage of determining the spatial distributions of molecules, such as those involved in the biosynthetic cascade leading to atropine and scopolamine, is that it could inform decisions on how best to retrieve them from plant material. The spatial distribution information obtained could then reduce the number of isolation and extraction steps required to obtain a purified product.

In principle, the LADI-MS approach described in Chapter 2 would be well-suited for application to determination of the locales of analytes of commercial interest in complex matrices such as plant tissue. To explore this possibility, we applied the technique to determination of the spatial distributions of atropine and scopolamine, and the molecules in the biosynthetic cascade leading to their formation, in seed tissue from *Datura leichhardtii*, which is a member of a genus that is particularly rich in these related alkaloids. The successful analysis, described below, revealed for the very first time, not only the spatial distributions of atropine

and scopolamine, but the localization of other major compounds known to be a part of the biosynthetic cascade leading to their formation.

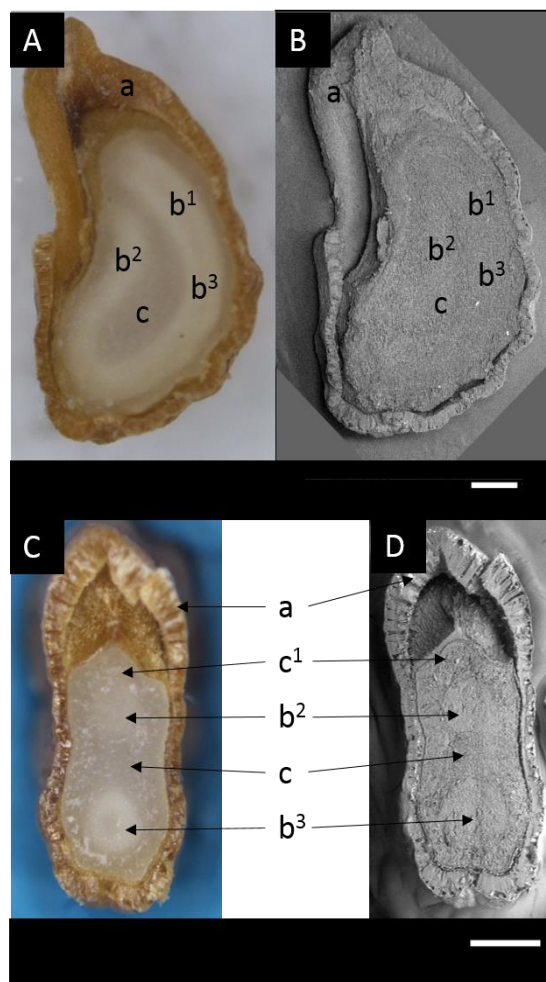
3.2. Results

3.2.1. Microscopy of the imaged tissue

To assist with visualization of the spatial localization of observed masses, light and SEM micrographs of both sagittal and transverse cross-sections of *D. leichhardtii* seeds were obtained. These are presented in Figure 3.1. Panels A and B are light and SEM micrographs of a sagittal cross-section of a *D. leichhardtii* seed, respectively, and Panels C and D feature the light and SEM micrographs of the transverse cross-section of a seed. The mature seed is discoid in shape. The embryo, which is linear, adopts a loop (annular) configuration and is embedded within the endosperm. In Figure 3.1 Panel A, this is illustrated by the light-colored areas labelled b¹-b³. The seed coat (testa), labelled as “a” in Panels A-D, is thickened in the region immediately surrounding the endosperm (an area known as the micropylar endosperm), and there is a cavity between the seed coat and micropylar endosperm. The curvature of the embryo results in the observation of two circles that are apparent in the transverse cross-section (Panels C and D), representing the embryonic root (radical-b²) and the stem between the radical and the cotyledon (i.e. the hypocotyl-b³).⁹⁶ In these representations, the seed is oriented so that the micropylar testa appears at the top. For the LADI-MS analysis, a transverse cross-section of the seed was surveyed.

3.2.2. Tropane alkaloid biosynthesis

One way to appreciate the comprehensiveness of the dataset acquired in our experiments (described below), is through consideration of what is known about the steps in atropine and scopolamine alkaloid biosynthesis in Solanaceae genera such as *Atropa*, *Brugmansia*, *Datura*, *Duboisia*, *Hyoscyamus* and *Mandragora*. It is believed to proceed by a common pathway that begins with arginine or ornithine, and features the steps shown in Figure 3.2. Either compound can serve as the precursor from which putrescine is derived.⁹⁷⁻⁹⁹ Transformation of arginine to putrescine involves the intermediacy of agmatine,⁹⁹ while formation of putrescine from ornithine is direct.⁹⁸ Putrescine is converted to *N*-methylputrescine via the action of putrescine *N*-methyltransferase.¹⁰⁰ The *N*-methylated amine is acted upon by *N*-methylputrescine oxidase which yields 4-methylaminobutanal, an aldehyde that undergoes spontaneous cyclization to form the



a = testa; b¹⁻³ = embryo tissue (b¹ = cotyledon, b² = radical, b³ = hypocotyl); c = endosperm (c¹ = micropylar endosperm)

Figure 3.1. Light (A and C) and scanning electron microscopy (SEM) micrographs (B and D) of *Datura leichhardtii* seeds. Sagittal (top) and transverse (bottom) cross-sections are presented. The scale bar shown in white corresponds to 500 μ m in both cases. Adapted with permission from: Fowble et al. Development of “laser ablation direct analysis in real time imaging” mass spectrometry (LADI-MS): Application to spatial distribution mapping of metabolites along the biosynthetic cascade leading to synthesis of atropine and scopolamine in plant tissue. *Anal Chem.* **89**, 3421-3429 (2017), Copyright 2017 American Chemical Society.⁷³

N-methyl- Δ^1 -pyrrolium cation.¹⁰¹ Complexation of the cation with acetoacetic acid furnishes 4-(1-methyl-2-pyrrolidiny)-3-oxobutanoate,¹⁰² the immediate precursor of both hygrine¹⁰³ and tropinone.^{102, 104} Tropinone then undergoes either tropinone reductase I catalyzed conversion to tropine, or transformation to pseudotropine¹⁰⁵ which serves as the precursor to the polyhydroxylated calystegine¹⁰⁶ alkaloids A3, B1 or B2. Condensation of tropine with phenyllactic

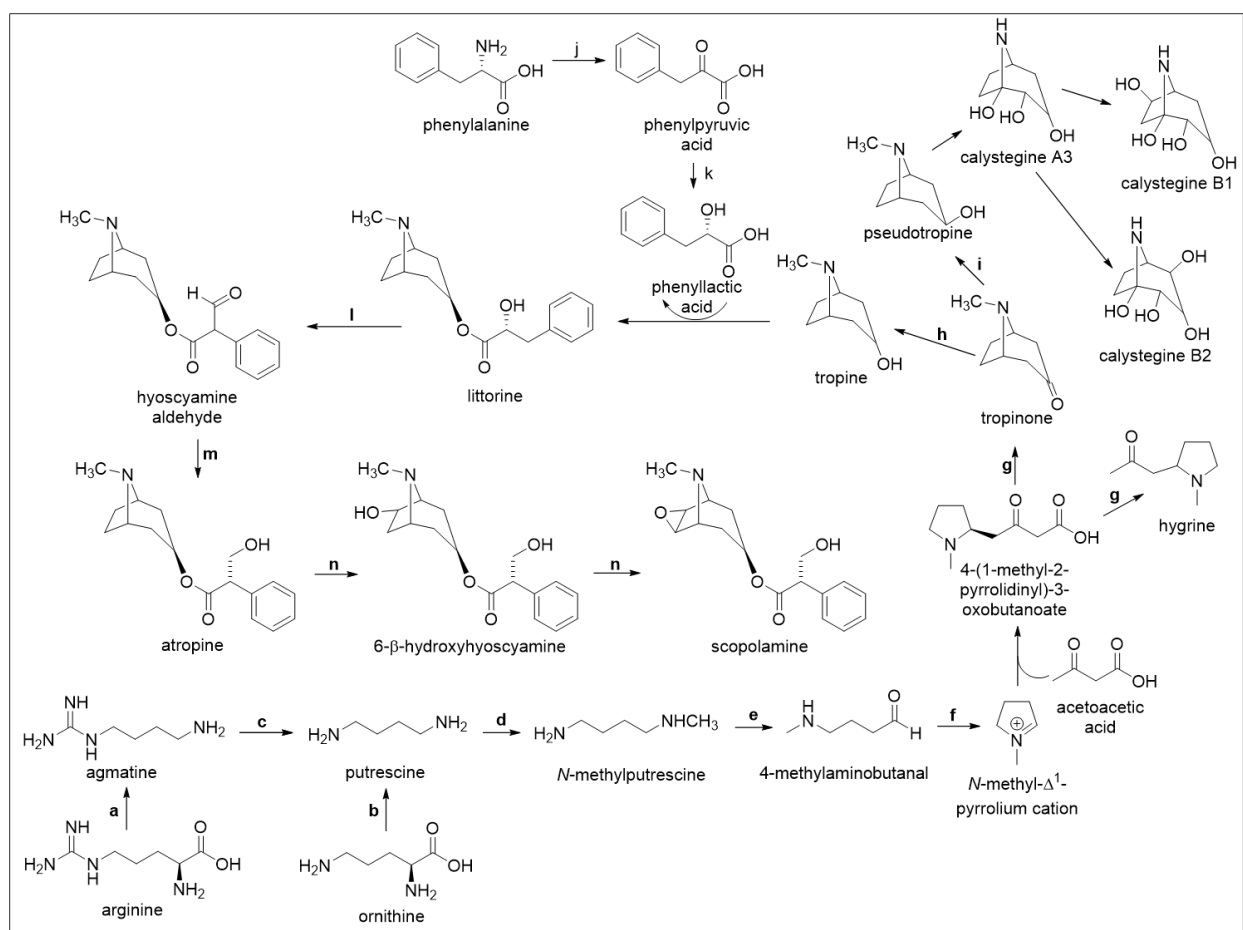


Figure 3.2. Proposed pathway for the biosynthesis of atropine and scopolamine in Solanaceae family plants. The enzymes known to be involved in the various steps are as follows: a = arginine decarboxylase; b = ornithine decarboxylase; c = putrescine *N*-methyltransferase; d = *N*-methylputrescine oxidase; e = tropinone reductase I; f = tropinone reductase II; g = CYP80F1; h = alcohol dehydrogenase; i = 6- β -hydroxylase. Adapted with permission from: Fowble et al. Development of “laser ablation direct analysis in real time imaging” mass spectrometry (LADI-MS): Application to spatial distribution mapping of metabolites along the biosynthetic cascade leading to synthesis of atropine and scopolamine in plant tissue. *Anal Chem.* **89**, 3421-3429 (2017), Copyright 2017 American Chemical Society.⁷³

acid gives littorine.¹⁰⁷ Phenyllactic acid is biosynthesized from phenylalanine via phenylpyruvic acid.¹⁰⁸ Through the action of CYP80F1, littorine is converted into hyoscyamine aldehyde, which serves as the direct precursor of atropine (aka hyoscyamine).¹⁰⁹ Atropine then undergoes hyoscyamine 6- β -hydroxylase-mediated conversion to scopolamine via 6- β -hydroxyhyoscyamine.¹¹⁰

3.2.3. Ion images acquired by LADI-MS

Figure 3.3 shows color overlaid ion images acquired from analysis of a transverse section of a *D. leichhardtii* seed. These thumbnail renderings show the spatial distribution of the specified masses with their assigned molecular identities. They are arranged to emphasize the relationship to one another of the compounds they represent in the proposed biosynthetic cascade leading to the formation of atropine and scopolamine. The dashed line surrounding each image indicates the outer edge of the seed coat, and the 1 mm scale bar shown for arginine applies to all the ion images. The bar shown at the bottom of each ion image is a color spectrum (based on empirical cumulative distribution function) ranging from black or dark red to yellow, indicating a low or zero intensity to a high relative intensity of the indicated ion. As discussed in Chapter 1, the ionization mechanism of DART is heavily reliant on the proton affinities of the analytes and may not necessarily reflect the relative amounts of the detected species. It is for this reason that the ion images shown in Figure 3.3 are not presented using the same color scale, as would usually be done in cases where the relative ion counts reflect the relative amounts of the detected ions. Thus, the color intensity scale for each ion image is independent of the others, and only represents the relative intensity of the indicated ion throughout the seed half.

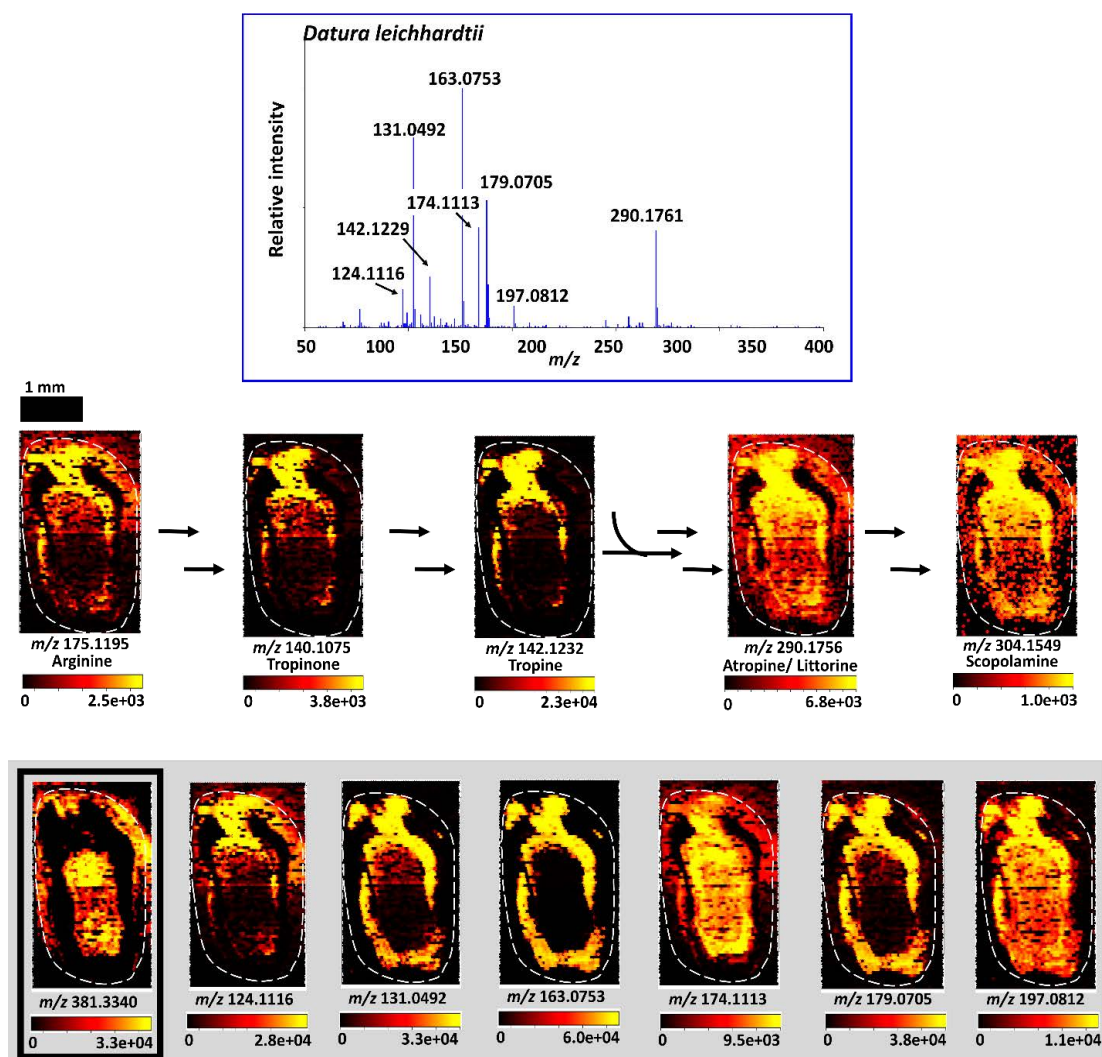


Figure 3.3. Color-overlaid ion images acquired from analysis of a transverse section of a *D. leichhardtii* seed by LADI-MS. The renderings show the spatial distribution of the specified masses. Assignments were confirmed by MS/MS analysis. The images are arranged to emphasize the relationship to one another of the compounds they represent in the biosynthetic cascade leading to the formation of atropine and scopolamine. The dashed line surrounding each image marks the outer edge of the seed coat, and the 1 mm scale bar shown for arginine applies to all the ion images. A typical DART mass spectrum representative of the area dominated by the unknown species (grey panel) is also presented. The mass measurement data for the ions featured are listed in Appendix 1. With the exception of the thumbnail which is enclosed in the black box, the images that appear in the grey-shaded area represent high-intensity masses of unknown identity. That which appears in the box features an ion (nominal m/z 381) which unlike the others featured, is highly concentrated in the embryo, although it is of relatively low intensity. Adapted with permission from: Fowble et al. Development of “laser ablation direct analysis in real time imaging” mass spectrometry (LADI-MS): Application to spatial distribution mapping of metabolites along the biosynthetic cascade leading to synthesis of atropine and scopolamine in plant tissue. *Anal Chem.* **89**, 3421-3429 (2017), Copyright 2017 American Chemical Society.⁷³

The mass spectrum depicted in the inset is representative of the micropylar endosperm, an area dominated by the presence of the ions represented in the grey panel in Figure 3.3. Other areas of the seed, such as the seed coat or embryo, produced spectra whose chemical fingerprint profiles were different from those of the micropylar endosperm (data not shown). The mass measurement data for the ions featured in this study are shown in Appendix 1. With the exception of the thumbnail which is enclosed in the black box (representing nominal m/z 381), the images that appear in the shaded area in Figure 3.3 represent high-intensity masses of unknown identity. That which appears in the box features an ion that is highly concentrated in the embryo, although it is of relatively low intensity. High-resolution masses corresponding to formulas consistent with the presence of protonated atropine, scopolamine and the protonated forms of some of the intermediates so far reported to be involved in their biosynthesis in Solanaceae plants (Figure 3.2) were observed. In some cases, the availability of authentic standards made it possible to confirm the tentative structural assignments by high-energy collision induced dissociation MALDI-MS/MS experiments. These included the precursor arginine, the intermediates tropinone and tropine, and the end products atropine and scopolamine. These data are presented in Appendices 2-7. The ion images for the molecules confirmed to be present showed that they were compartmentalized within the seed tissue. High-resolution masses consistent with the presence of a number of other compounds known to be associated with tropane alkaloid biosynthesis such as *N*-methyl- Δ^1 -pyrrolium cation, acetoacetic acid, 4-(1-methyl-2-pyrrolidinyl)-3-oxobutanoate, hygrine, pseudotropine, calystegines A3, B1, and B2, littorine and hyoscyamine aldehyde were also observed. However, the absence of authentic standards precluded confirmation of their presence by MALDI-MS/MS analysis. High-

resolution masses consistent with ornithine, phenylalanine, phenylpyruvic acid, and phenyllactic acid were also observed. The identities of these masses could not be confirmed however, because their intensities, even when using purified authentic standards with a variety of matrices, were too weak to conduct MADLI-MS/MS experiments. Thus, the ion images shown in the top panel are only of those compounds whose identities were confirmed by MS/MS analysis (Appendices 2-7).

Figure 3.4 utilizes artificially shaded SEM micrographs to provide a color-coded key that highlights the spatial distribution relationships between the observed masses. In these images, darker colors reflect higher levels of the detected masses. Several compounds were distributed throughout the tissue (indicated by red and pink shading in Figure 3.4 Panel A) including in the seed coat, all parts of the endosperm and the visible embryo (i.e. radical and hypocotyl). Among the ions represented were the end product scopolamine (m/z 304.1549) and its precursor atropine (m/z 290.1756). Littorine is a constitutional isomer of atropine. The absence of an analytical standard of littorine precluded definitive determination of its presence. The orange shading in Figure 3.4 Panel B shows the area of the amino acid arginine (m/z 175.1195). Its distribution was similar to that represented in Figure 3.4 Panel A, with the exception that it did not appear in the seed coat area that was proximal to the non-micropylar endosperm. Tropine, the precursor to littorine was more narrowly distributed, appearing as shown by blue shading in Figure 3.4 Panel C. It was concentrated in the micropylar testa, micropylar endosperm, and along the periphery of the endosperm to its midpoint. Tropinone (m/z 140.1075), the precursor of tropine was distributed similarly (Figure 3.4 Panel C).

There were several prominent masses of unknown identity that were also differentially distributed (see mass spectrum in Figure 3.3). These included one which appeared in the endosperm perimeter and the micropylar testa (m/z 163.0753—Figure 3.4 Panel D), some that were localized to the micropylar testa and the endosperm periphery, with small amounts in the radical (m/z 131.0492 and 179.0705—Figure 3.4 Panel E), one that was distributed throughout the endosperm and half of the seed coat (m/z 124.1116—Figure 3.4 Panel F) and one that was distributed throughout the tissue except in testa areas beyond the micropylar region (m/z 197.0812—Figure 3.4 Panel G). The compound represented by mass m/z 174.1113, which has the distribution shown in Figure 3.4 Panel B is also unknown. A mass of unknown identity at m/z 381.3340 was found to be located mostly in the embryo as well as surrounding endosperm and half of the seed coat (Figure 3.4 Panel H).

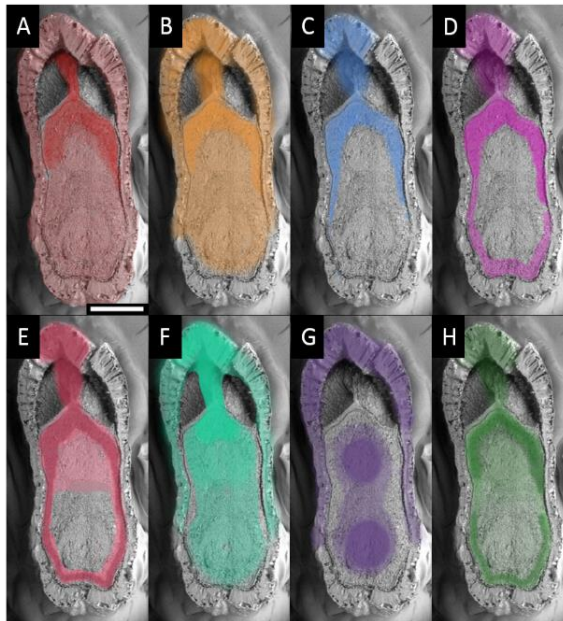


Figure 3.4. Illustration of differential distribution of detected ions as color overlays on the SEM micrograph of the transverse cross-section of the *D. leichhardtii* seed shown in Figure 3.1. The scale bar shown in white represents 500 μm and corresponds to all panels. The shading in each case shows the spatial distribution of various ions, with darker colors indicating greater ion intensity. Panel A: m/z 290.1756 (atropine and/or littorine), m/z 304.1549 (scopolamine); Panel B: m/z 174.1113 (unknown), m/z 175.1195 (arginine); Panel C: m/z 140.1075 (tropinone), m/z 142.1232 (tropine); Panel D: m/z 163.0753 (unknown); Panel E: m/z 131.0492 (unknown), m/z 179.0705 (unknown); Panel F: m/z 124.1116 (unknown); Panel G m/z 381.3340 (unknown); Panel H: m/z 197.0812 (unknown). Adapted with permission from: Fowble et al. Development of “laser ablation direct analysis in real time imaging” mass spectrometry (LADIMS): Application to spatial distribution mapping of metabolites along the biosynthetic cascade leading to synthesis of atropine and scopolamine in plant tissue. *Anal Chem.* **89**, 3421-3429 (2017), Copyright 2017 American Chemical Society.⁷³

3.3. Discussion

MALDI-MS/MS was used to confirm the identities of several of the observed masses. However, this technique was not optimal for the imaging study described here because although several MALDI matrix compounds were evaluated, the ion current from specific target molecules measured by MALDI directly from the seed was too low to obtain high-quality MS/MS data. In addition, it was nearly impossible to consistently obtain thin homogeneous slices from the very hard seeds to permit high-quality imaging with the MALDI system. While it may be possible to overcome these limitations with sufficient effort, we were able to circumvent these and other challenges often encountered with small molecule imaging by conventional IMS approaches, by transporting the ablation plume created by the laser under atmospheric conditions, through tubing to a DART ion source in open air, and directing the ionized sample to the MS inlet. We chose to use MALDI-MS/MS to confirm the presence of the compounds of interest from seed extracts, which were much more conveniently analyzed by this method, and which provided higher analyte concentrations and better spectral quality.

The assignments made for the compounds represented by the observed masses are based not only on the observations presented in this study, but also on the very well-established chemistry associated with tropane alkaloid biosynthesis in plants, including *Datura* species.^{97, 100, 102-104, 109, 111-114} However, the details regarding localization of tropane alkaloid-related compounds in plant tissue is poorly understood. The LADI-MS derived data not only show that compounds with exact masses consistent with those established in the literature to be observed in *Datura* seeds are present, but it also indicates their specific spatial distributions in the seed. In

addition, the MALDI-MS/MS measurements furnished results that were consistent with the assignments for a number of specific compounds in the seeds whose involvement in tropane alkaloid biosynthesis is well-known.

Cell-specific accumulation of alkaloids in plants, a phenomenon proposed to protect tissues from the often cytotoxic effects of these compounds, is a well-known occurrence,^{115,116,113, 117} and compartmentalization of scopolamine, atropine and other related alkaloids in both roots and aerial tissues has been observed.^{118,119} However, visual demonstration of differential tissue distribution of this range of small molecules related by their involvement in a common metabolic cascade in seeds or other plant tissues has not been reported. The intermediates, enzymes and end products in alkaloid synthesis are thought to be translocated within cells as well as between different cell types located in various tissues.¹²⁰ In *Atropa belladonna* and *Hyoscyamus muticus* plants, the enzymes required for the biosynthesis of the alkaloids atropine and scopolamine are located differentially throughout the plant tissue.¹¹⁷ The two enzymes located at the first and last steps of the biosynthetic cascade are found in the plant roots, while intermediate enzymes are located within different cell types. Thus, their alkaloid substrates are accordingly differentially distributed, and some trafficking must occur between tissues and cell types in order for the biosynthetic cascade leading to alkaloid end products to progress. Previous reports have demonstrated that tropane alkaloid biosynthesis occurs in the roots,¹¹⁴ and that the compounds are subsequently translocated to other plant parts in low amounts. Since they appeared in high concentrations in the seeds, they are either transported there during seed development, synthesized within the seed during its development, or perhaps both. Although it has been postulated that the alkaloids have a chemical defense function,^{111,121}

one intriguing possibility is that they are required for seed germination. In support of this hypothesis, it has been observed that during germination of *D. stramonium* seeds, the amounts of atropine and scopolamine decrease immediately after the seeds are moistened with water, and drop to undetectable levels until 4 days after germination, at which point the levels increase dramatically.¹²² Since neither compound was detected in the germination medium, it was suggested that these alkaloids were in some way utilized in metabolic processes related to the growth of the cotyledon. Further studies will be required to investigate this hypothesis.

Within the past five years, a number of reports of MS-based imaging of seeds have appeared. These include spatial mapping of: (1) lipids in *Camelina sativa* embryos,¹²³ rice grains¹²⁴ and cotton seeds;¹²⁵ (2) anthocyanins in black rice grains,¹²⁶ (3) a subset of amino acids and sugars in wheat;¹²⁷ and (4) hordatines in barley.¹²⁸ These studies were accomplished by MALDI- or DESI-MS imaging. In all the MALDI cases, high vacuum was required and prior to analysis the samples had to be subjected to cryosectioning, drying, fixation, embedment in gelatin, carboxymethyl cellulose or polyethylene glycol and/or application of a carefully selected matrix among other techniques. The resolutions varied from 25-300 μm . In all cases, the utilization of a matrix complicated interpretation of the data and the range of compounds that were ionized and detected was limited. A further challenge with the use of a matrix is that IMS images can misrepresent the true distribution of detected compounds when the tissue to which the matrix has been applied is heterogeneous.¹²⁹ Recently, indirect DESI-IMS methods were used to detect atropine and scopolamine in *D. stramonium* leaf tissue,¹³⁰ malabaricone C in *Myristica malabarica* seed,¹³¹ and rohitukline in *Dysoxylum binectariferum* seed.⁵⁰ This was done by creating an imprint of a leaf on a porous surface and scanning the imprint. Although these

analyses were accomplished by an ambient ionization method, the approach contrasts with ours in that: (1) it does not accommodate dry samples because these do not form an imprint; (2) the pixel size for the former was 125-250 μm while that achieved here was 50 μm^2 and could be reduced to 10 μm^2 . Furthermore, our method allowed direct analysis of the tissue and did not require solvent. This enabled detection of a much broader range of compounds, such that the spatial distributions of molecules involved in an entire metabolic cascade could be determined.

3.4. Conclusions

The observed spatial distribution profiles of the analyzed seeds imply the presence of highly refined inter- and intracellular small molecule transport machinery in order to accomplish and retain compartmentalization, as well as traffic substrates to locations where they can react with other partners or serve as precursors to form other molecules. Furthermore, the results hint at the likely locales of the enzymes involved in the biosynthesis of the observed compounds. Of potential practical utility is the identification of tissues in which economically important natural products are concentrated. This information could be exploited for the development of efficient and streamlined isolations protocols that might prove to be more economically viable than current approaches.

3.5. Materials and Methods

3.5.1. Seeds

Fifty *Datura leichhardtii* seeds were purchased from J.L Hudson, Seedsman (La Honda, CA, USA).

3.5.2. Chemicals

High-purity helium was obtained from Airgas (Albany, NY, USA). Phenylpyruvic acid, phenyllactic acid, and ornithine hydrochloride standards were purchased from Krackeler Scientific (Albany, NY, USA). Scopolamine hydrobromide, atropine, tropinone, phenylalanine, arginine and 2,5-dihydroxybenzoic acid (DHB) were purchased from Sigma Aldrich (St. Louis, MO, USA). Tropine was purchased from Alfa Aesar (Tewksbury, MA, USA). Trifluoroacetic acid was purchased from Acros Organics (NJ, USA).

3.5.3. Microscopy

A Nikon stereozoom SMZ800 microscope equipped with a Nikon DS Fi2 microscope camera was used to image the sagittal and transverse cross-sections. Scanning electron microscopy was achieved using a JSM-IT300LV scanning electron microscope (JEOL USA, Peabody, MA, USA). The seed cross-sections were affixed to carbon glue on an SEM sampling block (JEOL USA, Peabody, MA, USA) for imaging.

3.5.4. Sample preparation for MALDI-MS/MS

An aqueous extract was prepared by slicing three *D. leichhardtii* seeds in half using a razor blade and submerging them in 50 μL of distilled water. The mixture was sonicated for 30 min. Solutions of authentic standards at a concentration of 10 mg mL^{-1} were made using 1% trifluoroacetic acid in water:acetonitrile (1:1).

3.5.5. MALDI-MS/MS analysis

A matrix solution comprised of 10 mg mL⁻¹ DHB in acetonitrile and 0.5% trifluoroacetic acid in water (1:1) was used. A mixture of 1 µL of aqueous seed extract in 10 µL of matrix solution was pipetted onto a stainless-steel target plate. The sample was then allowed to dry in air. A JMS-S3000 SpiralTOF (JEOL, Tokyo, Japan) equipped with the TOF/TOF option was used for observation of MALDI mass spectra. Ions generated by irradiation with a 349 nm Nd:YLF laser were accelerated at 20 kV. Mass calibration of the seed extract was carried out by internal calibration using 5 peaks of PEG 200 ([M + Na]⁺).

3.5.6. Sample preparation for LADI-MS

A *D. leichhardtii* seed was cut in half, transverse wise, using a razor blade. The seed was deposited on a bed of LOCTITE silicone putty (Westlake, Ohio, USA) to keep it stable, with the cut face exposed. The putty to which the seed had been affixed was then mounted on the sample plate within the laser system sample chamber.

3.5.7. LADI-MS analysis

Ion images were acquired using an ESL NWR213 laser imaging system (Elemental Scientific Lasers, Bozeman, MT, USA) coupled with a DART-SVP ion source (IonSense, Saugus, MA, USA) and JEOL AccuTOF LC-plus JMS-T100LP HRMS (JEOL USA, Peabody, MA, USA) as described in Chapter 2. Spectra were collected at a rate of 0.5 s scan⁻¹. Spectra in the mass range of m/z 60-

800 were acquired in positive ion mode at 350 °C. The soft ionization-MS conditions set for the analyses included an orifice 1 voltage of 20 V and orifice 2 and ring lens voltages of 5 V each. The ion guide voltage was set to 600 V to allow for the analysis of ions over m/z 60. The rate of helium flow for the DART-SVP ion source was 2.0 L s⁻¹. Calibration was achieved using PEG as a reference standard. TSSPro3 software (Shrader Software Solutions) was used for peak calibration and determining the peak centroid. Mass spectral analysis, elemental composition determination and isotope analysis were performed using Mass Mountaineer software (Mass-spec-software.com, RBC Software, Portsmouth, NH, USA).

3.5.8. LADI-MS seed analysis

The *D. leichhardtii* seed cross-section was placed in the laser ablation system's airtight 800 mL sample chamber which is mounted on a motorized, computer-controlled x,y-moveable stage. Multiple laser parameters were optimized to achieve the strongest MS signals. These included: laser beam energy density (fluence) = 21 J cm⁻³; frequency = 20 Hz; scan speed = 50 μm sec⁻¹; spot size = 50 x 50 μm²; line width = 45 μm; and He flow rate = 600 mL min⁻¹. Based on the experimental parameters used, the spatial resolution attained was 110 x 50 μm².

Chapter 4: Application of LADI-MS to Determination of the Spatial Distributions of Furan and 5-Hydroxymethylfurfural in Unroasted and Roasted *Coffea arabica* Beans

4.1. Introduction

One of the prevailing challenges in the field of food chemistry is understanding how heat and other processes impact the molecular profile of food, and how that in turn affects flavor, odor, organoleptic properties, nutrient loss, and/or the generation of undesirable compounds (such as carcinogens) that have negative impacts on human and animal health. Knowledge of the presence of the precursor compounds of which food is comprised is essential to tracking the ways in which they are transformed during food processing, so that if necessary, steps can be taken to mitigate the formation of undesirable molecules by simply removing the compounds from which they are derived. In this regard, when a food or beverage material matrix is milled (e.g. ground coffee), undesired molecules can generally be more readily removed (e.g. extraction of caffeine from ground coffee to generate “decaf”; removal of lactose from milk to accommodate the lactose intolerant, etc.). However, when the food or beverage material cannot be made uniform, removal of offending precursor molecules can be much more difficult. Whole coffee beans are a case in point.

Aside from the influence of the chemicals whose appearance is defined by the genetic makeup of the specific coffee species, as well as the cultivar and growth conditions, the organoleptic properties of roasted coffee arise from compounds formed through a cascade of

heat-promoted chemical transformations including Maillard and Strecker degradation reactions and caramelization that occur more or less simultaneously during heat processing. The precursors for the formation of these compounds include sugars, amino acids, vitamins, lipids and fatty acids. The identities of the compounds produced, and their formation levels are impacted by the relative concentrations of the precursors themselves. However, it is likely that they are also influenced by their relative distributions within the bean, although this latter possibility has been little investigated because information on the localization of the molecular precursors within the bean remains largely unknown. Several reports have appeared detailing both the health benefits and detriments of coffee brews and their constituent components.¹³²⁻¹³⁴ While some compounds have been documented to impart health benefits, such as chlorogenic acids which exhibit antioxidant and anti-inflammatory effects,¹³⁴ others are perceived to have negative health impacts.^{133, 135-137}

Although both are purported to contribute to the sensory properties of the foods in which they appear,¹³⁸ furan and 5-hydroxymethylfurfural (HMF) are two compounds whose detection in coffee has raised concerns. Their concentrations in roasted coffee have been observed to range from 38.7-51.341 ng g⁻¹ and 0.452-6.27 mg g⁻¹ respectively.¹³⁹⁻¹⁴² Both compounds can be derived from several reactions involving a range of different precursors and/or intermediates.¹⁴³⁻¹⁴⁴ HMF has been shown to induce mutagenic and genotoxic effects in bacteria and human cells and promote colon and liver cancer in rats and mice,¹³³ although it remains unclear if these effects extend to humans.¹⁴³ HMF formation in foods has been found to be affected by sugar type, pH, water content and the presence of divalent cations.¹⁴⁵⁻¹⁴⁷ HMF can be formed from the caramelization of sugars such as sucrose¹⁴⁷ or fructose¹⁴⁸ through formation of a fructofuranosyl

cation under thermal treatment and acidic catalysis. Glucose and fructose can also generate HMF through the formation of a dicarbonyl intermediate, 3-deoxyglucosone (3-DG), from the Maillard reaction and caramelization.¹⁴⁹

Several mechanisms for the formation of furan have been discovered, largely through studies of various model systems,^{138, 144, 150-152} food-simulating systems¹⁵³⁻¹⁵⁴ and foods themselves.¹⁵⁰ Furan is classified as a known carcinogen in rats,¹³⁶ and a possible carcinogen in humans (Group 2B).¹³⁵ Its harmful effects have been proposed to be a consequence of cytochrome P450-mediated oxidation which furnishes a reactive *cis*-butene-1,4-dial metabolite which in turn can bind to various cellular components.¹³⁷

Concerns over the potential harmful effects of furan and HMF in foods and beverages have spurred efforts to develop methods to reduce their concentrations or eliminate them altogether.^{141, 155} However, this remains a formidable challenge because both can be formed from several precursors. In principle, one approach to the systematic development of mitigating strategies to reduce or eliminate the formation of compounds of concern is to better understand the areas within the bean where the molecules and their precursors reside, as the localization of these compounds might suggest approaches for their removal. However, little is known about the spatial distributions of the molecular components in green and roasted coffee beans. Previous investigations of the tissue specific appearance of small molecules within *Coffea* spp. have focused on bulk materials including beans, bark, leaves, and roots of *C. arabica* plants,¹⁵⁶⁻¹⁵⁷ thus losing spatial distribution information. A number of more recent studies have sought to address this through alternative methods. For example, tissular distribution of pentacyclic diterpenoids in coffee beans was accomplished by Dias et al. through manual separation of the

different tissues followed by analysis of each.¹⁵⁸ Conéjéro et al. were able to determine the tissue localization of chlorogenic acid and mangiferin in leaf cross-sections of several members of the *Coffea* genus by exploiting their autofluorescence characteristics.¹⁵⁹

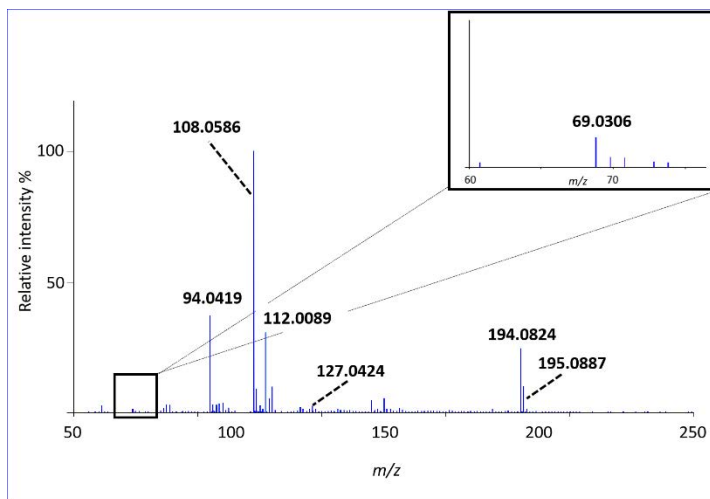
The information gleaned from these efforts implies that IMS could serve as a powerful tool for determination of the tissular localization of a broad variety of small molecules within the complex coffee bean matrix. Here, we demonstrate the use of LADI-MS for the detection of the highly volatile compounds furan and HMF in unroasted and roasted *C. arabica* beans to reveal for the first time the spatial distributions of each, and determine the impact of roasting on their distributions within the tissue.

4.2. Results

4.2.1. *Detection of furan and HMF in roasted coffee beans by dopant-assisted argon direct analysis in real time-high-resolution mass spectrometry (DART-HRMS)*

A prerequisite for determination of the spatial distributions of molecules by LADI-MS is the ability to observe them in the sample of interest by DART-HRMS. As discussed in Chapter 1, conventional DART-HRMS relies on metastable helium which when exposed to atmospheric water results in the formation of protonated water clusters via Penning ionization. Proton transfer from the clusters to the analytes serves as the ionization mechanism for species detected in positive ion mode. Although a range of molecules may be detected because their proton affinities are greater than that of water, the relative intensities of their representative peaks

might not necessarily reflect their relative amounts (as discussed in Chapter 1). In the case of coffee, the presence of caffeine and other alkaloids has the potential to dominate the mass spectrum and make the presence of other compounds of interest less apparent. We circumvented this issue by utilizing argon DART-HRMS with chlorobenzene as a dopant. In contrast to helium DART-HRMS, this approach generates ions by Penning ionization, followed by proton and/or charge transfer from the dopant, with charge transfer being the favored mechanism. Thus, analytes with high proton affinity such as caffeine do not dominate the argon DART mass spectrum and other compounds (with lower ionization energies than chlorobenzene) such as furan and 5-HMF, can be readily detected. Furan and HMF are ionized by an initial charge transfer from the dopant chlorobenzene followed by proton transfer from other ions in the mixture in the open-air gap between the ion source and the mass spectrometer inlet. A typical argon DART-high-resolution mass spectrum collected over the range m/z 50-250 is presented in Figure 4.1. The inset shows an expansion of the m/z 60-75 region which features the high-resolution mass of protonated furan at m/z 69.0306. The peak at m/z



collected over the range m/z 50-250 is presented in Figure 4.1. The inset shows an expansion of the m/z 60-75 region which features the high-resolution mass of protonated furan at m/z 69.0306. The peak at m/z

Figure 4.1. A representative dopant-assisted argon DART-mass spectrum of a roasted coffee bean over a mass range of m/z 50-250. The inset (upper right corner) is an expansion of the mass spectrum in the range of nominal m/z 60-75. The peaks at m/z 69.0306 and 127.0424 are consistent with those of the protonated masses of furan and 5-hydroxymethylfurfural, respectively. Adapted with permission from: Fowble, K. L., Okuda, K., Cody, R. B., and Musah, R. A. "Spatial distributions of furan and 5-hydroxymethylfurfural in unroasted and roasted *Coffea arabica* beans." *Food Res Int.* **119**, 725-732 (2019), Copyright 2019, Elsevier.⁷⁴

127.0424 is representative of protonated HMF. The other high intensity peaks at nominal m/z 94, 108, 112 and 194 are representative of phenol, anisole, chlorobenzene and caffeine, respectively. The phenol and anisole are derived from the tubing used to introduce the dopant. The identities of both furan and HMF were independently confirmed by GC-MS and comparison of their fragmentation patterns to those of authentic standards. The detection of furan and HMF by DART-HRMS indicated that in principle, their spatial distributions could be mapped by LADI-MS.

4.2.2. *Independent confirmation of furan in unroasted and roasted coffee beans by GC-MS*

Although many studies have reported that furan is a product of roasting and is found readily in roasted beans,^{132,160} only one has reported detection of furan in green unroasted coffee beans, albeit at very low levels.¹⁶¹ We were able to independently confirm the results of previous studies that showed the presence of furan in both unroasted and roasted coffee beans.

A gas-tight syringe was used to sample the headspace of aqueous coffee bean extracts for its subsequent analysis using GC-TOF-MS. Furan was detected with a retention time of 2.27 min in each standard solution. The areas under the peaks were integrated for each standard solution and a calibration curve was created for the quantification of furan in coffee beans. The standard curve, ranging in concentrations from 0 ng g⁻¹ to 100 ng g⁻¹ of furan is shown in Figure

4.2. The limit of detection and limit of quantification were determined to be 0.94 ng g⁻¹ and 3.12 ng g⁻¹, respectively. Furan was detected in the headspace of the solutions of both the unroasted and roasted coffee bean extracts, also at 2.27 min. The resulting GC chromatograms (of one of the replicates) are illustrated in Figure 4.3 Panels A and B, showing an expansion of the extracted ion chromatogram for furan in the 1-3 min range. The roasted and unroasted GC traces appear in Panel A and Panel B,

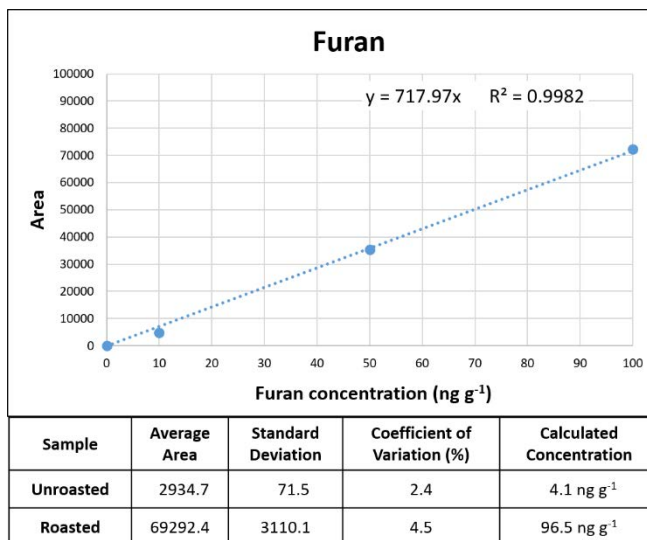


Figure 4.2. The standard curve for the quantification of furan (peak area vs concentration (ng g⁻¹)) over a range of 0-100 ng g⁻¹. The R² value for the curve is 0.9982. The average peak areas, standard deviations, coefficients of variation and calculated concentrations of furan for the unroasted and roasted coffee beans are shown. Adapted with permission from: Fowble et al. "Spatial distributions of furan and 5-hydroxymethylfurfural in unroasted and roasted *Coffea arabica* beans." *Food Res Int.* **119**, 725-732 (2019), Copyright 2019, Elsevier.⁷⁴

respectively. Analysis of the area under the curve compared to the standard curve (Figure 4.2) furnished approximate furan concentrations in both the unroasted and roasted coffee bean of 4.1 ng g⁻¹ and 96.5 ng g⁻¹, respectively. The coffee bean samples were run in triplicate, with coefficients of variation of less than 5% in both unroasted and roasted beans (Figure 4.2). While it could be argued that furan detected in unroasted beans could be formed during the heating of the coffee bean extract prior to headspace sampling, the consistency between the three analyses that required reheating of the same coffee bean extract suggests that little to no furan was created through the heating of the samples. The results are consistent with the report that observed the presence of low quantities of furan in unroasted beans.¹⁶¹ The detection of furan

in the green beans, however, does not negate the finding that roasting is a major contributor to its formation. As confirmed here, the level of furan was found to be significantly higher in the beans which had undergone the roasting process.

4.2.3. Independent confirmation of HMF in unroasted and roasted coffee beans by GC-MS

There are several reports of the detection of HMF in roasted coffee samples.¹⁶²⁻¹⁶⁴ Many focus on how the roasting process and steps taken by the consumer affect HMF levels in brewed coffee. A few groups have shown that the concentration of HMF decreases the longer the beans are roasted.¹⁶²⁻¹⁶³ This

could be due to the compound's instability and its role as a precursor for other molecules. Although many studies have determined the presence of HMF in roasted beans and brews, there are conflicting results on its presence in green unroasted beans, with only one confirming its detection.¹⁶⁴

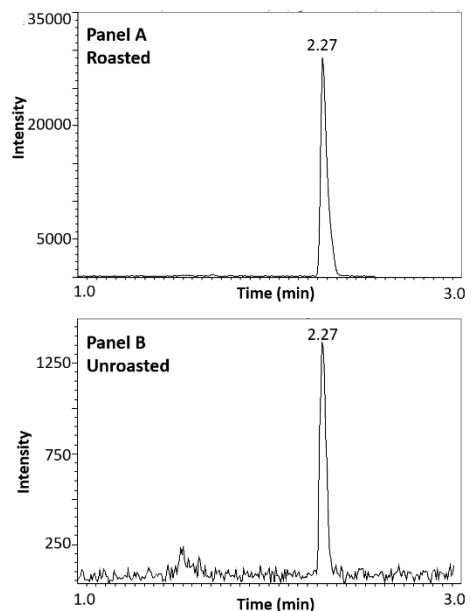


Figure 4.3. The GC extracted ion chromatograms (EIC) for furan in the roasted and unroasted coffee bean headspace gases in the time range of 1-3 min are shown in Panels A and B, respectively. Adapted with permission from: Fowble et al. "Spatial distributions of furan and 5-hydroxymethylfurfural in unroasted and roasted *Coffea arabica* beans." *Food Res Int.* **119**, 725-732 (2019), Copyright 2019, Elsevier.⁷⁴

A direct injection of 1 μL of a methanol:dichloromethane 1:1 extract was used for the GC-MS analysis. HMF was detected at 14.78 min in the standard solution, the unroasted coffee extract and the roasted coffee extract. The extracted GC chromatograms of HMF in roasted and unroasted coffee bean extracts are shown in Figure 4.4 Panels A and B, respectively in the time range of 14.5-15 min, within which HMF elutes. Although there are conflicting results in the literature on the presence of HMF in unroasted beans, our results confirm its presence in both the roasted and unroasted bean extract.

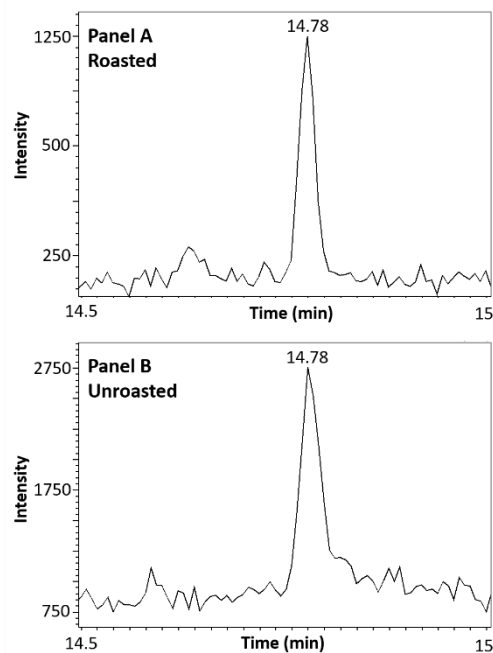


Figure 4.4. The GC extracted ion chromatograms (EIC) for HMF in the roasted and unroasted coffee bean 1:1 methanol:dichloromethane extracts in the time range of 14.5-15 min. Adapted with permission from: Fowble et al. "Spatial distributions of furan and 5-hydroxymethylfurfural in unroasted and roasted *Coffea arabica* beans." *Food Res Int.* **119**, 725-732 (2019), Copyright 2019, Elsevier.⁷⁴

4.2.4. Ion images acquired by LADI-MS

To facilitate the interpretation of the areas within the coffee bean where the compounds of interest were localized, Figure 4.5 shows a light microscopy image of an unroasted coffee bean to illustrate its internal anatomy. The apparent loop within the transverse cross-section is referred to as the perisperm or silver skin (A), while the surrounding tissue comprises the endosperm (B).¹⁶⁵ The perisperm which disintegrates during the roasting process, also covers the

exterior of the unroasted coffee beans (A). These terms will be used to describe the locales of the compounds of interest that were determined by LADI-MS.

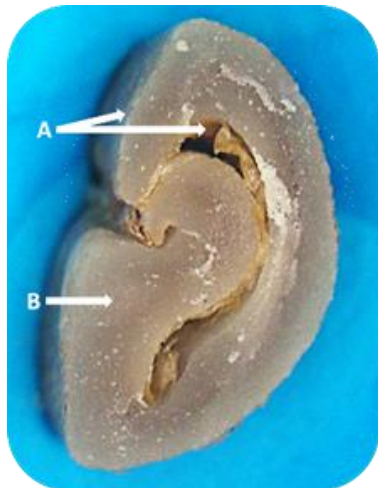


Figure 4.5. A light microscopy image of a transverse cross-section of a green (unroasted) coffee bean. The perisperm (silver skin) is the loop within the center of the coffee bean and a thin layer covering the outside (A). The surrounding tissue comprises the endosperm (B). Adapted with permission from: Fowble et al. "Spatial distributions of furan and 5-hydroxymethylfurfural in unroasted and roasted *Coffea arabica* beans." *Food Res Int.* **119**, 725-732 (2019), Copyright 2019, Elsevier.⁷⁴

Figure 4.6 shows the color-overlaid ion images that illustrate the observed spatial distributions of furan and HMF in the transverse cross-sections of unroasted (top row) and roasted (bottom row) coffee beans. The dashed line around each image represents the periphery of the beans. At the right of each image is a color scale bar ranging from black to yellow, representative of a low or zero intensity to a high intensity of the indicated ion, respectively. As detection of molecules by helium DART-HRMS is dependent on a molecule's proton affinity and not the relative amount of the observed analyte that is in a sample, the scale bars of the various ion images cannot be used to estimate the relative concentrations of the analytes in the coffee beans in comparison with another, and are only indicative of the varying relative concentration of that particular ion across the bean's tissue. The top two Panels A and B are ion images representative of furan and HMF respectively in an unroasted coffee bean. The bottom row of images (Panels C and D) are of the same compounds in a roasted coffee bean. The furan ion images show that this molecule is distributed throughout the endosperm in both the unroasted and roasted coffee beans, with higher levels located in some areas of the silver skin and relatively lower levels at the top of the ion image. However, it should be noted that these

ion images are not normalized to the same scale because of the large difference between the levels of furan in the unroasted versus roasted bean. This difference in furan levels is reflected in the GC-MS data showing that the approximate concentration of furan in the roasted and unroasted beans are 96.5 ng g^{-1} and 4.1 ng g^{-1} , respectively. After the LADI-MS analyses, there was a yellow discoloration observed on the surface of the unroasted bean. This could be interpreted as “roasting” caused by the laser ablation system. However, with the confirmation of furan in both unroasted and roasted beans by GC-MS, with consistency between all three injections (Figure 4.2), the effect of the laser is negligible on the furan spatial distribution mapping. Panels B and D illustrate the non-homogenous spatial

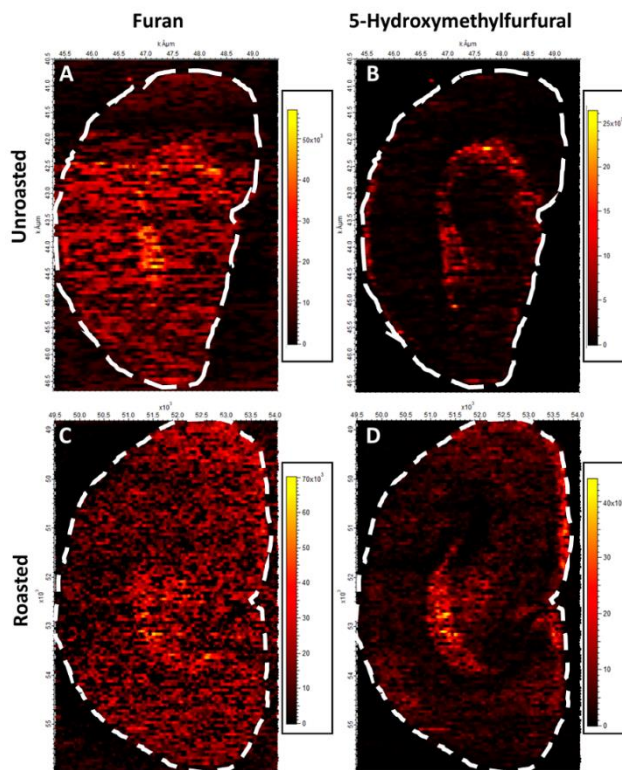


Figure 4.6. The color-overlaid ion images of the m/z values corresponding to furan and HMF in transverse cross-sections of unroasted (top) and roasted (bottom) coffee beans. Unroasted coffee bean: Panel A) furan; Panel B) 5-hydroxymethylfurfural. Roasted coffee bean: Panel C) furan; Panel D) 5-hydroxymethylfurfural. The color scale from black to yellow within each panel is indicative of zero or low intensity to a high intensity of the indicated ion. The white dashed line in each panel indicates the periphery of the coffee bean. Adapted with permission from: Fowble et al. “Spatial distributions of furan and 5-hydroxymethylfurfural in unroasted and roasted *Coffea arabica* beans.” *Food Res Int.* **119**, 725-732 (2019), Copyright 2019, Elsevier.⁷⁴

distributions of HMF in the unroasted and roasted coffee beans respectively. In the unroasted bean, HMF is localized to the silver skin within the loop and the thin layer on the outer surface of the bean. However, after roasting, HMF is more evenly distributed throughout the endosperm,

with higher levels within the silver skin found in the inner loop. The spatial distribution patterns for furan and HMF were found to be consistent in different roasted coffee beans (Appendix 8).

The LADI-MS experiments were carried out using high-purity helium as the carrier gas instead of argon. Although in typical DART-HRMS analyses of whole coffee beans, furan and HMF are more readily detected using argon-DART, the two compounds are also observed using helium-DART. In the case of LADI-MS experiments, since the laser is ablating a relatively small area ($70 \mu\text{m}^2$) and produces a relatively small ablation plume, the protons generated in the open-air gap are not depleted by the presence of molecules with high proton affinities (such as caffeine) and therefore, furan and HMF are more readily detected by the LADI-MS experiments than by typical helium-DART-HRMS analysis of large pieces of coffee beans that are sampled directly.

4.3. Discussion

The homogeneous distribution of furan within the entire tissue of the roasted coffee beans was not unexpected given that its proposed precursors would be expected to occur similarly. Furan can be formed by cyclization of aldotetrose derivatives derived from heat-promoted sugar degradation,^{138, 151-152, 166} Maillard reactions between sugars and amino acids,^{151-154, 167} and thermal degradations of amino acids¹⁵² among other pathways. All of these classes of precursor molecules would be expected to be represented throughout the coffee bean tissue. The homogeneous distribution of sucrose, for example, was demonstrated by Garrett et al. by

DESI-IMS.⁴⁸ The anticipated broad occurrence of precursors provides a rationale for the homogenous distribution of furan in the roasted bean after heat treatment of the green beans. The non-homogeneous occurrence of HMF is more intriguing. It too is proposed to be formed from carbohydrate and/or amino acid precursors that would be expected to be broadly distributed. Despite this, it is localized to the silver skin in the unroasted bean and to both the silver skin and the periphery in the roasted bean. This finding implies that either its precursors are localized to those areas, or that the regions where there is minimal to no HMF contain compounds that interfere with the formation of HMF and thus reduce its concentration. Studies of the molecular content of the silver skin may provide insight into some of the specific compounds that contribute to HMF formation *in situ* (as opposed to in model systems or experiments using model compounds), and this is the subject of ongoing studies in our laboratory. The finding that HMF is concentrated in the silver skin suggests that it may be possible to mitigate the formation of HMF by developing a green bean processing approach that involves removal of the areas such as the silver skin prior to roasting. This knowledge could not only eventually lead to the ability to track the production of desirable compounds as a function of species, cultivar and growth conditions, but also the ability to mitigate the production of undesirable molecules. The mechanism by which both furan and HMF are formed in the green beans is unclear, and the possibility that their formation is a function of the harvesting and processing of the green beans prior to roasting is also being investigated.

4.4. Conclusions

The spatial distribution maps of the small molecules furan and HMF in green and roasted coffee beans were demonstrated. The presence of each analyte mapped by LADI-MS was supported by the independent confirmation of their presence by argon DART-HRMS and GC-TOF-MS. The ability to detect these molecules by the LADI-MS approach is possible due to the absence of a high-vacuum requirement. These molecules, particularly furan with its low boiling point, would likely evaporate under the conditions required by other IMS techniques. The compound HMF was highly concentrated within the silver skin of the beans and distributed more widely after the roasting process. Furan on the other hand, was widely distributed in both the green and roasted beans with higher levels in some areas of the silver skin. The findings indicate that while the precursors for furan formation could appear in all parts of the bean, those for HMF could be localized to the silver skin. This information provides the opportunity to perform informed investigations of the chemical composition of those areas within the green bean, which on heat treatment result in the formation of localized compounds such as HMF, leading to development of informed methods for their potential removal during processing.

4.5. Materials and Methods

4.5.1. Chemicals

Furan standard and chlorobenzene were purchased from Sigma-Aldrich (St. Louis, MO, USA). 5-Hydroxymethylfurfural was purchased from Fisher Scientific (Hampton, NH, USA). High-

purity helium, nitrogen and argon gases were obtained either from Airgas (Albany, NY, USA) or Matheson (Manchester, NH, USA).

4.5.2. *Coffee beans*

Unroasted (green) and roasted *Coffea arabica* beans from Antigua, Colombia were purchased from Uncommon Grounds (Albany, NY, USA). The green unroasted beans were roasted onsite at Uncommon Grounds (Albany, NY, USA) using a Probat solid drum coffee roaster. Unroasted beans were introduced into the drum when it reached a temperature of 210 °C. The drum temperature was then raised 0.35 °C min⁻¹ for 11 min to a final temperature of 213.89 °C after which they were removed from the drum and stirred until they reached room temperature. The roasting parameters were those used at the Uncommon Grounds facility using the in-house coffee roaster, and are identical to those used for coffee beans sold to customers.

4.5.3. *Argon DART-HRMS analysis*

Argon DART-HRMS experiments were conducted using a JEOL AccuTOF-LP 4G mass spectrometer (JEOL USA, Peabody, MA, USA) with a resolving power of 10,000 FWHM, coupled to a DART-SVP ion source (Ionsense LLC, Saugus, MA). Chlorobenzene was used as a dopant for analyses and was infused by a syringe pump at a flow rate of 9 µL min⁻¹ through deactivated fused-silica tubing positioned at the open-air gap. The DART ion source was operated in positive ion mode with a gas heater temperature of 400 °C and a gas flow rate of 2.0 L min⁻¹. The mass

spectrometer was operated with an orifice 1 voltage of 20 V and orifice 2 and ring lens voltages of 5 V each. The ion guide voltage was set to 500 V to allow for the detection of ions above m/z 50. A roasted coffee bean was crushed to produce a number of smaller pieces for analysis. Tweezers were used to suspend portions of the roasted coffee bean in the open-air sample gap between the DART ion source and the AccuTOF mass spectrometer inlet. Multiple pieces of two coffee beans were analyzed and the spectra were averaged together.

4.5.4. Coffee bean extract sample preparation

Extract for furan confirmation

Unroasted and roasted coffee beans were crushed. One gram of crushed unroasted coffee beans was suspended in 10 mL of room temperature water in a capped 22 mL vial with a septum-containing screw cap (Supelco, Bellefonte, PA, USA) and placed in a hot water bath (95 °C) for 10 min. The vial was removed, shaken for 30 s to establish gas/liquid equilibration, and allowed to cool for 10 min before headspace extraction. A Pressure-Lok® precision analytical syringe (Supelco, Bellefonte, PA, USA) was used to withdraw 500 µL of the coffee extract headspace for injection. The vial was reheated in the same manner two more times for triplicate analysis. The vials were kept capped for the entire procedure to prevent furan from evaporating. This process was repeated using roasted coffee beans.

Extract for HMF confirmation

Unroasted and roasted coffee beans were ground and 10 mg of each were placed in separate 2 mL amber glass GC vials (Agilent, Santa Clara, CA, USA). A methanol:dichloromethane 1:1 solution (1 mL) was added to each vial. The extracts were allowed to stand at room temperature overnight before analysis. A small aliquot (200 μ L) was taken from the extract to be used for GC-MS analysis.

4.5.5. Standard samples preparation

A calibration series for furan was prepared by creating 10 ng g⁻¹, 50 ng g⁻¹, and 100 ng g⁻¹ standard solutions of furan in 10 mL of water in 22 mL septum-containing capped vials. Furan standard was refrigerated before opening and once vials were capped, the caps were not removed during analysis in order to prevent evaporation of furan. A 20 μ g g⁻¹ standard solution of HMF in 200 μ L of 1:1 methanol:dichloromethane was prepared.

4.5.6. GC-MS Analysis

GC-MS analyses were conducted using a JMS-T200GC AccuTOF GCx (JEOL USA, Inc., Peabody, MA, USA) mass spectrometer equipped with a 7890B Agilent GC. GC-MS data processing was completed by msAxel software (JEOL Ltd., Akishima, Japan).

Furan confirmation

The headspace (500 μL) was analyzed using an HP-FFAP column (30 m x 0.25 mm, 0.25 μm) (Agilent, Santa Clara, CA, USA) under the following conditions: oven temp: 30 $^{\circ}\text{C}$, held for 10 min, raised linearly 30 $^{\circ}\text{C min}^{-1}$ to 240 $^{\circ}\text{C}$ and held there for 9 min; inlet temperature: 200 $^{\circ}\text{C}$; carrier gas: helium, with a flow rate of 1 mL min^{-1} ; inlet mode: split 15:1; ionization mode: EI+, 70 V, 300 μA . Furan standards (including a blank) were analyzed once and coffee samples were run in triplicate.

HMF confirmation

Of the 200 μL solution, only 1 μL was injected into the GC. The sample was analyzed using a HP-FFAP column (30 m x 0.25 mm, 0.25 μm) under the following conditions: oven temp: 40 $^{\circ}\text{C}$, held for 1 min, raised linearly 15 $^{\circ}\text{C min}^{-1}$ to 240 $^{\circ}\text{C}$ and held there for 10 min; inlet temperature: 230 $^{\circ}\text{C}$; carrier gas: helium, with a flow rate of 1 mL min^{-1} ; inlet mode: split 50:1; ionization mode: EI+, 70 V, 300 μA . HMF standard was analyzed once, and coffee extracts were injected three times each.

4.5.7. LADI-MS coffee bean sample preparation

Unroasted and roasted coffee beans were sliced in half, transverse wise, using a razor blade. The bean halves were placed (separately) onto a bed of LOCTITE Fun Tak[®] mounting putty

with the cut face exposed. The putty was then placed on the sample plate which was then inserted into the laser ablation system air-tight sample chamber for analysis.

4.5.8. Light microscopy imaging of unroasted coffee beans

A Nikon stereozoom SMZ800 microscope coupled to a Nikon DS Fi2 microscope camera was used to collect light microscopy images of the transverse cross-section of an unroasted coffee bean.

4.5.9. LADI-MS analysis

LADI-MS was set up as previously described (Chapter 2).⁷³ Briefly, ion images were acquired using an NWR213 laser ablation imaging system (ESL, Bozeman, MT, USA) coupled with a DART ion source (IonSense, Saugus, MA, USA) and JEOL AccuTOF LC-plus JMS-T100LP HRMS (JEOL USA, Peabody, MA, USA) by way of tygon tubing. The mass spectrometer was operated under ambient conditions with an orifice 1 voltage of 20 V and orifice 2 and ring lens voltages of 5 V in positive ion mode with a scan collection rate of 0.6 s scan⁻¹. The resolving power of the HRMS used was 6,000 FWHM. The rate of the DART ion source helium flow was 2.0 L min⁻¹ at a heater temperature of 350 °C. An ion guide voltage of 600 V was used to collect spectra in the mass range of m/z 60-800. PEG was used as a reference standard for the calibration of the collected spectra. TSSPro3 software (Shrader Software Solutions, Grosse Pointe Park, MI, USA) was used for peak calibration and peak centroiding. Reconstructed ion currents were created for

each of the ions of interest and imported into Lolite imaging software (University of Melbourne, AUS). Mass spectral analysis, elemental composition determination and isotope analysis were performed using Mass Mountaineer software (Massmountaineer.com, Portsmouth, NH, USA).

The following laser parameters were used for the coffee bean analysis: laser beam energy density (fluence) = 21 J cm^{-2} ; laser frequency = 20 Hz ; scan speed = $65 \text{ } \mu\text{m s}^{-1}$; spot size = $70 \times 70 \text{ } \mu\text{m}^2$; line width = $60 \text{ } \mu\text{m}$; and He flow rate = 600 mL min^{-1} . Based on the experimental parameters used, the spatial resolution attained was $154.5 \times 70 \text{ } \mu\text{m}^2$.

Chapter 5: Application of LADI-MS to the Forensic Determination of the Spatial Distributions of Small Molecules in Endangered Wood

Samples

5.1. Introduction

The illegal trade in endangered woods occurs through the harvesting, transportation, and processing of protected species of woods in violation of national or international laws.¹⁶⁸ The trade in illegal woods is thought to be a billion-dollar industry that funds organized crime and terrorist organizations. Additionally, the illegal timber trade is leading to rapid deforestation and reduced biodiversity in the world's forests. To address this, regulatory agencies have been created for the enforcement of forest laws and to help track the trade of these endangered species.¹⁶⁸ One such agency is the Convention on International Trade in Endangered Species of Wild Fauna and Flora (CITES).¹⁶⁹ In the United States, the enforcement of these regulations typically falls to the Fish and Wildlife Service with the assistance of U.S. Border Patrol Agents that help with the identification of illegal species at border crossings.¹⁶⁹

There are several challenges associated with the tracking of illegally traded woods. One of these is how to discriminate between protected endangered woods and those that are legal to trade. Timber is typically transported across borders in large shipping containers that may contain many different species of wood. Thus, it can be quite difficult to ascertain species identity on this scale by visualization alone. While identification of wood species by visual examination of both macroscopic and microscopic features is a well-developed and mature field,¹⁷⁰ the paucity

of experts in this area, as well as the time consuming nature of the endeavor and the challenges in utilizing the approach for field identification at borders and in other forensic contexts, have spurred efforts to develop alternative approaches to accomplishing this task.¹⁷⁰ Several of these exploit the differences in chemical makeup between wood species, and feature techniques such as ion mobility MS,¹⁷¹ ambient sonic spray ionization MS,¹⁷² LC-MS,¹⁷³ and near IR spectroscopy.¹⁷⁴⁻¹⁷⁵ Recently DART-HRMS, employed by the U.S. Fish and Wildlife Service Forensics Laboratory, has also been used for the rapid species identification of woods protected under CITES,^{20-21, 28} as well as numerous other plant materials, with little to no sample preparation required.^{19, 22-25} Another approach to species identification is through DNA profiling.¹⁷⁶⁻¹⁷⁸ However, this relies on the existence of reliable reference libraries. Since the DNA profiles of most plant species are unknown, there are severe limitations to the use of this approach.

An additional challenge to enforcement of the CITES regulations is the falsification of the records regarding the origin of trees crossing the border. It would be useful to investigators to not only know what species of tree is being traded, but also the location where the tree was harvested. Such information is critical in cases where there are geographic restrictions on the locations from which a particular species of timber can be harvested (i.e. a given species can be legally harvested from one area but would be illegal to harvest from another). A number of chemical approaches have been applied to the determination of the geographical origin of logs. These include DNA-profiling,¹⁷⁹ stable isotope analysis,¹⁸⁰⁻¹⁸¹ and near IR spectroscopy.¹⁷⁵ The most prominent application of mass spectrometry to the forensic identification of wood origin has been isotope ratio MS.^{19, 25, 175} As trees grow, they incorporate specific stable isotopes into

the phytochemicals they produce, and the ratios of these isotopes can be linked to a geographical area based on the relative abundances of the isotopes in a given region.^{170, 180-181}

The science of the study of wooded plants is known as dendrology, and it includes the study of taxonomic relationships and species identification based on wood anatomy. Dendrochronology, a sub-discipline of dendrology, focuses on the study of growth rings which can reveal significant information about the timing of various conditions in the life of the tree, such as rainy seasons or droughts.¹⁷⁰ As a tree grows, the growth rings are formed from the outside in, meaning that those that appear in the center of the tree are the oldest, and those near the bark are newest.¹⁸² The growth rings are comprised of early and late wood stages. These correspond to areas of significant growth which are characterized by the appearance of larger cells (early), and those where the growth is slower and more compact (late), depending on the season.¹⁸² Climate is not the only factor that influences the development of growth rings.¹⁸²⁻¹⁸³ Exposure to forest fires or insect infestations can also manifest themselves in terms of characteristic features that appear in the growth rings.¹⁸² All of the information that can be extracted from the wood anatomy and growth rings can contribute to determination of the geographic origin of a felled tree, and the products derived from it.

The varying levels of success of spectroscopic and mass spectrometric approaches to species identification of logs and their derivative products, make clear that there are diagnostic small molecule profile characteristics that can be used for the forensic identification of wood. However, to date, very little work to investigate the identities of the small molecules involved, and correlating them to specific plant species and their geographic locations, or the environmental and climactic factors associated with their appearance, has been reported. This is

due in large part to the absence of enabling technologies that would facilitate not only determination of these molecules, but also revelation of their locales within the plant tissue. In this regard, the characteristics of LADI-MS appear particularly well-suited to addressing these concerns.

Accordingly, we investigated the application of LADI-MS to the mapping of the spatial distributions of small molecules localized to the growth rings in the four endangered wood species: *Dalbergia nigra*, *D. maritima*, *D. normandii*, and *Swietenia mahagoni*. The results, including application of LADI-MS-derived ion images for species identification, are discussed. One of the most important advantages of utilizing LADI-MS is that the sample chamber permits the analysis of large and irregularly shaped tree disc samples that span an area from pith to bark, allowing for all stages of growth to be analyzed in a single experiment. Figure 5.1 depicts the various morphological and anatomical features of trees to illustrate attributes of the types of samples analyzed in this work.

At the very center of the tree is a pulpy core, known as the pith.

The concentric circles in the image radiating out from the pith towards the bark

correspond to growth rings. The lines running perpendicular to the growth rings and extending from pith to bark are known as

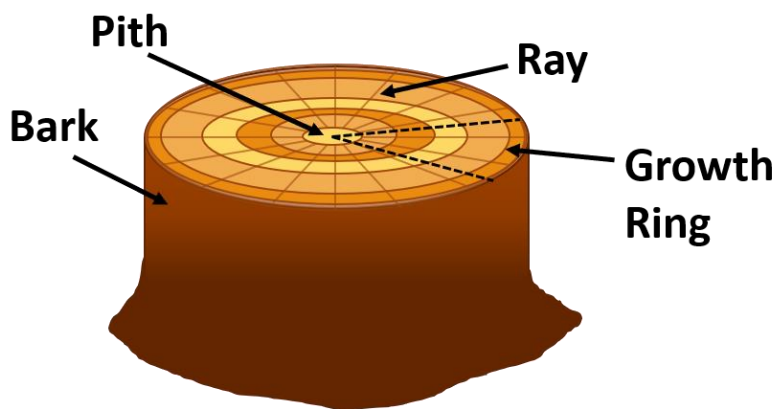


Figure 5.1. A diagram depicting the morphology and anatomy of a tree trunk. The outside corresponds to the bark of the tree. The very center is known as the pith, and the concentric circles radiating outwards from it are growth rings. The lines running perpendicular to the growth rings are rays. The black dotted lines, in a triangular shape, represent the type of pie-shaped segments that were analyzed by LADI-MS.

rays, and the black dotted lines represent where the logs are cut to provide the pie-slice samples that can be analyzed. The samples are up to 2 cm in depth, vary from ~6-10 cm from pith to bark, and were analyzed without the need for the further sectioning or sample pretreatment that is required in many other IMS techniques.¹⁸⁴⁻¹⁸⁸

5.2. Results

To determine if the analysis of wood samples by LADI-MS was possible, a *D. nigra* sample was ablated with a laser spot size of 80 μm^2 and a fluence of 2 J cm^{-2} . The ablated area did not travel the length of the tree from pith to bark, and was used only to determine if molecules could be detected by MS from this sample type. Figure 5.2 shows a representative mass spectrum from this analysis. In order to facilitate assignment of peaks, KNApSack, a database that contains small molecule metabolites and the plant species in which they have been observed, was consulted.¹⁸⁹ It contains a compilation of over 50,000 metabolites known to be present in over 20,000 species.

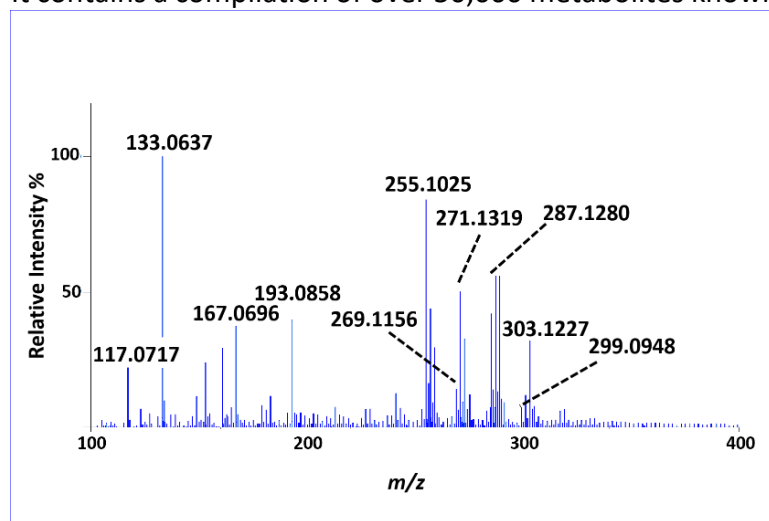


Figure 5.2. A representative mass spectrum acquired from ablating the surface of a *D. nigra* sample using LADI-MS.

From this database, a short list of compounds that have been isolated from *Dalbergia* spp. plants and subsequently structurally characterized were compiled. The high-resolution mass spectrum acquired by LADI-MS was then examined for the presence of

masses consistent with the presence of any of the short-listed molecules. From this exercise, tentative peak assignments could be made for m/z values 255.1025 (dalbergichromene— $M + H^+$: $C_{16}H_{15}O_3$), 269.1156 (dalbergin— $M + H^+$: $C_{16}H_{13}O_4$), and 299.0948 (afromosin or dalnigrin— $M + H^+$: $C_{17}H_{15}O_5$). While not listed in KNApSack as a compound present in *Dalbergia* spp., the peak at m/z 133.0637 corresponding to $M + H^+$: C_9H_9O , was consistent with cinnamaldehyde. This assignment was later confirmed by GC-MS analysis (data not shown).

The detection of masses consistent with molecules that are known to be present in *Dalbergia* spp. trees prompted the extension of the LADI-MS technique to the imaging of the spatial distributions of some of these molecules in the different wood samples. All four of the endangered wood samples (*D. nigra*, *D. maritima*, *D. normandii*, and *S. mahagoni*) were analyzed with similar DART-HRMS and laser parameters (Section 5.5, Materials and Methods), resulting in a spatial resolution of 155 x 80

μm^2 for each experiment.

Visible light optical images of all four samples were provided by

Dr. Edgard Espinoza of the U.S. Fish and Wildlife Service Forensics Laboratory and are shown in Figure 5.3. The

samples were analyzed by LADI-MS with the line scan extending from the inner core (pith) to the

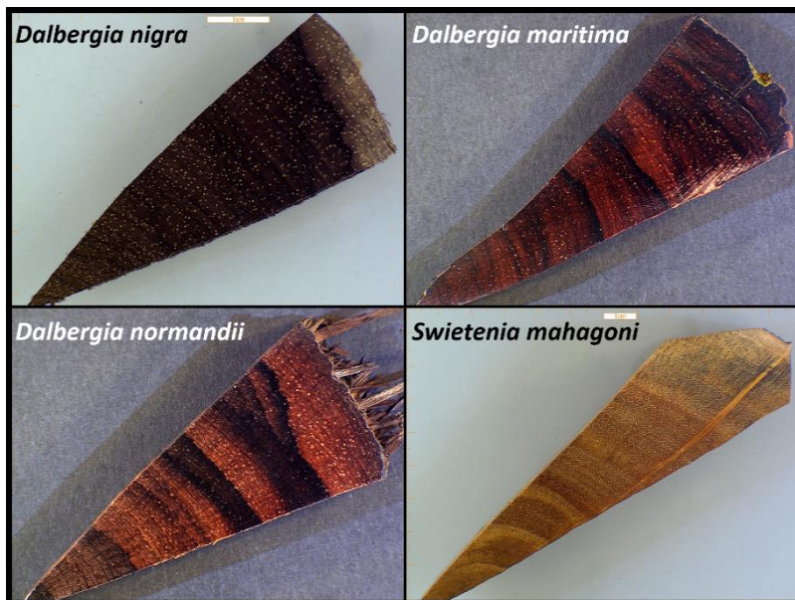


Figure 5.3. Visible light optical images of the four samples of wood analyzed by LADI-MS. The species analyzed were *D. nigra*, *D. maritima*, *D. normandii*, and *Swietenia mahagoni*. The samples ranged from ~6-10 cm in length from pith to bark and were ≤ 2 cm in depth.

outer edge (bark) as shown in Figure 5.1. Depending on the sample, the total length varied between ~6-10 cm.

The first sample analyzed was that of the *D. nigra* species at a laser spot size of 80 μm^2 , yielding a spatial resolution of 155 x 80 μm^2 .

This species is classified as Appendix I by CITES, meaning it is threatened with extinction and there is no trade allowed. This particular species, also known as Brazilian Rosewood, tends to be harvested illegally for use in the fashioning of furniture and musical instruments.

A hyperspectral image, taken at a wavelength of 645 nm, is shown in Figure 5.4 Panel A, and reveals features that are not visually

apparent in ambient light. The dark lines illuminated in Figure 5.4 Panel A correspond to the compacted areas of the growth rings. Color-overlaid ion images corresponding to masses consistent with caviunin (listed in KNApSack as being present in *Dalbergia* spp.), afrormosin/dalnigrin, and dalbergin are shown in Panels B, C, and D, respectively. In all three

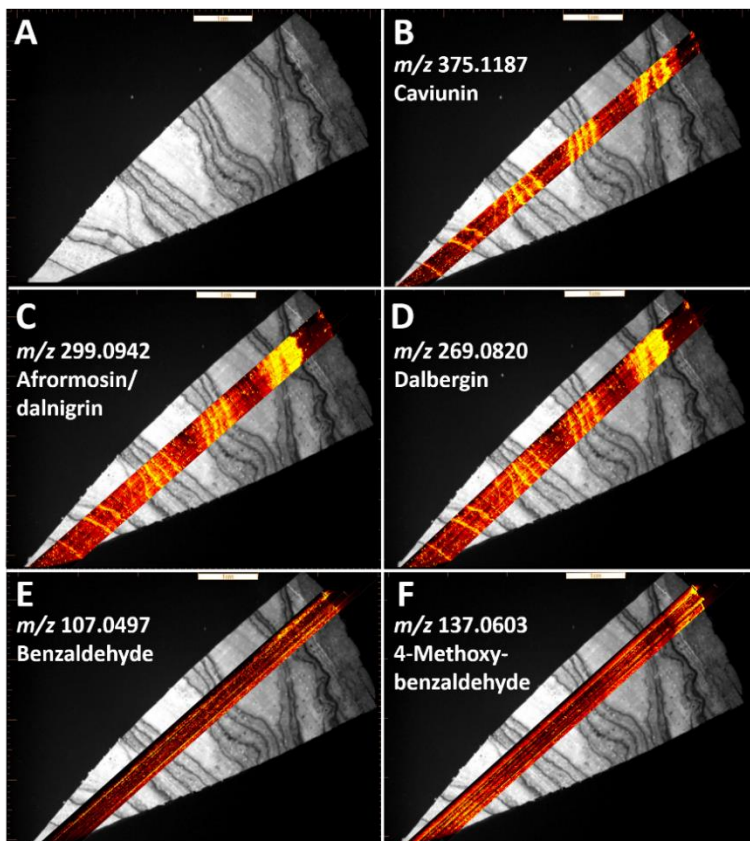


Figure 5.4. Ion images overlaid onto hyperspectral images acquired at 645 nm (Panel A) of the *D. nigra* sample. Panels B-D illustrate those masses localized within the dark growth ring areas, and are consistent with the presence of caviunin, afrormosin/dalnigrin, and dalbergin, respectively. Panels E and F feature ion images of benzaldehyde and 4-methoxybenzaldehyde, both of which appear to be evenly distributed throughout the wood tissue.

cases, the high intensity areas (indicated in yellow) were found to correlate to the dark growth ring areas. In contrast, the ion images for benzaldehyde (Panel E) and 4-methoxybenzaldehyde (Panel F), both of which were confirmed to be present by GC-MS analysis (data not shown), indicated that these molecules were distributed evenly throughout most of the wood tissue.

The second *Dalbergia* sp. analyzed was a sample of *D. maritima*, classified by CITES as Appendix II. The hyperspectral image of the wood, taken at a wavelength of 725 nm, is shown in Panel A of Figure 5.5. The color-overlaid ion images for dalbergin (m/z 269.0810) and dalbergichromene (m/z 255.1024) are shown in Figure 5.5 Panels B and C respectively. These two molecules show spatial distributions that are the opposite of one another. Dalbergin, shown in Panel B, is localized with high intensity in the dark rings that are visible using 725 nm wavelength light. On the other hand, dalbergichromene (Panel C) is absent, or at a lower intensity, in those same areas.

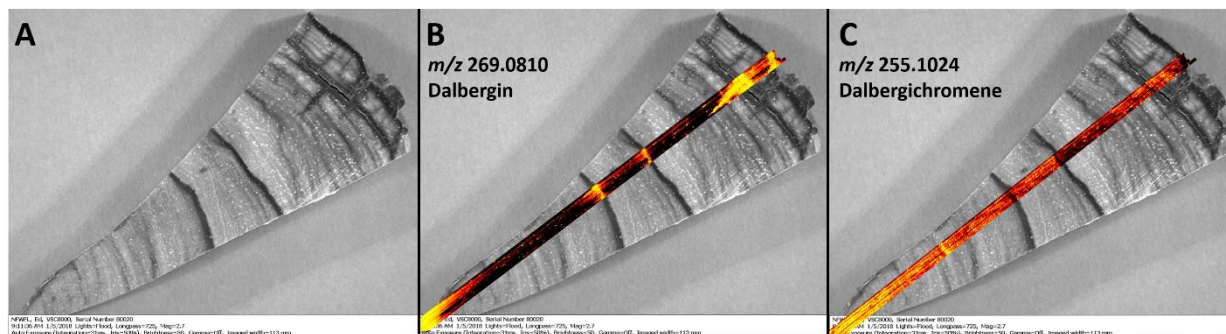


Figure 5.5. Ion images acquired using LADI-MS, overlaid onto hyperspectral images of a *D. maritima* sample. Panel A features a hyperspectral image of the *D. maritima* sample taken at a wavelength of 725 nm. Panels B and C show LADI-MS ion images of masses consistent with dalbergin and dalbergichromene overlaid on the hyperspectral image, respectively. The spatial distributions of the two featured ions are the opposite of one another, with dalbergin being found within the dark growth ring areas, and dalbergichromene mostly absent in those same areas.

The third sample analyzed was of the *D. normandii* tree species, which is also classified as Appendix II. The hyperspectral image, taken at a wavelength of 725 nm, is shown in Figure 5.6

Panel A. The ion images for masses consistent with afrormosin or dalnigrin (m/z 299.0942) and cinnamaldehyde (m/z 133.0667) are shown in Figure 5.6 Panels B and C. In both ion images, the compounds are shown to have a high intensity at the pith of the tree sample. The mass at m/z 299.0942, consistent with afrormosin or dalnigrin, was found to

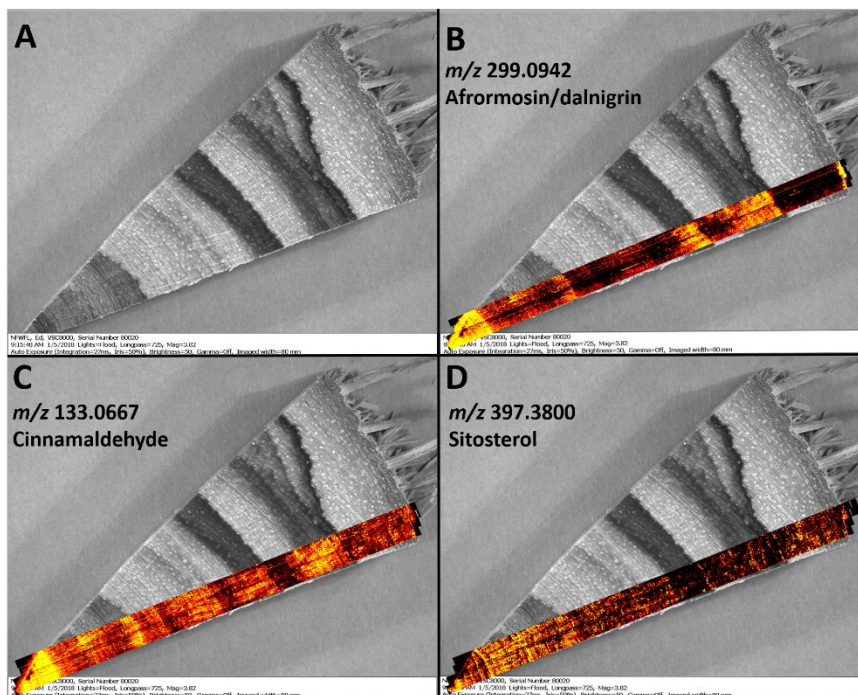


Figure 5.6. LADI-MS ion images overlaid onto a hyperspectral image of the *D. normandii* sample acquired at a wavelength of 725 nm (Panel A). Panels B-D show LADI-MS ion images of masses consistent with afrormosin/dalnigrin, cinnamaldehyde, and sitosterol, respectively. The spatial distributions of afrormosin/dalnigrin and cinnamaldehyde show a high intensity of these ions at the pith of the tree sample, but a difference in relative intensities near the bark. The ion image for dehydroxylated sitosterol (Panel D) shows striations radiating out from the pith towards the bark.

be mostly absent near the bark, whereas the ion image for cinnamaldehyde shows this ion with a relatively high intensity in the same area. The ion image for a mass consistent with dehydroxylated sitosterol (m/z 397.3800) in Panel D, features individual striations that radiate out from the pith towards the bark. Additionally, this molecule is found with a lower intensity in the darker growth ring areas.

To investigate whether the spatial distributions of small molecules in wood tissue could potentially be utilized for the differentiation of one species from another member of the same genus, ion images for a mass consistent with 3,4-dimethoxydalbergione (m/z 285.1127— $M + H^+$):

C₁₇H₁₇O₄), overlaid on the corresponding hyperspectral images of each sample are shown in Figure 5.7. Although the observed mass is consistent with that of 3,4-dimethoxydalbergione, which has been previously isolated from *Dalbergia* spp. trees and characterized, the presence of this molecule in the wood analyzed in this study has not been confirmed. As such, the ion images depicted could correspond to a second compound with the same molecular formula. In Panels A and B, the ion images of the *m/z* value 285.1127 in the *D. nigra* and *D. maritima* samples are shown. In these two species, the spatial distributions of this mass are the opposite of one another. The mass is found with a high intensity in the dark growth ring areas in the *D. nigra* sample (Panel A) but is mostly absent in the same dark areas in the *D. maritima* sample (Panel B). In the *D. normandii* sample shown in Panel C, the ion image for a mass consistent with 3,4-

dimethoxydalbergione (*m/z* 285.1127) is localized with a higher relative intensity in the dark compacted areas of the growth rings, similar to the spatial distribution found in *D. nigra*. Next, we compared the ion distributions in two samples representing the same species (*D. normandii*). The

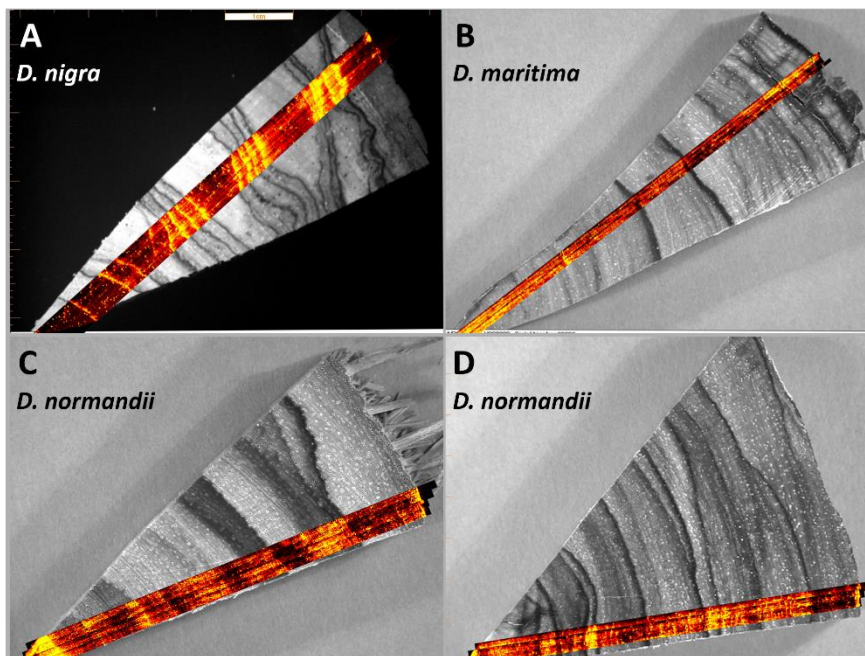


Figure 5.7. Color-overlaid ion images of a mass consistent with 3,4-dimethoxydalbergione overlaid onto the corresponding hyperspectral images of the *Dalbergia* spp. tree samples analyzed. The spatial distribution of this molecule shows inter- and intra-species differences.

spatial distribution of the same mass in a second *D. normandii* sample (Figure 5.7 Panel D) exhibits a lower relative intensity in the darker growth ring areas.

In addition to the *Dalbergia* spp., a sample from a second genus was analyzed by LADI-MS. The hyperspectral and overlaid ion images from the Appendix II species *S. mahagoni* are shown in Figure 5.8. For this species, the hyperspectral image was taken in the UV range at a wavelength of 365 nm (Panel A), which reveals fluorescence of the wood tissue near the bark. The dark line running perpendicular to the growth rings is a “ray” (Figure 5.1). Rays are thought to contain cells that help transport different biologically active molecules to various areas of the tree tissue. Panel B shows the ion image for dehydroxylated cycloartenol, a triterpenoid. The spatial distribution of this molecule features higher intensities in the lighter growth ring areas, with a much higher relative intensity near the bark. However, this molecule does not seem to be localized in the ray.

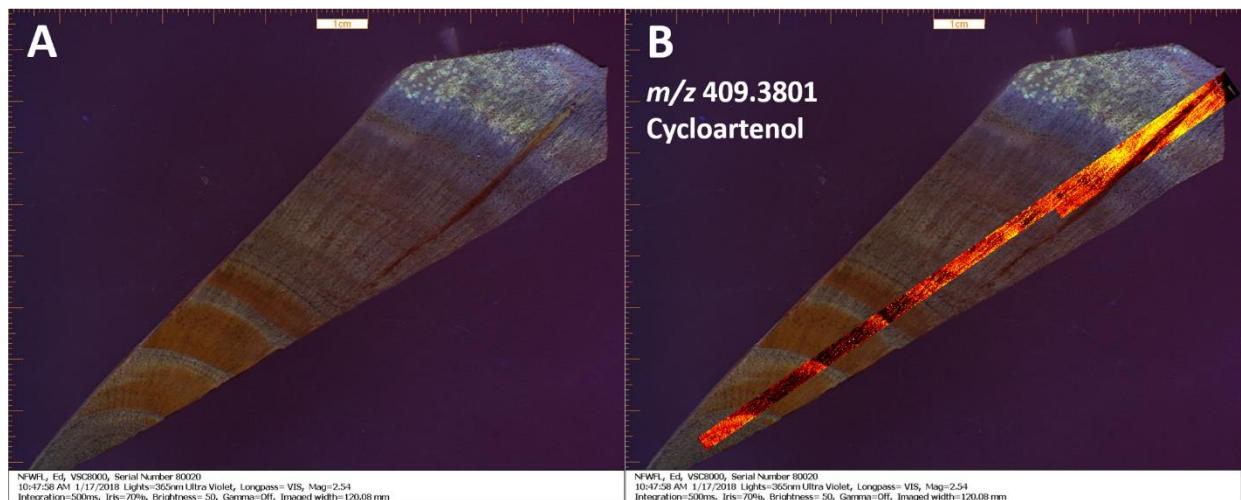


Figure 5.8. The hyperspectral and ion images for the *S. mahagoni* tree sample. Panel A consists of the hyperspectral image taken at a wavelength of 365 nm, with fluorescence appearing near the bark. The color-overlaid ion image of a mass consistent with cycloartenol is shown in Panel B. This molecule is localized with little to no intensity in the ray cells.

5.3. Discussion

The ion images featured in this study of the LADI-MS analysis of endangered woods were highlighted because they represented masses consistent with those of compounds previously found in *Dalbergia* spp., *Swietenia* spp., or other tree samples described in the literature or the KNApSack database.^{21, 173, 189-190} Definitive confirmation of the identities of these molecules, (with the exception of cinnamaldehyde, benzaldehyde and 4-methoxybenzaldehyde), has not been completed, although this is an area of active investigation. One mass featured in this work, m/z 299.0942, could correspond to both afrormosin and dalnigrin, as these molecules share the same molecular formula. Dalnigrin has been confirmed by LC-MS studies in *D. nigra* samples.¹⁷³ However, it was not found in *D. cearensis*, *D. congestiflora*, *D. cubilquitzensis*, *D. cultrate*, *D. frutesens*, *D. granadillo*, *D. inundata*, *D. melanoxylon*, *D. miscolobium*, *D. retusa*, *D. sissoo*, or *D. spruceana*.¹⁷³ No work has been done to confirm its presence in the other species featured in this chapter.

We investigated the potential of using the spatial distributions of molecules for species identification within the same genus by mapping the ion images for the same mass in three *Dalbergia* spp. samples. However, as shown in Figure 5.7, the results could not be used for differentiation between the three analyzed *Dalbergia* spp. The localization of a mass consistent with 3,4-dimethoxydalbergione, with high intensity in the dark areas of the growth rings, was the same in both *D. nigra* and one of the *D. normandii* samples. On the other hand, the spatial distribution of the same mass in the *D. maritima* species was found to differ, showing a lower intensity in the dark growth ring areas. Additionally, the distribution of m/z 285.1127 in both *D.*

normandii samples differed. Further investigations are required to determine whether there are other ions whose LADI-MS-derived spatial distributions may have utility in enabling species identification for members of the same genus.

One potential explanation for the differences in the spatial distributions of a given mass between two samples of the same species is that the mass corresponds to more than one molecule of the same molecular formula. As discussed in the case of m/z 299.0942, which can be indicative of the presence of dalnigrin or afrormosin, the m/z value of 285.1127 may reflect the presence of two molecules with a shared formula of $C_{17}H_{17}O_4$, and not only 3,4-dimethoxydalbergione. Thus, the differences in the spatial distributions may signify that they represent entirely different molecules. If analysis of the samples following isolation and characterization by a confirmatory technique like GC-MS results in confirmation of the same molecule detected in all the samples, a second explanation of the disparity between the spatial distributions in different samples of the same species is that there may be external factors that impact compound localization. For example, it could be a function of the climate or local environment in which the tree was grown. Cinnamaldehyde may serve as a case in point. It has been shown to function in plants as an insecticide and antimicrobial,¹⁹¹ and thus its localization to the growth rings in trees may indicate a function in protecting trees from insect infestations. Although the purpose of the compartmentalization of some of these molecules to different areas of the wood tissue is unknown, LADI-MS provides a means for the investigation of this phenomenon more thoroughly.

The utilization of LADI-MS permits the analysis of large wood samples not previously amenable to imaging by other techniques. Although the imaging of a variety of molecules in wood

tissues has been accomplished,^{184-188, 192} these studies have focused only on very small areas of the wood tissue, with the largest area analyzed being ~8 mm.¹⁹² Additionally, only one of these studies imaged the tree sample from pith to bark.¹⁸⁵ Most research has focused on the analysis of the spatial distribution of small molecules localized to the plant cell wall.^{184, 186, 188} In the study presented here, the smallest sample analyzed was ~6 cm from pith to bark, and the focus was on the determination of the macro-spatial distribution of molecules localized to different wood tissues in the sample. Although this study focuses on the large scale distribution of molecules spanning the entire length of the sample from pith to bark, LADI-MS also permits the analysis of molecular features on a much smaller scale. The lower limit of the laser spot size (as discussed in Chapter 2) is 4 μm^2 allowing for the interrogation of microscopic tissues such as individual vessels in the tree samples (data not shown), which are typically on the scale of a few mm. The sample chamber of the LADI-MS system permits imaging without prior tedious sample preparation such as microtome-sectioning and embedment, which is required for most other techniques.¹⁸⁴⁻¹⁸⁸

5.4. Conclusions

The mapping of the spatial distributions of several small molecules in endangered wood samples by LADI-MS was demonstrated. The development of LADI-MS provides a means for the determination of the physiological relevance to the localizations of some of the small molecules to different wood tissues, like growth rings and rays. The technique allowed for the facile imaging of large and irregularly shaped sample types not amenable to imaging by other means, with little to no sample preparation. The data acquired by the LADI-MS analyses has the potential to inform

an investigator to the climate or geographical region in which a tree was grown based on the spatial distributions of the small molecules within the growth rings related to the corresponding dendrochronological data. Additionally, the detection of molecules consistent with pollution could pinpoint the location of a tree's growth.

5.5. Materials and Methods

5.5.1. Chemicals

High-purity helium and nitrogen gases were purchased from Matheson (Manchester, NH, USA).

5.5.2. Endangered wood samples

Four species of wood, including *Dalbergia nigra*, *D. normandii*, *D. maritima*, and *Swietenia mahagoni*, were provided by the U.S. Fish and Wildlife Forensics Laboratory. Each sample was provided in the form of a pie-shaped segment cut from a tree stump or felled log, and extended over the entire length from the pith to the bark (Figures 5.1 and 5.2). The samples were each less than 2 cm in depth and varied from between ~6-10 cm in length from pith to bark. The cut surface was sanded to a polished finish, using a Work Sharp WS3000 tool sharpener (Ashland, OR, USA), prior to analysis.

5.5.3. LADI-MS analysis

LADI-MS was set-up as previously described in Chapter 2 with the JEOL AccuTOF-LP 4G HRMS (JEOL USA, Inc., Peabody, MA, USA) and a heated stainless-steel transfer line. The wood samples were placed polished side up in the sample chamber for analysis. The DART ion source was operated with a gas flow rate of 2.0 L min⁻¹. The orifice 1 voltage was set to 20 V and the orifice 2 and ring lens voltages were set to 5 V each. The ion guide voltage of the MS was set to 1,000 V for the detection of ions over m/z 100. The mass range detected was m/z 100-800. In all experiments, the ion source was operated in positive ion mode with a gas heater temperature of 500 °C. The MS acquisition rate was 0.3 s scan⁻¹. The laser parameters used in these experiments included: laser beam energy density (fluence) = 2 J cm⁻²; frequency = 20 Hz; scan speed = 75 μm sec⁻¹; spot size = 80 x 80 μm²; and He flow rate = 450 mL min⁻¹. PEG was used as a reference standard for the calibration of the collected spectra. The msAxel Data Processing software package (JEOL USA, Inc., Peabody, MA, USA) was used for peak calibration and peak centroiding. Reconstructed ion currents were created for each of the ions of interest and imported into Iolite imaging software (University of Melbourne, AUS). Mass spectral analysis, elemental composition determination and isotope analysis were performed using Mass Mountaineer software (Massmountaineer.com, Portsmouth, NH, USA). Based on the experimental parameters used, the spatial resolution attained was 155 x 80 μm².

Chapter 6: Simultaneous Imaging of Latent Fingermarks and Detection of Analytes of Forensic Relevance

6.1. Introduction

In a forensics context, fingermarks left behind by individuals can directly link them to a crime scene and are thus of high value to investigators. Historically, their visualization has been accomplished using a variety of techniques including dusting with powders, cyanoacrylate fuming, and the application of ninhydrin, among other approaches.¹⁹³ Fingerprint visualization by these methods exploits the presence of amino acids and endogenous molecules such as lipids in the latent fingermarks.¹⁹³ However, in principle, any chemical with which the fingers come into contact can be registered in the print, a fact that provides the opportunity to extract immense amounts of information about the owner. Chemical compounds found within latent fingermarks can include illicit drugs, psychoactive plant materials and explosive compounds. The observation of such substances can provide important information about exposures that may be directly relevant to a crime.

Recognition of the potential utility of knowing the chemical content of fingermarks has spurred development of various analysis methods. Swabbing followed by extraction of materials found in smudged fingerprints and analyzing their contents by GC- or LC-MS techniques,¹⁹⁴⁻¹⁹⁸ as well as by DART-HR- and DESI-MS have been used.^{194, 198-201} These techniques are able to reveal the presence of both endogenous and exogenous molecules found in fingerprints, including fatty acids, drugs of abuse, drug metabolites, and explosive materials. However, in using these

approaches, the fingerprint image that establishes a link between an individual and substances to which they have been exposed is destroyed.

In recent years, this challenge has been overcome through imaging spectroscopic and mass spectrometric techniques. For example, fingerprint imaging has been accomplished using IR and Raman spectroscopies.²⁰²⁻²⁰⁴ However, these approaches have limited ability to provide definitive information on the identity of chemical constituents.²⁰⁵⁻²⁰⁷ On the other hand, IMS techniques have proven to be well-suited to chemical imaging of latent fingerprints.^{198, 205-206} Their power lies in the ability to reveal fingerprint patterns made from any one of a range of substances that are present, all from a single experiment. If the fingerprint contains an illicit substance or other molecules of concern such as explosive materials, the MS ion images could provide a direct link to a specific individual. Additionally, if metabolites of illicit and psychoactive substances can be detected within a latent fingerprint, a distinction can be made between those individuals who have only handled the materials, and those who have ingested the product. Several MS techniques have been used to map the spatial distributions of endogenous and exogenous materials in latent fingerprints, with the most common being SIMS, MALDI-MS, SALDI-MS, and DESI-MS.^{198, 205-206, 208-221}

While current IMS techniques enable spatial distributions of molecules to be obtained, there are several reasons why it would be advantageous if LADI-MS could be used. Experiments are performed in open-air and under ambient conditions, and do not require high-vacuum. LADI-MS can be completed on non-conductive surfaces which permits analysis of samples on a variety of matrices, such as packing tape. As it utilizes a soft ionization source, LADI-MS does not cause extensive fragmentation of the molecules detected. The possible utility of the technique in

fingerprint analysis is demonstrated through the imaging of endogenous molecules within latent fingerprints, and the detection of cocaine, yanonin and other kavalactones derived from a psychoactive plant, and pseudoephedrine. Micro-ablation and detection of RDX, an explosive, are also demonstrated.

6.2. Results

The handling of a variety of materials was used to assess the utility of LADI-MS for detection of compounds of potential forensic interest in latent fingerprints. These included an illicit drug (cocaine), an unregulated psychoactive plant material (*P. methysticum*), the active ingredient in an over-the-counter medication (pseudoephedrine) that can also be used to synthesize illicit drugs, and an explosive material (RDX). Imaging of the latent fingerprints was completed using a laser spot size of 60 μm^2 , resulting in spatial resolutions of 126 x 60 μm^2 for each experiment.

6.2.1. LADI-MS analysis of a cocaine-laden latent fingerprint

Figure 6.1 shows representative results of a typical LADI-MS experiment that was performed on a fingerprint that was deposited after the handling of cocaine. The mass spectrum in Figure 6.1 (Panel A) shows a composite of all the detected ions, including protonated cocaine (m/z 304.1505). Also presented are the color-overlaid ion images of endogenous dehydroxylated cholesterol (m/z 369.3475) and exogenous protonated cocaine (m/z 304.1505) in Panels B and C

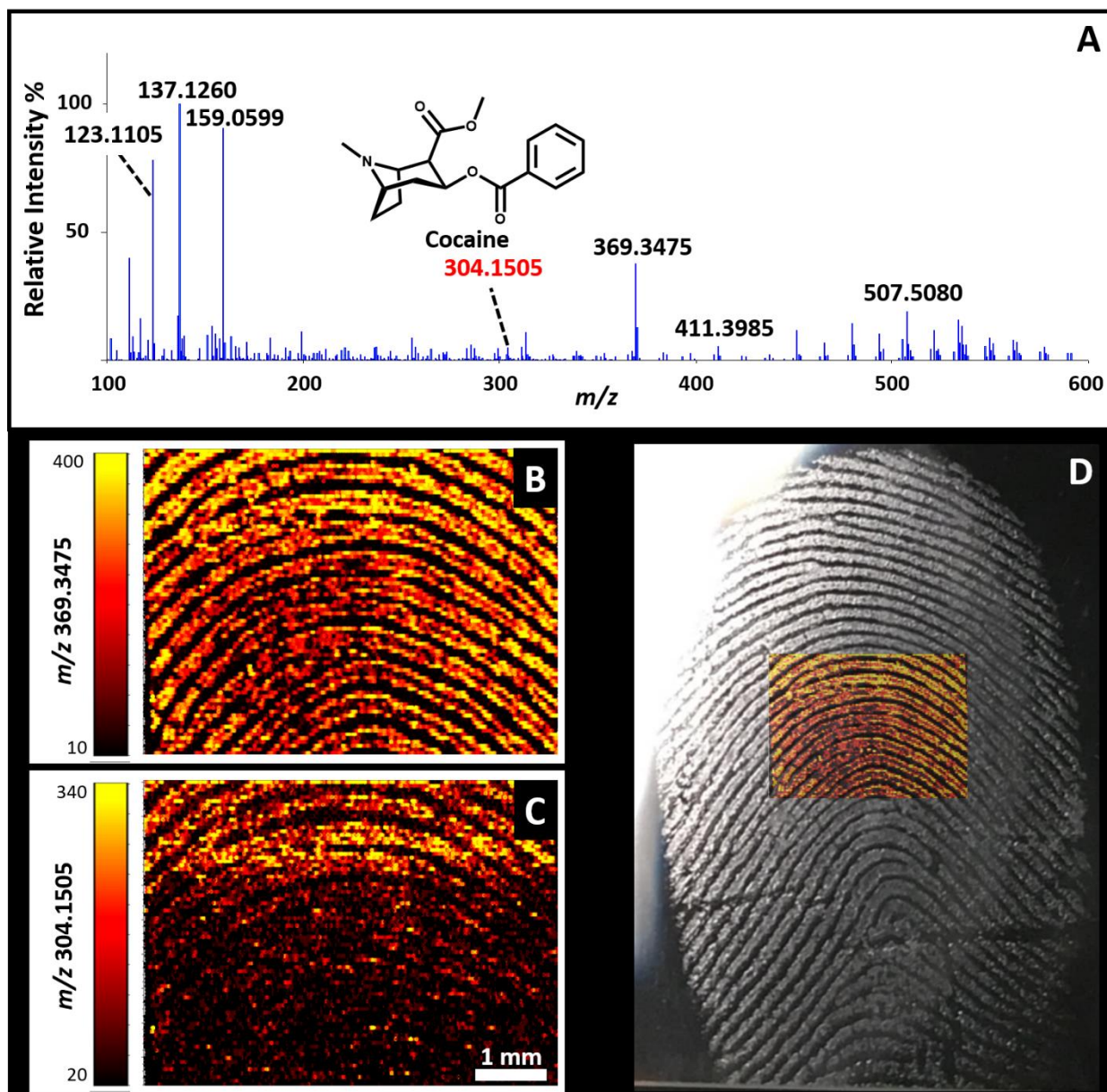


Figure 6.1. A mass spectrum and LADI-MS ion images resulting from the analysis of a fingerprint deposited after exposure to cocaine. Panel A shows a representative LADI-mass spectrum with the peak corresponding to protonated cocaine labeled in red (m/z 304.1505). The LADI-MS color-overlaid ion images of the masses consistent with dehydroxylated cholesterol (Panel B) and protonated cocaine (Panel C) in the same latent fingerprint are shown. The 1 mm scale bar applies to both ion images. The color scale bar ranging from black to yellow is representative of a zero or low intensity to high intensity of the indicated ions. The ion image of the mass consistent with dehydroxylated cholesterol is overlaid on a photograph of the latent print that was acquired prior to LADI-MS analysis (Panel D). Adapted with permission from: Fowble, K. L., and Musah, R. A. "Simultaneous imaging of latent fingerprints and detection of analytes of forensic relevance by laser ablation direct analysis in real time imaging-mass spectrometry (LADI-MS)." *Forensic Chem*, **15**, 100173 (2019), Copyright 2019, Elsevier.⁷⁵

respectively. The 1 mm scale bar applies to both ion images and the color intensity bars ranging from black to yellow are representative of a zero or low intensity to a high intensity of the indicated ion. The cholesterol and cocaine ion images (Panels B and C), both of which were acquired in the same experiment, reveal a characteristic fingerprint pattern which is identical to, and therefore can be superimposed over, the area that they represent in the optical image of the print (Panel D). The observation of an ion image for the endogenous compound representing the fingerprint image itself, and the detection of cocaine in the form of an ion image that aligns with the ridge pattern of the print (in the same experiment) indicate exposure to cocaine by the owner of the print.

6.2.2. LADI-MS analysis of a psychoactive plant-laden latent fingerprint

To avoid prosecution for possession of illegal substances, many drug abusers are turning to plant materials that are not currently regulated but are psychoactive. The United Nations Office on Drugs and Crime (UNODC) has listed twenty of these as “plants of concern”.²²² As shown in Figure 6.2 (Panel A), the mass associated with a psychoactive biomarker, yangonin, for one such plant of concern, *Piper methysticum* (commonly known as Kava), was detected (m/z 259.0980) in a print after bulk plant material had been handled. Other kavalactones that were also observed included methysticin (m/z 275.0960) and dihydromethysticin (m/z 277.1040). Fingerprint ridge details are displayed in the ion image for endogenous dehydroxylated cholesterol (m/z 369.3520) that was acquired from the same experiment (Panel B). Figure 6.2 Panel C shows the magnified optical image of the same area represented by the cholesterol ion

image, while Panel D shows the cholesterol ion image overlaid on the full latent fingerprint photograph.

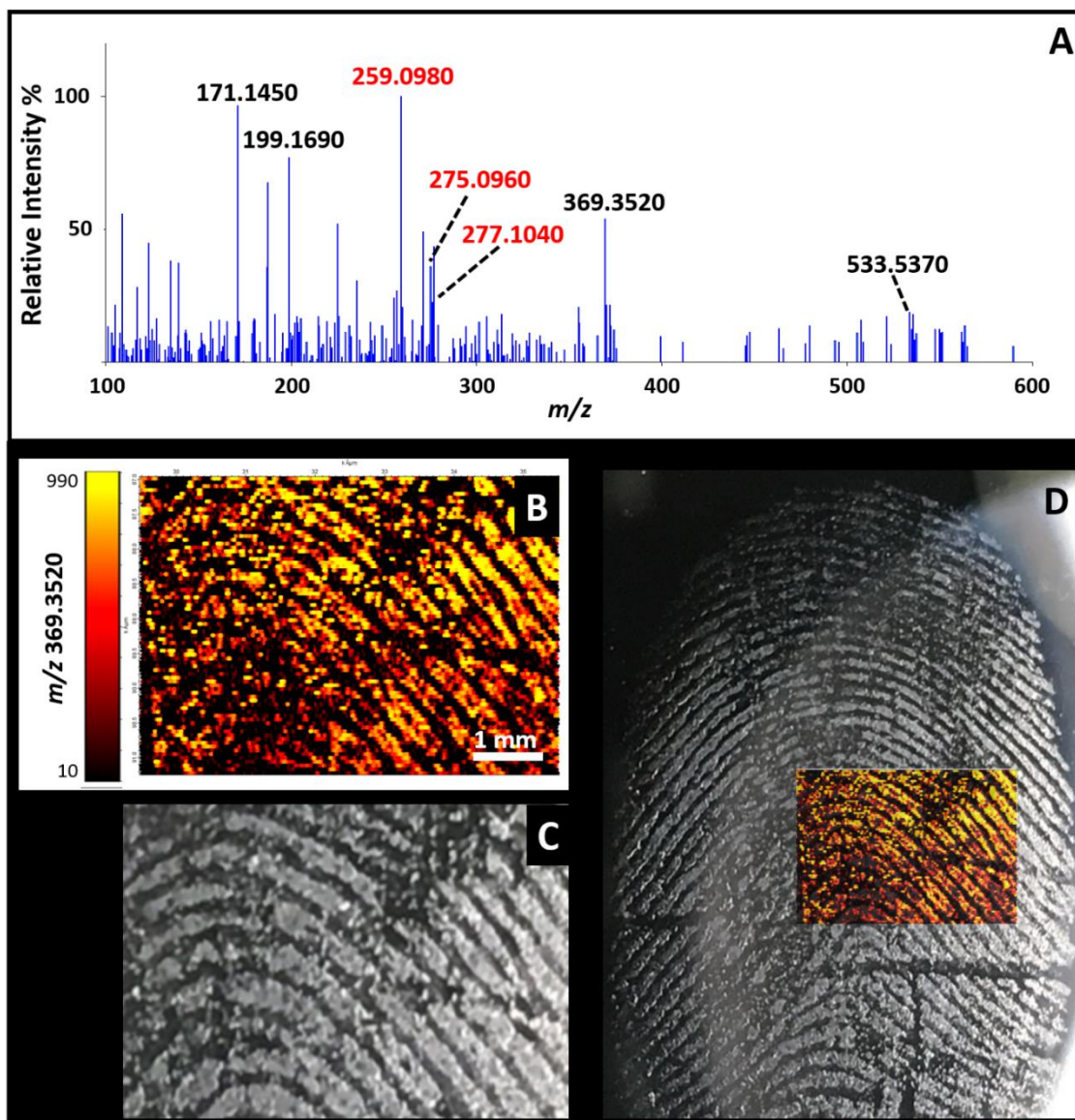


Figure 6.2. A LADI-MS-derived ion image and a representative LADI-mass spectrum obtained from the analysis of a fingerprint deposited after handling of *P. methysticum* plant material. The masses for several kavalactones are labelled in the mass spectrum (Panel A): m/z 259.0980-yangonin; m/z 275.0960-methysticin; and m/z 277.1040-dihydromethysticin. The LADI-MS ion image is shown of m/z 369.3520, a mass that is consistent with that of dehydroxylated cholesterol (Panel B). Panel C shows an optical image of the area of the fingerprint that was ablated in the experiment. Panel D shows the cholesterol ion image overlaid on a photograph of the latent fingerprint. Adapted with permission from: Fowble, K. L., and Musah, R. A. "Simultaneous imaging of latent fingerprints and detection of analytes of forensic relevance by laser ablation direct analysis in real time imaging-mass spectrometry (LADI-MS)." *Forensic Chem*, **15**, 100173 (2019), Copyright 2019, Elsevier.⁷⁵

6.2.3. LADI-MS analysis of a pseudoephedrine-laden latent fingerprint

Drug manufacturers have a history of turning to over-the-counter sources of pseudoephedrine for use in the production of methamphetamine. Decongestants containing this compound are typically packaged and ingested in capsule form, thereby making direct exposure of the hands and fingers to pseudoephedrine highly unlikely. Therefore, the detection of pseudoephedrine in a latent fingerprint may suggest that the drug was removed from the capsule for the purpose of being misused. Figure 6.3 shows a mass spectrum and ion images of molecules detected in a print that was deposited after the handling of pseudoephedrine. Fingerprint ridge patterns for endogenous dehydroxylated cholesterol (m/z 369.3480) and exogenous protonated pseudoephedrine (m/z 166.1240) are presented in Panels B and C, respectively, and the mass spectrum in Figure 6.3 (Panel A) shows the peak for protonated pseudoephedrine (m/z 166.1240), thus confirming the exposure of the individual's fingers to this material. Panel D shows an overlay of the ion image of dehydroxylated cholesterol on a photograph of the latent print prior to LADI-MS analysis, to reveal that the ridge patterns in the ion image match those in the latent print.

6.2.4. LADI-MS analysis of a developed and lifted latent fingerprint

While the aforementioned results demonstrate proof-of-principle that LADI-MS can be applied to latent print imaging under ideal conditions, the approach would be most useful if it could be applied to prints lifted from surfaces, including the tape used to lift developed fingerprints at a crime scene. To investigate whether this could be accomplished, a fingerprint

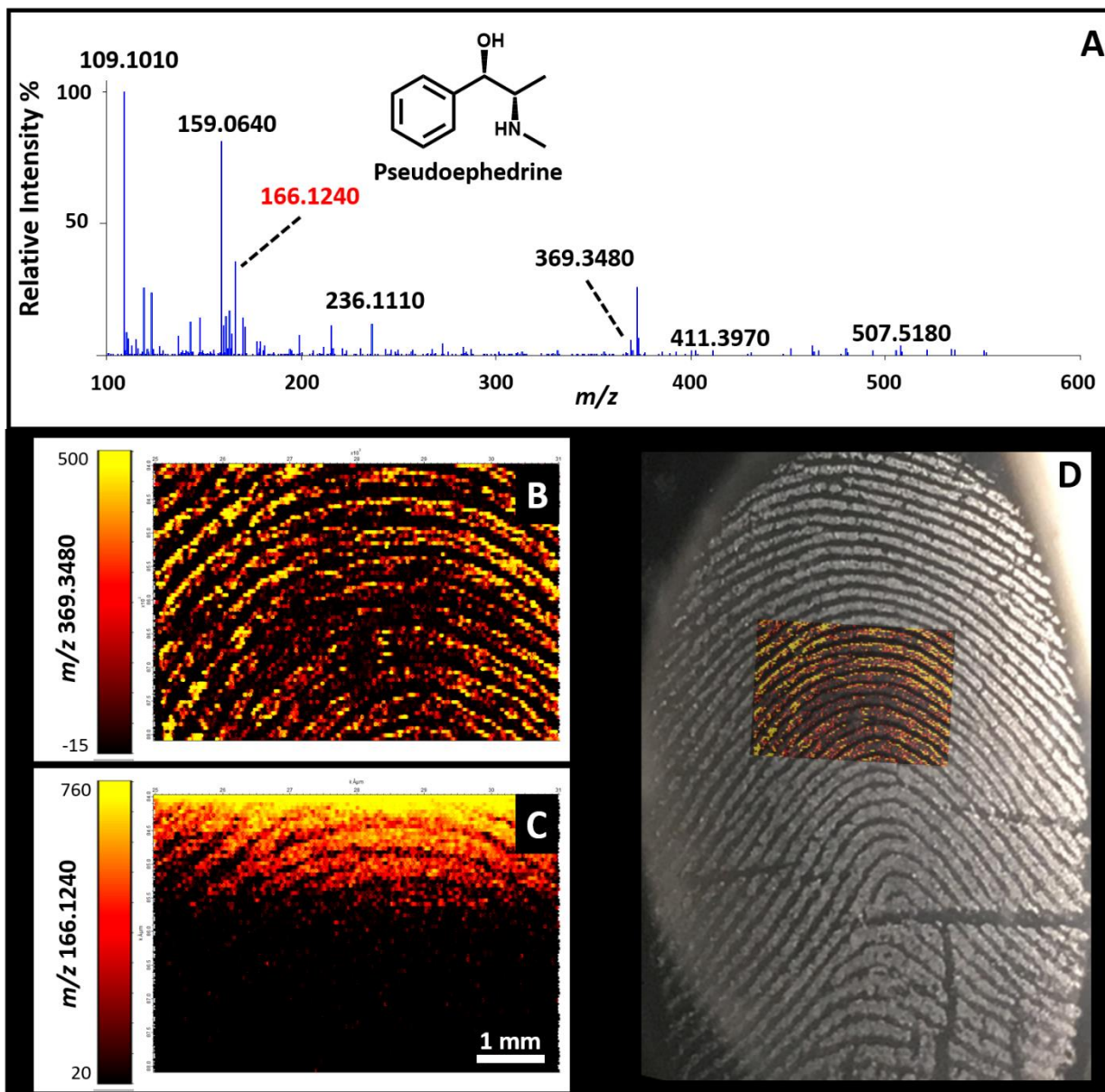


Figure 6.3. A LADI-MS-derived mass spectrum and ion images showing the presence of endogenous and exogenous molecules in a pseudoephedrine-laden fingerprint. Panel A shows the mass spectrum of a fingerprint deposited after exposure to pseudoephedrine with the mass for protonated pseudoephedrine (m/z 166.1240) labelled in red. The color-overlaid LADI-MS ion images of endogenous cholesterol (Panel B) and exogenous pseudoephedrine (Panel C) in a latent fingerprint are shown. The 1 mm scale bar in the ion image applies to both images. The ion image of cholesterol is shown overlaid on a photograph of the latent print (Panel D). Adapted with permission from: Fowble, K. L., and Musah, R. A. "Simultaneous imaging of latent fingerprints and detection of analytes of forensic relevance by laser ablation direct analysis in real time imaging-mass spectrometry (LADI-MS)." *Forensic Chem*, **15**, 100173 (2019), Copyright 2019, Elsevier.⁷⁵

was deposited onto a glass slide and subsequently dusted with fingerprint dusting powder. The dusted print was lifted using clear packing tape. The tape was then deposited onto the sample plate (adhesive side up) for analysis. Figure 6.4 shows the ion image of dehydroxylated cholesterol (m/z 369.3536) on the lifted tape. Some fingerprint ridge detail is revealed in the ion image. The loss of ridge detail in this ion image may be a result of the unpracticed hand used for the dusting of the fingerprint prior to lifting, or the use of a fingerprint development technique that is suboptimal for subsequent LADI-MS analysis.

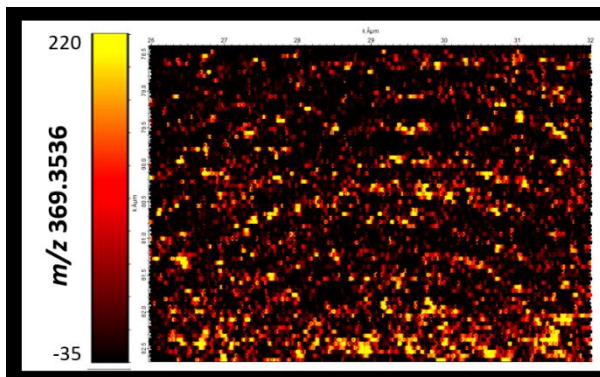


Figure 6.4. Ion image of dehydroxylated cholesterol in a lifted latent fingerprint, imaged on the adhesive side of packing tape by LADI-MS. Adapted with permission from: Fowble, K. L., and Musah, R. A. “Simultaneous imaging of latent fingerprints and detection of analytes of forensic relevance by laser ablation direct analysis in real time imaging-mass spectrometry (LADI-MS).” *Forensic Chem*, **15**, 100173 (2019), Copyright 2019, Elsevier.⁷⁵

6.2.5. *Micro-ablation of an explosive material located within a latent fingerprint*

Another way to link an individual to an illicit substance while retaining the fingerprint image, is by completing an analysis without disturbing the print at all. As an example, the LADI-MS system’s objective magnifying lens enabled visual detection in a fingerprint of a particle of the explosive RDX post exposure of this substance to the fingers. This is illustrated in the Figure 6.5 inset. The laser, with a spot size of $80\ \mu\text{m}^2$, was used to ablate the RDX particle, thus

preserving the full fingerprint for further subsequent analysis by other forensic techniques. The mass spectrum in Figure 6.5 clearly shows chlorinated RDX (m/z 257.0058) as the base peak.

6.2.6. Demonstration of the advantages of an ambient ionization mass spectrometric approach for latent fingerprint analysis

Unlike many of the most widely used IMS techniques, LADI-MS experiments are conducted in open air without the need for high-vacuum. This is important, as the chemical composition of fingerprints has been shown to change

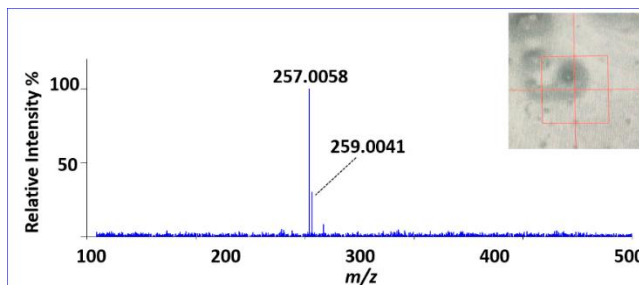


Figure 6.5. Laser ablation DART-mass spectrum of an RDX particle located in a latent fingerprint and detected using methylene chloride as a dopant. The m/z value 257.0058 is chlorinated RDX explosive. The inset shows a photograph of the magnified image of the RDX particle. Adapted with permission from: Fowble, K. L., and Musah, R. A. "Simultaneous imaging of latent fingerprints and detection of analytes of forensic relevance by laser ablation direct analysis in real time imaging-mass spectrometry (LADI-MS)." *Forensic Chem*, **15**, 100173 (2019), Copyright 2019, Elsevier.⁷⁵

within time frames as short as an hour on exposure to high-vacuum conditions.²²³ Typical high spatial resolution IMS experiments require at least a few hours for analysis, during which the fingerprint is exposed to high-vacuum conditions which change its composition over time. For example, squalene, tetradecanoic acid, pentadecanoic acid, hexadecanoic acid, and octadecanoic acid (with protonated masses of m/z 411.3991, m/z 229.2168, m/z 243.2324, m/z 285.2794, and m/z 257.2481, respectively) in fingerprints have been shown to be depleted after exposure to a high-vacuum environment.²²³ In a LADI-MS spectrum (Figure 6.6-top panel) acquired under ambient conditions, all five of the aforementioned molecules were detected within 6 mmu of their calculated protonated high-resolution masses (labelled in red). Additionally, to confirm that these molecules remained detectable in aged fingerprints, analysis of an aged print was

performed. Figure 6.6 shows a comparison of LADI-MS spectra of a fresh ~1 h print (top panel) versus a 96 h print (bottom panel). Although the mass spectrum of the aged print does not contain all of the molecules observed in the fresh print, the endogenous species tetradecanoic acid and squalene, in their protonated forms at m/z 229.2089 and m/z 411.3967 respectively, were detectable.

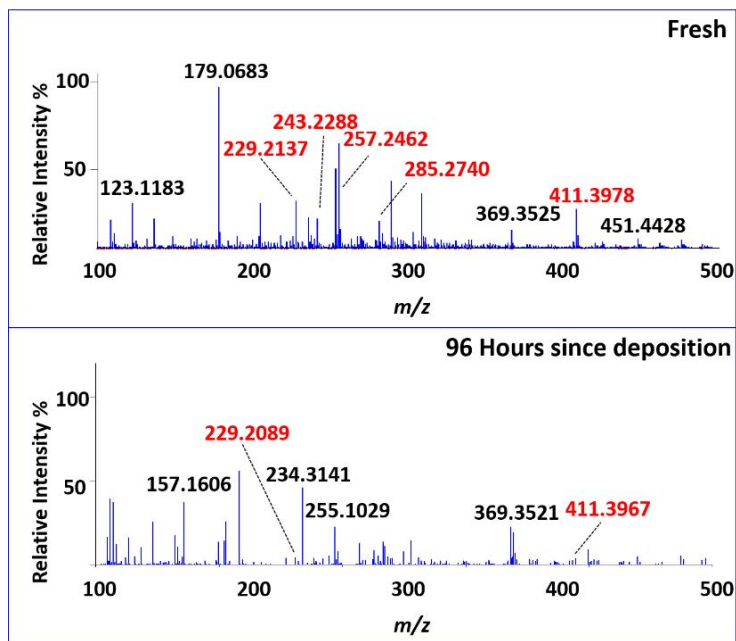


Figure 6.6. LADI-mass spectra of a “fresh” blank fingerprint (top) and a blank latent fingerprint analyzed after 96 h (bottom). The masses indicated in red represent tetradecanoic acid (nominal m/z 229), pentadecanoic acid (nominal m/z 243), hexadecanoic acid (nominal m/z 257), octadecanoic acid (nominal m/z 285), and squalene (nominal m/z 411). Adapted with permission from: Fowble, K. L., and Musah, R. A. “Simultaneous imaging of latent fingerprints and detection of analytes of forensic relevance by laser ablation direct analysis in real time imaging-mass spectrometry (LADI-MS).” *Forensic Chem*, **15**, 100173 (2019), Copyright 2019, Elsevier.⁷⁵

6.3. Discussion

While a variety of IMS techniques have been directed to latent fingerprint detection, the method described here is distinguished from these in that there are no sample preparation steps necessitated by the MS approach, and the experiments are completed under ambient and soft ionization conditions. The imaging experiments are also completed in a short time frame (not exceeding 3 h for a single analysis), which when combined with the limited sample preparation required is more rapid than most other techniques. The absence of a vacuum circumvents the problem of outgassing and thus avoids instrument depressurization time²²⁴ and the loss

(evaporation) of analytes of interest.²²³ As a soft ionization source, the DART does not cause extensive analyte fragmentation, which can occur in SIMS imaging experiments. However, SIMS is distinguished in providing high enough spatial resolution to reveal the locations of individual sweat glands in fingerprints.²⁰⁹

In comparison to MALDI-MS, SALDI-MS and SIMS, DESI-MS and desorption electro-flow focusing ionization (DEFFI)-MS are some of the only other ambient ionization IMS techniques (both utilizing a flow of solvent), that have been applied to latent fingerprints.^{37, 214, 225-226} Although both approaches were successful in revealing them, the requirement for the application of solvent could potentially result in changes in the spatial distribution of analytes through molecule translocation caused by solvent.²²⁷ Since LADI-MS does not require solvent, changes in small-molecule distributions are less likely. Also, because LADI-MS does not rely on solvent desorption, a broader range of molecules of varying polarities can be detected simultaneously in a single experiment. However, the ionization mechanism of the DART ion source relies heavily upon the proton affinity of the analytes. This can affect the sensitivity of the LADI-MS instrumentation for the detection of some analytes of forensic relevance. Additionally, it should be noted that for DEFFI- and DESI-MS experiments, the solvent selection could be optimized for the detection of specific molecules, and both have been successfully used to detect cocaine and the explosive RDX.^{37, 71, 228-229} In comparison to traditional DESI-MS imaging experiments which typically have a spot size of ~200 μm ,²³⁰ LADI-MS can obtain higher spatial resolution ion images. However, the development of *nano*-DESI-MS and DEFFI-MS has improved upon these spatial resolutions. Sensitivity experiments to explore analyte detection limits for the LADI-MS technique are the subject of ongoing investigations.

The micro-ablation application of LADI-MS described here is promising in its applicability to forensic fingerprint analysis. The latent fingermark is not destroyed and can be further analyzed using traditional development techniques with ninhydrin, cyanoacrylate fuming, or dusting with powders, all techniques that are broadly accepted in the courts. In addition, the sample can be micro-ablated to yield simplified spectra of materials of interest in a specific area of the print. This latter capability is similar to the approach reported by Clemons et al.²³¹ in which an area of a print was nanoextracted and the extract was subsequently analyzed by DART-MS to reveal the presence of explosives. However, the LADI-MS approach differs from this in that no solvent extraction step is required.

6.4. Conclusions

The LADI-MS technique was used to map the spatial distributions of endogenous fingerprint compounds and detect the psychoactive compounds cocaine and yanonin, and non-psychoactive pseudoephedrine, as well as the explosive RDX in latent fingermarks. The combination of the detection of psychoactive materials and the spatial distribution mapping of endogenous molecules in the same experiments can provide a direct link between an individual (through fingerprint identification) and substances with which they have come into contact. The laser was used to ablate a single particle of RDX in a latent fingermark without disturbing the rest of the print, thus allowing for further testing and photography by conventional methods. This technique could be applied to a range of psychoactive and explosive molecules in fingerprints and can be operated in positive or negative ion mode, permitting the detection of a variety of

molecules. The ambient ionization conditions of the technique allow for the detection of molecules that would be lost under the high-vacuum conditions required by other methods, and prevent extensive fragmentation of the analytes of interest. LADI-MS requires no sample pretreatment steps and can be performed on non-conductive surfaces. The application of LADI-MS to the detection in fingerprints of other small molecules such as endogenous/semi-endogenous drug metabolites are the subjects of ongoing investigations and could help distinguish between individuals who have handled forensically relevant material versus those who have ingested it.

6.5. Materials and Methods

6.5.1. Chemicals

RDX, pseudoephedrine in methanol, and exempt preparations of cocaine in acetonitrile were purchased from Cerilliant (Round Rock, TX, USA). *P. methysticum* powder was purchased from Bouncing Bear Botanicals (Lawrence, KS, USA). Methylene chloride (HPLC grade) was purchased from Fisher Scientific (Pittsburgh, PA, USA). High-purity helium and nitrogen gases were purchased from Matheson (Manchester, NH, USA) or Airgas (Albany, NY, USA).

6.5.2. Fingerprint residues

All of the handling and deposition of fingerprint experiments were approved and conducted in accordance with the University at Albany's Institutional Review Board.

Cocaine-laden print

An aliquot (30 μL) of a solution of cocaine in acetonitrile (1 mg mL^{-1}) was deposited on a clean glass microscope slide (Thermo Fisher Scientific, Waltham, MA, USA) and allowed to dry. A finger was then rubbed on the dried residue and a fingermark was subsequently deposited onto a clean glass microscope slide for analysis.

Kava-laden print

A small amount (< 3 mg) of *P. methysticum* (Kava) powder was rubbed between the thumb and index finger. A fingermark was then deposited onto a clean glass microscope slide.

Pseudoephedrine-laden print

An aliquot (30 μL) of pseudoephedrine in methanol (1 mg mL^{-1}) was deposited onto a glass slide and allowed to dry. The residue was rubbed with the index finger and a fingermark was subsequently deposited onto a clean glass slide.

Lifted print

A human sebum-enriched fingermark was created by rubbing a clean index finger across the forehead and applying it to a clean glass microscope slide. The latent print was then dusted with black latent print powder (Sirchie, Youngsville, NC, USA). Clear single-sided adhesive packing

tape (Staples, Albany, NY, USA) was then placed on the deposited and dusted fingerprint to lift it. The tape was placed adhesive side up on the sample plate for analysis, and was affixed to the sample plate by the use of additional packing tape.

RDX-laden print

RDX solution (1 mg mL⁻¹) was allowed to dry to a residue on a clean glass slide. A clean index finger was then swiped across the forehead and subsequently exposed to the RDX residue and a fingerprint was deposited onto a clean glass microscope slide.

Blank print

A clean index finger was rubbed across the forehead to provide a human sebum-enriched fingerprint that was then deposited on a glass microscope slide for LADI-MS analysis. A second fingerprint was deposited in the same manner and analyzed approximately 96 hours later.

6.5.3. LADI-MS analysis

The LADI-MS system was set up as previously described (Chapter 2).⁷³ Ion images were acquired through the coupling of an ESL NWR 213 laser ablation system (ESL, Bozeman, MT, USA) and a DART-HRMS instrument by way of a heated stainless-steel transfer line. A glass tee was used to direct the flow from the transfer line to the DART-HRMS interface. The high-resolution mass spectrometers used for the imaging and RDX experiments were a JEOL AccuTOF LC-plus

JMS-T100LP HRMS and a JEOL AccuTOF-LP 4G HRMS (JEOL USA, Inc., Peabody, MA, USA) with resolving powers of 6,000 and 10,000 FWHM, respectively. The mass spectrometers were operated with an orifice 1 voltage of 20 V and orifice 2 and ring lens voltages of 5 V each in positive and negative ion mode. The mass ranges collected for the experiments were m/z 100-700, with the exception of the RDX print which was collected with a mass range of m/z 150-700. The rate of the DART ion source helium flow was 2.0 L min⁻¹. PEG was used as a reference standard for the calibration of the collected spectra. TssPro 3.0 (Shrader Analytical Software Solutions, Grosse Pointe, MI, USA) and the msAxel Data Processing software package (JEOL USA, Inc., Peabody, MA, USA) were used for peak calibration and peak centroiding. Reconstructed ion currents were created for each of the ions of interest and imported into Lolite imaging software (University of Melbourne, AUS). Mass spectral analysis, elemental composition determination and isotope analysis were performed using Mass Mountaineer software (Massmountaineer.com, Portsmouth, NH, USA).

The DART-HRMS and laser parameters used for the imaging experiments are listed in Tables 6.1 and 6.2, respectively. Each imaging experiment was completed within 3 h.

Table 6.1. DART-HRMS parameters used for fingerprint analyses.*			
Sample	Ion mode	Ion guide voltage**	MS acquisition rate
Cocaine	+	1000 V	0.5 s scan ⁻¹
<i>P. methysticum</i>	+	1000 V	0.5 s scan ⁻¹
Pseudoephedrine	+	1000 V	0.5 s scan ⁻¹
Lifted (blank)	+	1000 V	0.5 s scan ⁻¹
RDX	-	1500 V	0.3 s scan ⁻¹

*All analyses were performed at a DART heater temperature of 500 °C, except RDX which was conducted at 350 °C.

**The ion guide voltage is also referred to as the “peaks voltage” of a JMS-T100LP instrument.

Sample	Fluence	Scan speed	Spot size	Spatial resolution
Cocaine	1.7 J cm ⁻²	55 μm s ⁻¹	60 x 60 μm ²	126 x 60 μm ²
<i>P. methysticum</i>	1.7 J cm ⁻²	55 μm s ⁻¹	60 x 60 μm ²	126 x 60 μm ²
Pseudoephedrine	1.7 J cm ⁻²	55 μm s ⁻¹	60 x 60 μm ²	126 x 60 μm ²
Lifted (blank)	1.7 J cm ⁻²	55 μm s ⁻¹	60 x 60 μm ²	126 x 60 μm ²
RDX	1.1 J cm ⁻²	-	80 x 80 μm ²	-

*The RDX detection experiment was not an imaging-based analysis, and thus does not have imaging-relevant parameters listed.

In the case of the RDX detection experiment, the laser was used to ablate a single particle and the fingerprint was not imaged. Methylene chloride was used as a dopant to assist in the detection of RDX. A syringe pump, operating at 0.03 mL h⁻¹ was used to introduce methylene chloride to the glass tee junction at the DART-HRMS interface.

Chapter 7: Other Forensic Applications of LADI-MS—Analysis of Inks on Paper and Gunshot Residue

7.1. Introduction

In Chapter 6, the utility of LADI-MS in the mapping of forensically relevant exogenous compounds in fingerprints was demonstrated. However, there are many more issues related to crime scene investigation to which LADI-MS can be applied. A benefit of LADI-MS is that it can be employed for analysis of a multitude of forensic samples, including ammunition and questioned documents. Currently, there are many different instruments and technologies that are used to analyze forensically relevant sample types. These include GC-MS, scanning electron microscopy-energy-dispersive X-ray spectroscopy (SEM/EDX), colorimetric assays, and Raman, NMR, and IR spectroscopy, among others. Given the usual circumstance that the available forensic evidence is limited, it would be highly advantageous if the output of multiple forms of analyses (e.g. imaging as well as chemical content information) could be acquired within a single experiment. This would streamline and speed up the data acquisition process, reduce the amount of evidence required, and potentially reveal additional information essential to solving a crime. In this chapter, we demonstrate the utility of LADI-MS in the forensic mapping of the spatial distributions of ink constituents when applied on paper, and to the detection of both the organic and inorganic components of gunshot residue (GSR).

7.1.1. Analysis of inks on paper

An important area of investigation in criminal cases is the examination of paper records or artistic works. These can include legal documents, wills, deeds, bank checks, or even art pieces. In this regard, confirming authenticity and assessing whether unauthorized changes have been made are critical. For example, one way to determine if modifications have been made to a written document after its original creation is to assess whether the handwriting is consistent throughout. However, this approach can be quite subjective. Another is to determine whether there are inconsistencies in the composition of the inks used. If there are multiple sources of ink, such as what might occur if multiple numbers are added to the value previously inscribed on a check, this may indicate that a crime has been committed.

Inks used in ballpoint and gel pens are comprised of a variety of components that contribute to its color as well as the viscosity and fastness.²³² These compounds, which are often proprietary, can include pigments, dyes, solvents, resins, lubricants, and surfactants.²³² Due to this, the chemical composition of inks can vary drastically between brands, and these variations can be used to discriminate between different pens used on a document, and even assist in brand attribution.

Commonly, forensic examiners use spectroscopic techniques, including hyperspectral imaging, for the detection of alterations made to a document.²³²⁻²³⁵ These non-destructive approaches can help distinguish between different ink compositions. Hyperspectral imaging, for example, consists of shining different wavelengths of light on the surface of the questioned document.²³³⁻²³⁸ Different inks will fluoresce under different wavelengths, thereby alerting the

examiner to the presence of a potential forgery or other alteration made to a painting or document. However, it was recently reported that even with the coupling of hyperspectral imaging and chemometric analysis, some inks are so similar to one another that identification of unique brands could not be accomplished.²³³ Although the fluorescence under different wavelengths of light could provide a confirmation of the use of a second pen, ink, or marker, the determination of the specific brand or compounds in the inks cannot generally be accomplished by hyperspectral imaging alone.

Mass spectrometric techniques can provide more definitive discrimination between the pens or markers used to alter a document, and have been applied to the determination of the chemical compositions of different inks. The approaches used include GC-MS, LC-MS, DESI-MS, DART-MS, MALDI-MS, LDI-MS, and paper spray-MS.^{232, 239-248} Some of the work accomplished has focused on the identification of dyes and pigments used for the coloring of the inks,^{240, 242-243, 248} while others focused on alternative components in the mixture such as solvents and resins.^{241, 248} DART-MS has been successfully applied to the determination of both dyes and other constituents of ink, as well as to the identification of a brand of pen based on library matching of the DART-derived spectra.²⁴⁵⁻²⁴⁶

The disadvantage of using typical MS approaches alone is the absence of spatial distribution information. It would be helpful to determine where on the document an alteration has occurred. With the previously mentioned MS studies, samples from all areas of the document would have to be used to determine where a change in ink has occurred. Again, IMS would provide this information. A number of IMS techniques including SIMS, LDI-MS, SALDI-MS, DESI-MS, and desorption atmospheric pressure chemical ionization MS imaging (DAPCI-MS), have been applied

to the imaging of the spatial distributions of the components of inks on paper.^{54, 232, 249-252} The advantages of an IMS approach are the ability to determine exactly where in a document an alteration was made and also, in some cases, the order of deposition.²⁵¹⁻²⁵² In this chapter, successful application of LADI-MS to the mapping of the spatial distributions of small molecules in inks on paper is described.

7.1.2. *Gunshot residue analysis (GSR)*

When a firearm is discharged, the components of the gunpowder used to propel the projectile are transferred to the surface of the bullet. The major organic components of smokeless gunpowder include plasticizers, propellants, and stabilizers composed of nitrocellulose, nitroglycerine, diphenylamine, and ethylcentralite, among other compounds.²⁵³ Also contained within GSR are inorganic constituents, including barium, antimony, and lead. The majority of analytical techniques used in the identification of GSR focus on the detection of these inorganics.²⁵⁴⁻²⁵⁶ However, the ability to detect and identify the organic compounds in GSR has become important because of the increasingly common absence of heavy metals in ammunition.²⁵⁷⁻²⁶¹ The most common technique for the detection of metals in GSR (i.e. Ba, Sb, Pb) is SEM/EDX. It is a highly sensitive technique that can map the morphology (by SEM) and composition (by EDX) of a single particle of GSR.²⁶² However, with the advent of heavy-metal free smokeless powders, this technique can lead to false negatives for GSR if Ba, Pb, and Sb are not detected.

In response to the more widespread use of smokeless powders, there has been an increase in the development of techniques used to detect the organic components of GSR. These include LC-MS, LC-MS/MS and LC-QTOF.^{257, 261, 263} Nitrocellulose and nitroglycerine, two common components in GSR, are found in many other products, such as varnishes and lacquers. This complicates the assessment of whether the source of these compounds is smokeless powder material or an innocuous household product. When stabilizers such as diphenylamine are observed along with nitrocellulose and nitroglycerine, the results are a more definitive indication of GSR. However, the LC-MS techniques used in such analyses can require extensive extraction procedures and sample preparation steps. Moreover, they do not permit the simultaneous detection of inorganic components.^{257, 261, 263}

There are currently no routine methods that permit the detection of both organic and inorganic components of GSR. However, in a recent report, LAESI-MS was used to detect both organics and inorganics using a single instrument, and the acquired data was subjected to statistical analysis processing which revealed that manufacturer identification is feasible.²⁶⁴

Herein, we describe the application of LADI-MS to the two aforementioned forensic areas of interest (i.e. analysis of inks on paper and GSR). The spatial distributions of small molecules unique to different pens and markers are presented to reveal document alteration. Additionally, we demonstrate the capability of LADI-MS to detect both inorganic and organic components of GSR and fired bullets.

7.2. Results

7.2.1. Application to inks on paper

To demonstrate the utility of LADI-MS to the mapping of small molecule spatial distributions within inks that have been applied to paper, a peace sign was drawn using two different colors of Sharpie® markers (Figure 7.1 Panel A). The blue Sharpie® was used to draw the outer circle and the orange Sharpie® was used to draw the inner lines. To determine the masses that could be used to distinguish between the two colored inks, a piece of paper was saturated with each color of ink and analyzed by DART-MS directly. The resulting mass spectra are shown in Figure 7.1 (Panels B and C). Along with a photograph of the peace sign (Panel A) that was imaged by LADI-MS with a laser spot size of $70 \mu\text{m}^2$, Figure 7.1 shows the spatial distribution

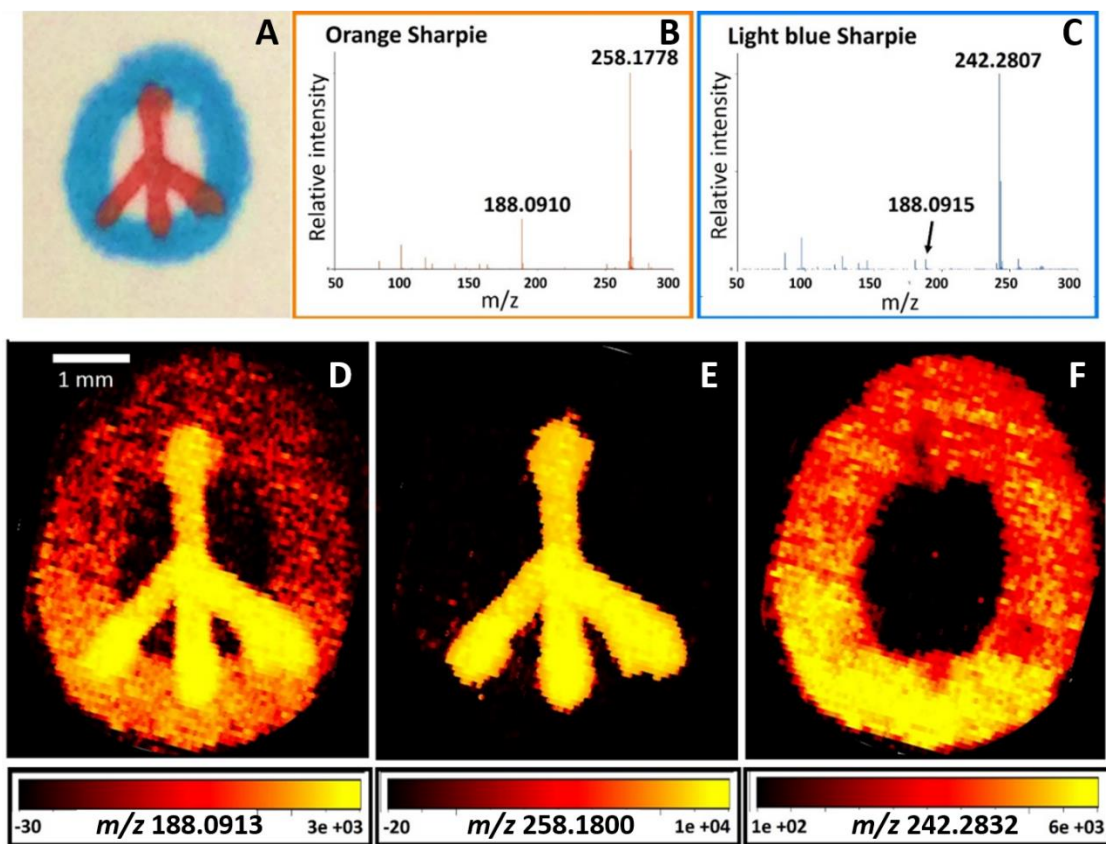


Figure 7.1. A peace sign image drawn with blue (outer circle) and orange (inner lines) Sharpie® markers (Panel A), and the corresponding DART-mass spectra and LADI-MS ion images. The representative DART-mass spectra of the orange and blue ink on computer paper are shown in Panels B and C respectively. The color-overlaid ion images of the m/z values 188.0913, 258.1800, and 242.2832 showing the full peace sign image, only the inner lines, and only the outer circle are featured in Panels D, E, and F respectively.

maps of three compounds found in the Sharpie® markers. The identity of m/z 188 is unknown, but it is a compound common to both the light blue and orange Sharpie® inks, as shown in Panel D of Figure 7.1. The spatial distribution of this analyte gives the full image of the peace sign. The identity of m/z 258 is also unknown, but it is only found in the orange ink (Panel E). The mass of m/z 242 is the base peak in the light blue marker mass spectrum, and it was not detected in the orange ink (Panel F).

As blue and orange markers of the same brand can easily be visually distinguished, the same analysis was applied to the imaging of a peace sign drawn with two different brands of black marker that looked identical on visual examination (Figure 7.2. Panel A). In this case, the

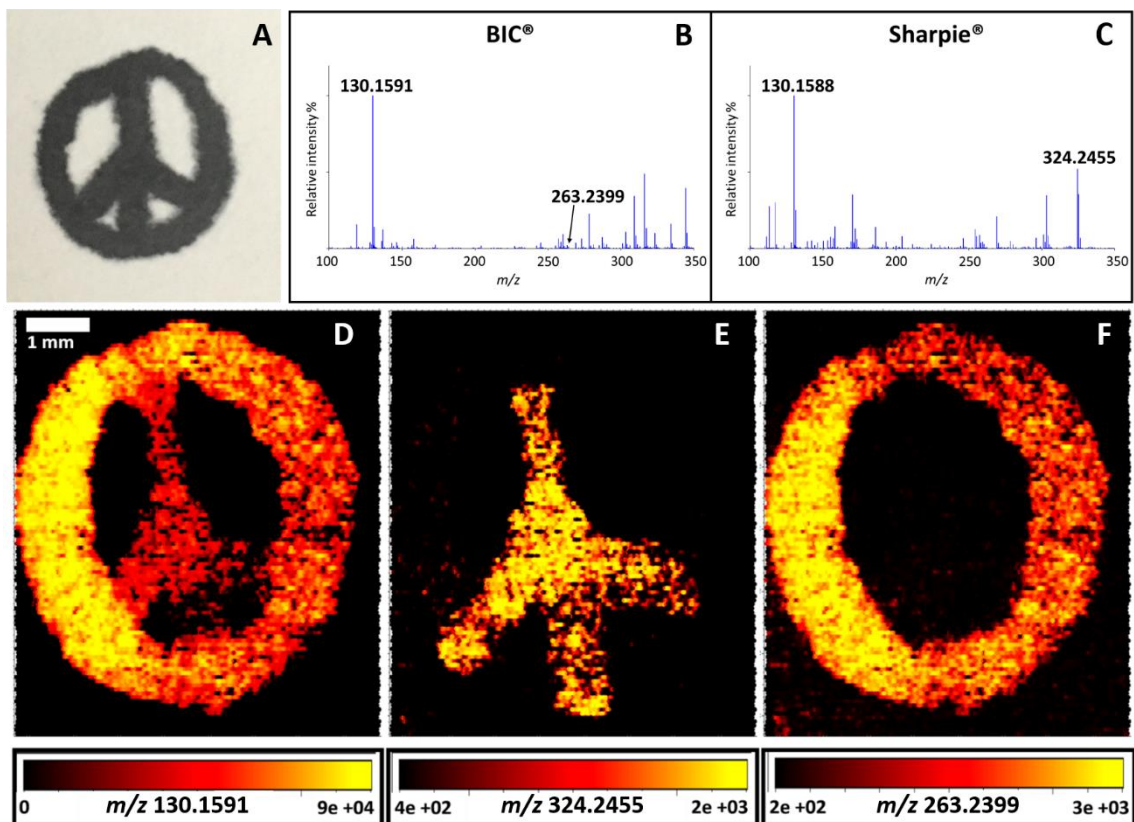


Figure 7.2. A peace sign image drawn with Bic® and Sharpie® black markers (Panel A), and the corresponding DART-mass spectra and LADI-MS ion images. The representative DART-mass spectra of the inks on computer paper are shown in Panels B and C. The color-overlaid ion images of the m/z values 130.1591, 324.2455, and 263.2399 showing the full peace sign image, only the inner lines, and only the outer circle are featured in Panels D, E, and F respectively.

outer circle was drawn using a black Bic® marker and the inner lines were completed with a Sharpie® black marker. Figure 7.2 shows the peace sign image (Panel A), the associated mass spectra obtained from direct analysis of the inks (Panels B and C), and the ion images of three analytes (Panels D, E, and F) acquired with a spatial resolution of 170 x 80 μm². Again, the spatial distributions of the unique ions in each brand of ink showed the two distinct areas of the peace sign drawn with the respective marker.

To represent a more realistic sample, two numbers were written in black pen and subsequently altered to read a different value using a second black pen. The two brands used were Paper mate® and Uni-ball®. In the first instance, the number 9 was converted into an 8. The resulting LADI-MS ion images revealed the alterations. In Figure 7.3 Panel A, the full number 8 is

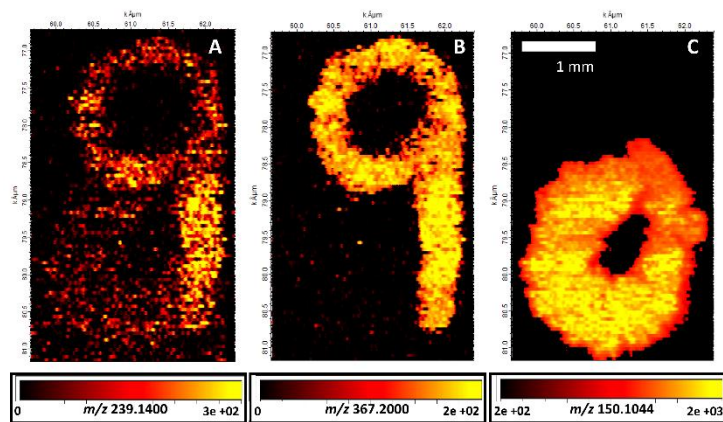


Figure 7.3. The color-overlaid ion images for three compounds of interest detected in black pen inks. Panel A shows the spatial distribution of a mass of a compound found in both inks in the form of “8”. Panels B and C show the ion images for components unique to the individual pen brands Paper mate® and Uni-ball®, respectively. The 1 mm scale bar applies to all images.

shown with the ion image of m/z 239.1400. Although this mass was found in both brands of inks, it is found with a higher intensity in the brand used to draw the original 9 (Paper mate®). Panels B and C (Figure 7.3) show the spatial distributions of two m/z values, 367.2000 and 150.1044, unique to the Paper mate® and Uni-ball® brands of ink, respectively. Another example of this application of LADI-MS is the adding of a 0 at the end of a number. In this case, the number 10, written with the Paper mate® pen, was changed to 100 with the addition of a 0 with the Uni-ball®

ink. In Figure 7.4 Panels A, B, and C, three ion images for the m/z values 239.1350, 367.2200, and 327.2052 are shown. The ion images reveal the full number (100) and the 10 and 0 written in different inks.

7.2.2. Application to fired bullets and other inorganic materials

Organic components

A Speer .40 caliber S&W copper-jacketed bullet was fired from a handgun into a phone book that served to

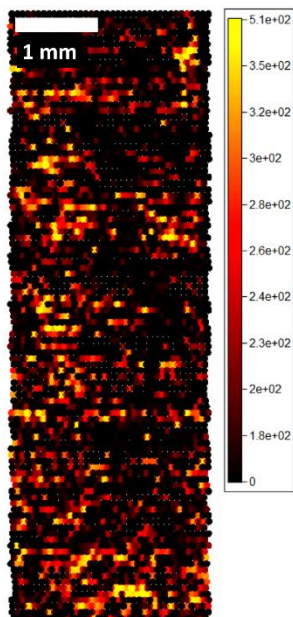


Figure 7.5. The color-overlaid ion image of m/z 170.0970, a mass consistent with that of diphenylamine. The scale bar in the upper left represents 1 mm.

capture it. The ActiveView software used to control the laser ablation pattern was operated to select one area of the fired bullet for ablation. The entire rectangular area (~2 mm x 7 mm)

was ablated using the DART-HRMS and laser parameters listed in Tables 7.1 and 7.2, resulting in a spatial resolution of 220.5 x 90 μm^2 .

Several components of gunpowder residue, including the plasticizers were monitored. Figure 7.5 shows the spatial distribution of m/z 170.0970, consistent with protonated diphenylamine, a known component of smokeless gunpowder. An m/z value consistent with

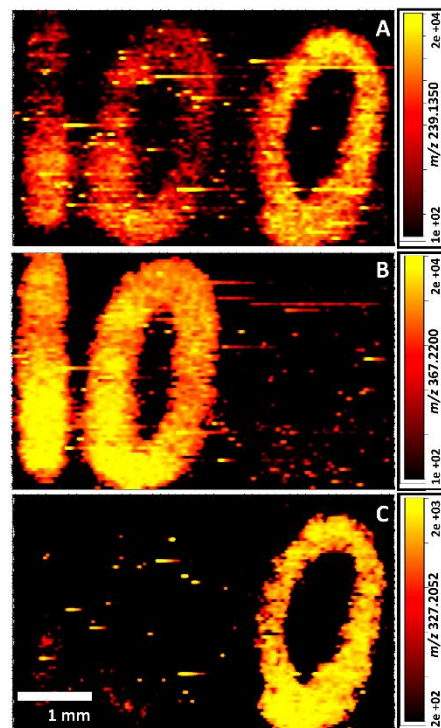


Figure 7.4. The color-overlaid ion images for three masses detected in black pen inks. Panel A shows the spatial distribution of a mass of a compound found in both inks in the form of “100”. Panels B and C show the ion images for components unique to the individual pen brands Paper mate® and Uni-ball®, respectively. The 1 mm scale bar applies to all images.

diphenylamine was found to cover the entirety of the area ablated by the laser, albeit with different relative intensities, as expected. Other m/z values consistent with components of smokeless powder (data not shown) were also detected including a mass of unknown identity at m/z 227.

Inorganic components

By coupling the laser ablation system to the DART-MS instrument, the detection of metals with the use of the chelating agent acetylacetonate (acac), was accomplished. Typically, metals are undetectable by DART-MS. The surface of a copper (Cu) jacketed bullet was ablated, and Cu (m/z 62.9) and its isotope (m/z 64.9) were detected as shown in Figure 7.6 Panel A. The base peak of the mass spectrum is associated with copper. A similar experiment was completed on the surface of a lead (Pb) plate. In Figure 7.6 Panel B, the mass spectrum contains the m/z values 203.9, 205.9, 206.9, and

207.9 at the appropriate relative intensities to confirm the detection of Pb and its isotopes. In the case of Pb, a number of other compounds were detected and thus the mass spectrum shown

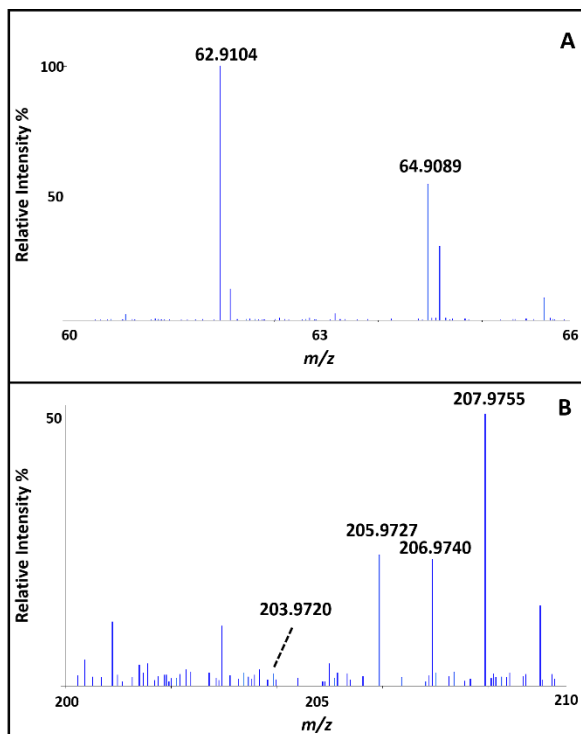


Figure 7.6. Mass spectra showing the detection of copper (Panel A) and lead (Panel B) after the application of acac to the surface of the metal. The labelled peaks correspond to copper and lead and their respective isotopes.

focuses on the narrow m/z range indicated, and the overall relative intensity of the most abundant Pb isotope (m/z 207.9755) is only 50%. Although these were not imaging experiments, the results illustrate that LADI-MS can be used to detect inorganics as well as image organics found in gunshot residue or other matrices.

7.3. Discussion

Although the compounds used for the mapping of the spatial distributions of two different brands of inks and markers were not identified, the presence of unique molecules for each brand implies that the identification of a specific marker/pen or manufacturer may be possible. This is further confirmed by work done previously that has shown the identification of pen inks by library matching and statistical analysis processing of MS-derived data.²⁴⁶⁻²⁴⁷ Currently, the disadvantage of the proposed application of LADI-MS to imaging of inks on paper is that the technique is destructive. Even at low fluences, the top layer of the paper and ink are ablated, resulting in a loss of ink on the surface of the paper. Further optimization of the approach could lower the amount of material ablated, thus making the destructiveness of the technique negligible, and permitting the retention of some of the ink on the surface of the document after ablation.

The application of LADI-MS to the detection of both organic and inorganic components of GSR is promising. The organic components can easily be detected, as DART-HRMS is optimized for the analysis of small organic molecules. The detection of the inorganic species is more surprising, as few other approaches can detect both inorganics and organics. To apply the

technique to the imaging of both organic and inorganic species, two experiments would have to be conducted. First, the analysis of the organic GSR components could be completed during a typical LADI-MS analysis as described in Chapters 3-6. Subsequently, the parameters of both the laser ablation system and the MS could be altered to run another imaging experiment for the analysis of inorganic species. A chelating agent like acac could be applied to a fired bullet surface or any other material exposed to GSR, and the collection of data would be completed. The reason for the imaging of the inorganic components after the analysis to detect organics is because the laser power needed for the detection of these species would most likely destroy the organic compounds.

7.4. Conclusions

The LADI-MS approach was utilized to map the spatial distributions of both organic and inorganic species in the forensically relevant applications of analysis of inks on paper and GSR. The ability to distinguish between inks applied using two different markers/inks was demonstrated. In principle, the chemical composition information obtained could be used for the determination of a specific brand of ink used. Additionally, LADI-MS can detect both the organic and inorganic species found in GSR, thus permitting the collection of data typically only obtained using multiple instruments. LADI-MS, like other IMS techniques, permits the acquisition of spatial distribution information as well as the chemical composition of the molecules detected. This is particularly important for forensics applications where evidence can be limited.

7.5. Materials and Methods

7.5.1. *Materials*

Whatman™ brand chromatography paper (Cat. No. 3001-851) and acetylacetone were purchased from Sigma Aldrich (St. Louis, MO, USA). The markers and pens used to draw peace sign images and numbers were obtained from an office supply store. Speer brand copper-jacketed ammunition (.40 caliber) was purchased from a sporting goods store. A small piece of lead was obtained from the University at Albany's machine shop (Albany, NY, USA). High-purity helium and nitrogen gases were bought from Airgas (Albany, NY, USA) or Matheson (Manchester, NH, USA).

7.5.2. *Inks on paper sample preparation*

Peace sign image (colored inks)

A peace sign was drawn using two different colors of Sharpie® brand markers. A light blue marker was used to draw the outer circle and the orange marker was used to draw the inner lines on computer paper. The small piece of paper was affixed to the sample drawer insert using double-sided carbon tape.

Peace sign image (black inks)

A peace sign was drawn using two different brands of black markers (Bic® and Sharpie®). The outer circle was created using the Bic® brand marker, and the inner lines were created using

the Sharpie® brand marker on computer paper. The resulting sample was affixed to the sample drawer insert using double-sided carbon tape and placed into the sample chamber for analysis.

Number images (black inks)

The number “9” was drawn on white computer paper. Subsequently, a circle was drawn, using a different pen, underneath the top part of “9” to simulate the number “8”. The original number was written using a Paper mate® brand pen, and the alteration was made using a Uni-ball® pen. In a second experiment, the number “10” was drawn on white computer paper using a Paper mate® brand pen. A second “0” was added using a black Uni-ball® pen to create the number “100”. Both pieces of paper were affixed to carbon tape and inserted into the sample chamber for LADI-MS analysis.

7.5.3. Ammunition and lead plate

The .40 caliber copper-jacketed bullet was fired, using a .40 caliber handgun, into a stack of phone books. The phone books served to capture the fired bullet. The bullet was retrieved and placed on silicone putty in the sample drawer for LADI-MS analysis. A dilute solution of acetylacetone in methanol was applied to the surface of the fired bullet prior to the analysis for the detection of inorganic species. For the detection of Pb, a lead plate (~7.5 cm²) was placed directly into the sample chamber for analysis. A small amount (< 20 µL) of acetylacetone in methanol was also applied to the surface prior to ablation.

7.5.4. LADI-MS analysis

The LADI-MS approach was set-up as described previously in Chapter 2.⁷³ The mass spectrometer used for both peace sign images and the fired bullet experiment was the JEOL AccuTOF LC-plus JMS-T100LP HRMS (JEOL USA, Inc., Peabody, MA, USA) with a resolving power of 6,000 FWHM coupled to the NWR213 unit by way of tygon tubing. The mass spectrometer used for the “number” experiments and the detection of lead experiment was a JEOL AccuTOF-LP 4G HRMS (JEOL USA, Inc., Peabody, MA, USA) with a resolving power of 10,000 FWHM coupled to the NWR213 unit with a heated stainless-steel transfer line. The DART ion source was operated with a helium flow rate of 2.0 L min⁻¹. The orifice 1 voltage was operated at 20 V with orifice 2 and ring lens voltages of 5 V each (unless otherwise noted). The DART-HRMS and laser ablation system parameters for each experiment are shown in Tables 7.1 and 7.2.

Sample	Gas heater temp	Ion guide voltage	MS acquisition rate
Color peace sign	350 °C	600 V	0.6 s scan ⁻¹
Black peace sign	550 °C	1000 V	0.5 s scan ⁻¹
9 to 8	500 °C	1000 V	0.3 s scan ⁻¹
10 to 100	550 °C	1000 V	0.5 s scan ⁻¹
Organic GSR	350 °C	600 V	0.75 s scan ⁻¹
Inorganic GSR (Cu)**	350 °C	400 V	0.75 s scan ⁻¹
Lead**	500 °C	1000 V	0.3 s scan ⁻¹

*All analyses were carried out in positive ion mode.

**The orifice 1 voltage for the detection of inorganic species was raised to 180 V.

Sample	Fluence	Scan speed	Spot size	Spatial resolution
Color peace sign	21 J cm ⁻²	75 μm s ⁻¹	70 x 70 μm ²	167.5 x 70 μm ²
Black peace sign	15 J cm ⁻²	75 μm s ⁻¹	80 x 80 μm ²	170 x 80 μm ²
9 to 8	2 J cm ⁻²	45 μm s ⁻¹	50 x 50 μm ²	95 x 50 μm ²
10 to 100	4.5 J cm ⁻²	45 μm s ⁻¹	50 x 50 μm ²	104 x 50 μm ²
Organic GSR	15 J cm ⁻²	90 μm s ⁻¹	90 x 90 μm ²	220.5 x 90 μm ²
Inorganic GSR (Cu)	30 J cm ⁻²	-	90 x 90 μm ²	-
Lead	110 μm**	-	-	-

*A circular spot size with a diameter of 110 μm was used for the detection of lead.

Concluding Remarks

The work presented here describes the development of a novel ambient ionization imaging technique termed laser ablation direct analysis in real time imaging-mass spectrometry (LADI-MS) through the coupling of a laser ablation system with a DART-HRMS instrument. The approach was optimized for the detection and mapping of the spatial distributions of small molecules in complex matrices and circumvented many of the challenges associated with current IMS methods. The technique permitted the analysis of small molecules without the need for tedious sample preparation steps, solvent, matrix, or high-vacuum conditions.

The utility of LADI-MS was demonstrated through its application to the detection of a wide variety of molecules in different sample types including coffee beans, *Datura* sp. seeds, and endangered woods. The approach was also applied to samples of forensic relevance such as latent fingerprints, inks on paper, and fired ammunition. The wide-ranging capabilities of LADI-MS establish it as a promising new method that can be applied to the interrogation of samples of relevance to numerous areas including medicinal chemistry, forensic science, plant biochemistry, food science and technology, agriculture, and environmental chemistry, among many others.

References

1. Watson, J. T.; Sparkman, O. D., *Introduction to Mass Spectrometry: Instrumentation, Applications and Strategies for Data Interpretation*. John Wiley & Sons, Ltd: England, 2007.
2. Kerrigan, S. *Improved detection of synthetic cathinones in forensic toxicology samples: Thermal degradation and analytical considerations*; U.S. Department of Justice: 2015.
3. Kerrigan, S.; Savage, M.; Cavazos, C.; Bella, P., Thermal degradation of synthetic cathinones: Implications for forensic toxicology. *J Anal Toxicol* **2016**, *40* (1), 1-11.
4. Munson, M. S. B.; Field, F. H., Chemical ionization mass spectrometry. I. General introduction. *J Am Chem Soc* **1966**, *88* (12), 2621-2630.
5. Harris, G. A.; Nyadong, L.; Fernandez, F. M., Recent developments in ambient ionization techniques for analytical mass spectrometry. *Analyst* **2008**, *133* (10), 1297-1301.
6. Weston, D. J., Ambient ionization mass spectrometry: Current understanding of mechanistic theory; analytical performance and application areas. *Analyst* **2010**, *135* (4), 661-668.
7. Li, L.-P.; Feng, B.-S.; Yang, J.-W.; Chang, C.-L.; Bai, Y.; Liu, H.-W., Applications of ambient mass spectrometry in high-throughput screening. *Analyst* **2013**, *138* (11), 3097-3103.
8. Venter, A.; Nefliu, M.; Graham Cooks, R., Ambient desorption ionization mass spectrometry. *TrAC Trend Anal Chem* **2008**, *27* (4), 284-290.
9. Cody, R. B.; Laramée, J. A.; Durst, H. D., Versatile new ion source for the analysis of materials in open air under ambient conditions *Anal Chem* **2005**, *77* (8), 2297-2302.
10. Gross, J., Direct analysis in real time-a critical review on DART-MS. *Anal Bioanal Chem* **2014**, *406* (1), 63-80.
11. Takáts, Z.; Wiseman, J. M.; Gologan, B.; Cooks, R. G., Mass spectrometry sampling under ambient conditions with desorption electrospray ionization. *Science (New York, N.Y.)* **2004**, *306* (5695), 471-473.
12. JEOL USA, I., Direct analysis in real time time-of-flight mass spectrometer training manual. 2013.
13. Bahrami, H.; Tabrizchi, M.; Farrokhpour, H., Protonation of caffeine: A theoretical and experimental study. *Chem Phys* **2013**, *415*, 222-227.
14. Tošović, J.; Marković, S., Structural and antioxidative features of chlorogenic acid. *Croat Chem Acta* **2016**, *89* (4), 535-541.
15. Cody, R. B.; Dane, A. J., Dopant-assisted direct analysis in real time mass spectrometry with argon gas. *Rapid Commun Mass Spectrom* **2016**, *30* (10), 1181-1189.
16. Yang, H.; Wan, D.; Song, F.; Liu, Z.; Liu, S., Argon direct analysis in real time mass spectrometry in conjunction with makeup solvents: A method for analysis of labile compounds. *Anal Chem* **2013**, *85* (3), 1305-1309.
17. Su, R.; Yu, W.; Sun, K.; Yang, J.; Chen, C.; Lian, W.; Liu, S.; Yang, H., The ion source of nitrogen direct analysis in real-time mass spectrometry as a highly efficient reactor: Generation of reactive oxygen species. *J Am Soc Mass Spectrom* **2019**, *30* (4), 581-587.

18. Beyramysoltan, S.; Abdul-Rahman, N.-H.; Musah, R. A., Call it a “nightshade”—A hierarchical classification approach to identification of hallucinogenic Solanaceae spp. using DART-HRMS-derived chemical signatures. *Talanta* **2019**, *204*, 739-746.
19. Cody, R. B.; Dane, A. J.; Dawson-Andoh, B.; Adedipe, E. O.; Nkansah, K., Rapid classification of White Oak (*Quercus alba*) and Northern Red Oak (*Quercus rubra*) by using pyrolysis direct analysis in real time (DART™) and time-of-flight mass spectrometry. *J Anal Appl Pyrol* **2012**, *95*, 134-137.
20. Espinoza, E. O.; Wiemann, M. C.; Barajas-Morales, J.; Chavarria, G. D.; McClure, P. J., Forensic analysis of CITES-protected Dalbergia timber from the Americas. *IAWA J* **2015**, *36* (3), 311.
21. Lancaster, C.; Espinoza, E., Analysis of select Dalbergia and trade timber using direct analysis in real time and time-of-flight mass spectrometry for CITES enforcement. *Rapid Commun Mass Spectrom* **2012**, *26* (9), 1147-56.
22. Lesiak, A. D.; Cody, R. B.; Dane, A. J.; Musah, R. A., Rapid detection by direct analysis in real time-mass spectrometry (DART-MS) of psychoactive plant drugs of abuse: The case of *Mitragyna speciosa* aka “Kratom”. *Forensic Sci Int* **2014**, *242*, 210-218.
23. Lesiak, A. D.; Cody, R. B.; Dane, A. J.; Musah, R. A., Plant seed species identification from chemical fingerprints: A high-throughput application of direct analysis in real time mass spectrometry. *Anal Chem* **2015**, *87* (17), 8748-8757.
24. Lesiak, A. D.; Musah, R. A., Application of ambient ionization high resolution mass spectrometry to determination of the botanical provenance of the constituents of psychoactive drug mixtures. *Forensic Sci Int* **2016**, *266*, 271-280.
25. Lesiak, A. D.; Musah, R. A., More than just heat: Ambient ionization mass spectrometry for determination of the species of origin of processed commercial products—Application to psychoactive pepper supplements. *Anal Methods-UK* **2016**, *8* (7), 1646-1658.
26. McClure, P. J.; Chavarria, G. D.; Espinoza, E., Metabolic chemotypes of CITES protected Dalbergia timbers from Africa, Madagascar, and Asia. *Rapid Commun Mass Spectrom* **2015**, *29* (9), 783-8.
27. Musah, R. A.; Cody, R. B.; Dane, A. J.; Vuong, A. L.; Shepard, J. R. E., Direct analysis in real time mass spectrometry for analysis of sexual assault evidence. *Rapid Commun Mass Spectrom* **2012**, *26* (9), 1039-1046.
28. Musah, R. A.; Espinoza, E. O.; Cody, R. B.; Lesiak, A. D.; Christensen, E. D.; Moore, H. E.; Maleknia, S.; Drijfhout, F. P., A high throughput ambient mass spectrometric approach to species identification and classification from chemical fingerprint signatures. *Sci Rep* **2015**, *5*, 11520.
29. Fernández, F. M.; Cody, R. B.; Green, M. D.; Hampton, C. Y.; McGready, R.; Sengaloundeth, S.; White, N. J.; Newton, P. N., Characterization of solid counterfeit drug samples by desorption electrospray ionization and direct-analysis-in-real-time coupled to time-of-flight mass spectrometry. *ChemMedChem* **2006**, *1* (7), 702-705.
30. Giffen, J. E.; Rosati, J. Y.; Longo, C. M.; Musah, R. A., Species identification of necrophagous insect eggs based on amino acid profile differences revealed by direct analysis in real time-high resolution mass spectrometry. *Anal Chem* **2017**, *89* (14), 7719-7726.

31. Bodzon-Kulakowska, A.; Suder, P., Imaging mass spectrometry: Instrumentation, applications, and combination with other visualization techniques. *Mass Spectrom Rev* **2016**, *35* (1), 147-169.
32. Watrous, J. D.; Dorrestein, P. C., Imaging mass spectrometry in microbiology. *Nat Rev Microbiol* **2011**, *9*, 683.
33. Buchberger, A. R.; DeLaney, K.; Johnson, J.; Li, L., Mass spectrometry imaging: A review of emerging advancements and future insights. *Anal Chem* **2018**, *90* (1), 240-265.
34. Boughton, B. A.; Thinagaran, D.; Sarabia, D.; Bacic, A.; Roessner, U., Mass spectrometry imaging for plant biology: A review. *Phytochem Rev* **2016**, *15* (3), 445-488.
35. Prideaux, B.; Stoeckli, M., Mass spectrometry imaging for drug distribution studies. *J Proteom* **2012**, *75* (16), 4999-5013.
36. Forbes, T. P.; Sisco, E., Mass spectrometry detection and imaging of inorganic and organic explosive device signatures using desorption electro-flow focusing ionization. *Anal Chem* **2014**, *86* (15), 7788-7797.
37. Forbes, T. P.; Sisco, E., Chemical imaging of artificial fingerprints by desorption electro-flow focusing ionization mass spectrometry. *Analyst* **2014**, *139* (12), 2982-2985.
38. Li, H.; Smith, B. K.; Shrestha, B.; Mark, L.; Vertes, A., Automated Cell-by-Cell Tissue Imaging and Single-Cell Analysis for Targeted Morphologies by Laser Ablation Electrospray Ionization Mass Spectrometry. In *Mass Spectrometry Imaging of Small Molecules*, 2014/11/02 ed.; He, L., Ed. Springer New York: New York, NY, 2015; Vol. 1203, pp 117-27.
39. Moreno-Pedraza, A.; Rosas-Román, I.; Garcia-Rojas, N. S.; Guillén-Alonso, H.; Ovando-Vázquez, C.; Díaz-Ramírez, D.; Cuevas-Contreras, J.; Vergara, F.; Marsch-Martínez, N.; Molina-Torres, J.; Winkler, R., Elucidating the distribution of plant metabolites from native tissues with laser desorption low-temperature plasma mass spectrometry imaging. *Anal Chem* **2019**, *91* (4), 2734-2743.
40. Nemes, P.; Barton, A. A.; Li, Y.; Vertes, A., Ambient molecular imaging and depth profiling of live tissue by infrared laser ablation electrospray ionization mass spectrometry. *Anal Chem* **2008**, *80* (12), 4575-4582.
41. Nemes, P.; Vertes, A., Laser ablation electrospray ionization for atmospheric pressure, *in vivo*, and imaging mass spectrometry. *Anal Chem* **2007**, *79* (21), 8098-8106.
42. Stopka, S. A.; Samarah, L. Z.; Shaw, J. B.; Liyu, A. V.; Veličković, D.; Agtuca, B. J.; Kukolj, C.; Koppelaar, D. W.; Stacey, G.; Paša-Tolić, L.; Anderton, C. R.; Vertes, A., Ambient metabolic profiling and imaging of biological samples with ultrahigh molecular resolution using laser ablation electrospray ionization 21 tesla FTICR mass spectrometry. *Anal Chem* **2019**, *91* (8), 5028-5035.
43. Araujo, D. P.; Tuan, M. J.; Yew, J. Y.; Meier, R., Analysing small insect glands with UV-LDI MS: high-resolution spatial analysis reveals the chemical composition and use of the osmeterium secretion in *Themira superba* (Sepsidae: Diptera). *J Evol Biol* **2014**, *27* (8), 1744-50.
44. Chen, B.-J.; Lee, P.-L.; Chen, W.-Y.; Mai, F.-D.; Ling, Y.-C., Hair dye distribution in human hair by ToF-SIMS. *Appl Surf Sci* **2006**, *252* (19), 6786-6788.
45. Claude, E.; Jones, E. A.; Pringle, S. D., DESI Mass Spectrometry Imaging (MSI). In *Imaging Mass Spectrometry : Methods and Protocols*, Cole, L. M., Ed. Springer New York: New York, NY, 2017; pp 65-75.

46. Forest, S.; Breault-Turcot, J.; Chaurand, P.; Masson, J. F., Surface plasmon resonance imaging-MALDI-TOF imaging mass spectrometry of thin tissue sections. *Anal Chem* **2016**, *88* (4), 2072-9.
47. Gamble, L. J.; Anderton, C. R., Secondary ion mass spectrometry imaging of tissues, cells, and microbial systems. *Micros Today* **2016**, *24* (2), 24-31.
48. Garrett, R.; Rezende, C. M.; Ifa, D. R., Revealing the spatial distribution of chlorogenic acids and sucrose across coffee bean endosperm by desorption electrospray ionization-mass spectrometry imaging. *LWT - Food Sci Technol* **2016**, *65* (Supplement C), 711-717.
49. Greer, T.; Sturm, R.; Li, L., Mass spectrometry imaging for drugs and metabolites. *J Proteom* **2011**, *74* (12), 2617-2631.
50. Mohana Kumara, P.; Srimany, A.; Ravikanth, G.; Uma Shaanker, R.; Pradeep, T., Ambient ionization mass spectrometry imaging of rohitukine, a chromone anti-cancer alkaloid, during seed development in *Dysoxylum binectariferum* Hook.f (Meliaceae). *Phytochemistry* **2015**, *116*, 104-110.
51. Mourino-Alvarez, L.; Iloro, I.; de la Cuesta, F.; Azkargorta, M.; Sastre-Oliva, T.; Escobes, I.; Lopez-Almodovar, L. F.; Sanchez, P. L.; Urreta, H.; Fernandez-Aviles, F.; Pinto, A.; Padiál, L. R.; Akerstrom, F.; Elortza, F.; Barderas, M. G., MALDI-imaging mass spectrometry: A step forward in the anatomopathological characterization of stenotic aortic valve tissue. *Sci Rep* **2016**, *6*, 27106.
52. Perez, C. J.; Bagga, A. K.; Prova, S. S.; Yousefi Taemeh, M.; Ifa, D. R., Review and perspectives on the applications of mass spectrometry imaging under ambient conditions. *Rapid Commun Mass Spectrom* **2018**.
53. Porta, T.; Grivet, C.; Kraemer, T.; Varesio, E.; Hopfgartner, G., Single hair cocaine consumption monitoring by mass spectrometric imaging. *Anal Chem* **2011**, *83* (11), 4266-72.
54. Voras, Z. E.; deGhetaldi, K.; Wiggins, M. B.; Buckley, B.; Baade, B.; Mass, J. L.; Beebe, T. P., Jr., ToF-SIMS imaging of molecular-level alteration mechanisms in Le Bonheur de vivre by Henri Matisse. *Appl Phys A-Mater* **2015**, *121* (3), 1015-1030.
55. Waki, M.; Sugiyama, E.; Kondo, T.; Sano, K.; Setou, M., Nanoparticle-assisted Laser Desorption/Ionization For Metabolite Imaging. In *Mass Spectrometry Imaging of Small Molecules*, 2014/11/02 ed.; He, L., Ed. Springer New York: New York, NY, 2015; Vol. 1203, pp 159-73.
56. Walker, H. J.; Steels, C.; Bendell, L.; Clench, M. R.; Read, D. J.; Cameron, D. D.; Burrell, M. M., Understanding metabolism of arginine in biological systems via MALDI imaging. *Proteomics* **2016**, *16* (11-12), 1690-4.
57. *Mass Spectrometry Imaging of Small Molecules*. Springer New York, 2015; Vol. 1203.
58. Yew, J. Y.; Soltwisch, J.; Pirkel, A.; Dreisewerd, K., Direct laser desorption ionization of endogenous and exogenous compounds from insect cuticles: practical and methodologic aspects. *J Am Soc Mass Spectrom* **2011**, *22* (7), 1273-84.
59. Karas, M.; Bahr, U.; Gießmann, U., Matrix-assisted laser desorption ionization mass spectrometry. *Mass Spectrom Rev* **1991**, *10* (5), 335-357.
60. Song, K.; Cheng, Q., Desorption and ionization mechanisms and signal enhancement in surface assisted laser desorption ionization mass spectrometry (SALDI-MS). *Appl Spectrosc Rev* **2019**, 1-23.

61. Tanaka, K.; Waki, H.; Ido, Y.; Akita, S.; Yoshida, Y.; Yoshida, T.; Matsuo, T., Protein and polymer analyses up to m/z 100,000 by laser ionization time-of-flight mass spectrometry. *Rapid Commun Mass Spectrom* **1988**, *2* (8), 151-153.
62. O'Rourke, M. B.; Raymond, B. B.; Djordjevic, S. P.; Padula, M. P., A versatile cost-effective method for the analysis of fresh frozen tissue sections via matrix-assisted laser desorption/ionisation imaging mass spectrometry. *Rapid Commun Mass Spectrom* **2015**, *29* (7), 637-44.
63. Bailey, M. J.; Bright, N. J.; Croxton, R. S.; Francese, S.; Ferguson, L. S.; Hinder, S.; Jickells, S.; Jones, B. J.; Jones, B. N.; Kazarian, S. G.; Ojeda, J. J.; Webb, R. P.; Wolstenholme, R.; Bleay, S., Chemical characterization of latent fingerprints by matrix-assisted laser desorption ionization, time-of-flight secondary ion mass spectrometry, mega electron volt secondary mass spectrometry, gas chromatography/mass spectrometry, x-ray photoelectron spectroscopy, and attenuated total reflection fourier transform infrared spectroscopic imaging: An intercomparison. *Anal Chem* **2012**, *84* (20), 8514-8523.
64. Kaplan-Sandquist, K. A.; LeBeau, M. A.; Miller, M. L., Evaluation of four fingerprint development methods for touch chemistry using matrix-assisted laser desorption ionization/time-of-flight mass spectrometry. *J Forensic Sci* **2015**, *60* (3), 611-8.
65. Caprioli, R. M.; Farmer, T. B.; Gile, J., Molecular imaging of biological samples: localization of peptides and proteins using MALDI-TOF MS. *Anal Chem* **1997**, *69* (23), 4751-60.
66. Winograd, N.; Bloom, A., Sample Preparation for 3D SIMS Chemical Imaging of Cells. In *Mass Spectrometry Imaging of Small Molecules*, He, L., Ed. Springer New York: New York, NY, 2015; pp 9-19.
67. Touboul, D.; Kollmer, F.; Niehuis, E.; Brunelle, A.; Laprevote, O., Improvement of biological time-of-flight-secondary ion mass spectrometry imaging with a bismuth cluster ion source. *J Am Soc Mass Spectrom* **2005**, *16* (10), 1608-18.
68. Bailey, M. J.; Jones, B. N.; Hinder, S.; Watts, J.; Bleay, S.; Webb, R. P., Depth profiling of fingerprint and ink signals by SIMS and MeV SIMS. *Nucl Instrum Meth B* **2010**, *268* (11), 1929-1932.
69. Dong, Y.; Guella, G.; Franceschi, P., Impact of tissue surface properties on the desorption electrospray ionization imaging of organic acids in grapevine stem. *Rapid Commun Mass Spectrom* **2016**, *30* (6), 711-8.
70. Roach, P. J.; Laskin, J.; Laskin, A., Nanospray desorption electrospray ionization: an ambient method for liquid-extraction surface sampling in mass spectrometry. *Analyst* **2010**, *135* (9), 2233-6.
71. Forbes, T. P.; Brewer, T. M.; Gillen, G., Desorption electro-flow focusing ionization of explosives and narcotics for ambient pressure mass spectrometry. *Analyst* **2013**, *138* (19), 5665-5673.
72. Muramoto, S.; Forbes, T. P.; van Asten, A. C.; Gillen, G., Test sample for the spatially resolved quantification of illicit drugs on fingerprints using imaging mass spectrometry. *Anal Chem* **2015**, *87* (10), 5444-5450.
73. Fowble, K. L.; Teramoto, K.; Cody, R. B.; Edwards, D.; Guarrera, D.; Musah, R. A., Development of "laser ablation direct analysis in real time imaging" mass spectrometry: Application to spatial distribution mapping of metabolites along the biosynthetic cascade

- leading to synthesis of atropine and scopolamine in plant tissue. *Anal Chem* **2017**, *89* (6), 3421-3429.
74. Fowble, K. L.; Okuda, K.; Cody, R. B.; Musah, R. A., Spatial distributions of furan and 5-hydroxymethylfurfural in unroasted and roasted *Coffea arabica* beans. *Food Res Int* **2019**, *119*, 725-732.
75. Fowble, K. L.; Musah, R. A., Simultaneous imaging of latent fingerprints and detection of analytes of forensic relevance by laser ablation direct analysis in real time imaging-mass spectrometry (LADI-MS). *Forensic Chem* **2019**, 100173.
76. Kiss, A.; Hopfgartner, G., Laser-based methods for the analysis of low molecular weight compounds in biological matrices. *Methods* **2016**, *104*, 142-153.
77. Dong, Y.; Li, B.; Malitsky, S.; Rogachev, I.; Aharoni, A.; Kaftan, F.; Svatoš, A.; Franceschi, P., Sample preparation for mass spectrometry imaging of plant tissues: A review. *Front Plant Sci* **2016**, *7*.
78. Brown, V. L.; He, L., Current Status and Future Prospects of Mass Spectrometry Imaging of Small Molecules. In *Mass Spectrometry Imaging of Small Molecules*, He, L., Ed. Springer New York: New York, NY, 2015; pp 1-7.
79. Heeren, R. M. A.; McDonnell, L. A.; Amstalden, E.; Luxembourg, S. L.; Altelaar, A. F. M.; Piersma, S. R., Why don't biologists use SIMS?: A critical evaluation of imaging MS. *Appl Surf Sci* **2006**, *252* (19), 6827-6835.
80. Tamura, J.; Osuga, J., New Generation LC-TOF/MS "AccuTOF". Application and Research Center, JEOL Ltd.: 2001.
81. Wilson, T. G.; Cryan, J. R., Lufenuron, a chitin-synthesis inhibitor, interrupts development of *Drosophila melanogaster*. *J Exp Zool* **1997**, *278* (1), 37-44.
82. Galhena, A. S.; Harris, G. A.; Nyadong, L.; Murray, K. K.; Fernández, F. M., Small molecule ambient mass spectrometry imaging by infrared laser ablation metastable-induced chemical ionization. *Anal Chem* **2010**, *82* (6), 2178-2181.
83. Liu, Y.; Ma, X.; Lin, Z.; He, M.; Han, G.; Yang, C.; Xing, Z.; Zhang, S.; Zhang, X., Imaging mass spectrometry with a low-temperature plasma probe for the analysis of works of art. *Angew Chem Int Ed* **2010**, *49* (26), 4435-4437.
84. Zhang, J.; Zhou, Z.; Yang, J.; Zhang, W.; Bai, Y.; Liu, H., Thin layer chromatography/plasma assisted multiwavelength laser desorption ionization mass spectrometry for facile separation and selective identification of low molecular weight compounds. *Anal Chem* **2012**, *84* (3), 1496-503.
85. Che, C.-T.; Zhang, H., Plant natural products for human health. *Int J Mol Sci* **2019**, *20* (4), 830.
86. Akram, M.; Hamid, A.; Khalil, A.; Ghaffar, A.; Tayyaba, N.; Saeed, A.; Ali, M.; Naveed, A., Review on medicinal uses, pharmacological, phytochemistry and immunomodulatory activity of plants. *Int J Immunopathol Pharmacol* **2014**, *27* (3), 313-9.
87. Senthilkumar, S.; Vijayakumari, K., Pharmacological review of important medicinal plants and uses. *Int J Univers Pharm Bio Sci* **2016**, *5* (2), 51-64.
88. Wangchuk, P.; Yeshi, K.; Jamphel, K., Pharmacological, ethnopharmacological, and botanical evaluation of subtropical medicinal plants of Lower Kheng region in Bhutan. *Integr Med Res* **2017**, *6* (4), 372-387.

89. Christen, P., Tropane alkaloids: Old drugs used in modern medicine. In *Studies in Natural Products Chemistry*, Atta-ur-Rahman, Ed. Elsevier: 2000; Vol. 22, pp 717-749.
90. Gurib-Fakim, A., Medicinal plants: Traditions of yesterday and drugs of tomorrow. *Mol Aspects Med* **2006**, *27* (1), 1-93.
91. Stockbrugger, R. W., Antimuscarinic drugs. *Methods Find Exp Clin Pharmacol* **1989**, *11 Suppl 1*, 79-86.
92. De Simone, R.; Margarucci, L.; De Feo, V., Tropane alkaloids: An overview. *Pharmacologyonline* **2008**, *1*, 70-89.
93. Lochner, M.; Thompson, A. J., The muscarinic antagonists scopolamine and atropine are competitive antagonists at 5-HT₃ receptors. *Neuropharmacology* **2016**, *108*, 220-8.
94. Friedman, M.; Levin, C. E., Composition of jimson weed (*Datura stramonium*) seeds. *J Agric Food Chem* **1989**, *37* (4), 998-1005.
95. Paul, B. D.; Dreka, C.; Knight, E. S.; Smith, M. L., Gas chromatographic/mass spectrometric detection of narcotine, papaverine, and thebaine in seeds of *Papaver somniferum*. *Planta Med* **1996**, *62* (06), 544-547.
96. Gunn, C. R., Gaffney, F. B., Seed characteristics of 42 economically important species of Solanaceae in the United States. 1471, U. S. D. o. A. T. B., Ed. United States Department of Agriculture: Washington D.C., 1974.
97. Hashimoto, T.; Yukimune, Y.; Yamada, Y., Putrescine and putrescine *N*-methyltransferase in the biosynthesis of tropane alkaloids in cultured roots of *Hyoscyamus albus*. *Planta* **1989**, *178* (1), 131-137.
98. Leete, E., The stereospecific incorporation of ornithine into the tropine moiety of hyoscyamine. *J Am Chem Soc* **1962**, *84* (1), 55-57.
99. Walton, N. J.; Robins, R. J.; Peerless, A. C. J., Enzymes of *N*-methylputrescine biosynthesis in relation to hyoscyamine formation in transformed root cultures of *Datura stramonium* and *Atropa belladonna*. *Planta* **1990**, *182* (1), 136-141.
100. Hibi, N.; Fujita, T.; Hatano, M.; Hashimoto, T.; Yamada, Y., Putrescine *N*-methyltransferase in cultured roots of *Hyoscyamus albus*: *n*-Butylamine as a potent inhibitor of the transferase both *in vitro* and *in vivo*. *Plant Physiol* **1992**, *100* (2), 826-835.
101. Katoh, A.; Shoji, T.; Hashimoto, T., Molecular cloning of *N*-methylputrescine oxidase from tobacco. *Plant Cell Physiol* **2007**, *48* (3), 550-554.
102. Robins, R. J.; Abraham, T. W.; Parr, A. J.; Eagles, J.; Walton, N. J., The biosynthesis of tropane alkaloids in *Datura stramonium*: The identity of the intermediates between *N*-methylpyrrolinium salt and tropinone. *J Am Chem Soc* **1997**, *119* (45), 10929-10934.
103. Abraham, T. W.; Leete, E., New intermediate in the biosynthesis of the tropane alkaloids in *Datura innoxia*. *J Am Chem Soc* **1995**, *117* (31), 8100-8105.
104. Portsteffen, A.; Draeger, B.; Nahrstedt, A., Two tropinone reducing enzymes from *Datura stramonium* transformed root cultures. *Phytochemistry* **1992**, *31* (4), 1135-1138.
105. Hashimoto, T.; Nakajima, K.; Ongena, G.; Yamada, Y., Two tropinone reductases with distinct stereospecificities from cultured roots of *Hyoscyamus niger*. *Plant Physiol* **1992**, *100* (2), 836-845.
106. Scholl, Y.; Schneider, B.; Dräger, B., Biosynthesis of calystegines: 15N NMR and kinetics of formation in root cultures of *Calystegia sepium*. *Phytochemistry* **2003**, *62* (3), 325-332.

107. Bedewitz, M. A.; Góngora-Castillo, E.; Uebler, J. B.; Gonzales-Vigil, E.; Wiegert-Rininger, K. E.; Childs, K. L.; Hamilton, J. P.; Vaillancourt, B.; Yeo, Y.-S.; Chappell, J.; DellaPenna, D.; Jones, A. D.; Buell, C. R.; Barry, C. S., A root-expressed l-phenylalanine:4-hydroxyphenylpyruvate aminotransferase is required for tropane alkaloid biosynthesis in *Atropa belladonna*. *Plant Cell* **2014**, *26* (9), 3745-3762.
108. Lakshmi Prasuna, M.; Mujahid, M.; Sasikala, C.; Ramana, C. V., l-Phenylalanine catabolism and l-phenyllactic acid production by a phototrophic bacterium, *Rubrivivax benzoatilyticus* JA2. *Microbiol Res* **2012**, *167* (9), 526-531.
109. Li, R.; Reed, D. W.; Liu, E.; Nowak, J.; Pelcher, L. E.; Page, J. E.; Covello, P. S., Functional genomic analysis of alkaloid biosynthesis in *Hyoscyamus niger* reveals a cytochrome P450 Involved in littorine rearrangement. *Chem Biol* **2006**, *13* (5), 513-520.
110. Hashimoto, T.; Matsuda, J.; Yamada, Y., Two-step epoxidation of hyoscyamine to scopolamine is catalyzed by bifunctional hyoscyamine 6 β -hydroxylase. *FEBS Lett* **1993**, *329* (1-2), 35-39.
111. Alves, M. N.; Sartoratto, A.; Trigo, J. R., Scopolamine in *Brugmansia suaveolens* (Solanaceae): Defense, allocation, costs, and induced response. *J Chem Ecol* **2006**, *33* (2), 297-309.
112. Berkov, S.; Philipov, S., Alkaloid production in diploid and autotetraploid plants of *Datura stramonium*. *Pharm Biol* **2002**, *40* (8), 617-621.
113. Berkov, S.; Zayed, R.; Doncheva, T., Alkaloid patterns in some varieties of *Datura stramonium*. *Fitoterapia* **2006**, *77* (3), 179-182.
114. Hashimoto, T.; Hayashi, A.; Amano, Y.; Kohno, J.; Iwanari, H.; Usuda, S.; Yamada, Y., Hyoscyamine 6 β -hydroxylase, an enzyme involved in tropane alkaloid biosynthesis, is localized at the pericycle of the root. *J Biol Chem* **1991**, *266* (7), 4648-53.
115. St-Pierre, B.; Vazquez-Flota, F. A.; De Luca, V., Multicellular compartmentation of *Catharanthus roseus* alkaloid biosynthesis predicts intercellular translocation of a pathway intermediate. *Plant Cell* **1999**, *11* (5), 887-900.
116. Bird, D. A.; Franceschi, V. R.; Facchini, P. J., A tale of three cell types: Alkaloid biosynthesis is localized to sieve elements in opium poppy. *Plant Cell* **2003**, *15* (11), 2626-2635.
117. Ziegler, J.; Facchini, P. J., Alkaloid biosynthesis: Metabolism and trafficking. *Annu Rev Plant Biol* **2008**, *59*, 735-69.
118. Berkov, S.; Philipov, S., Alkaloid production in diploid and autotetraploid plants of *Datura stramonium*. *Pharm Biol* **2002**, *40* (8), 617-621.
119. Zayed, R.; Wink, M.; El-Shamy, H., In vitro organogenesis and alkaloid accumulation in *Datura innoxia*. In *Zeitschrift für Naturforschung C*, 2006; Vol. 61, p 560.
120. Roze, L. V.; Chanda, A.; Linz, J. E., Compartmentalization and molecular traffic in secondary metabolism: A new understanding of established cellular processes. *Fungal Genet Biol* **2011**, *48* (1), 35-48.
121. Kariñho-Betancourt, E.; Agrawal, A. A.; Halitschke, R.; Núñez-Farfán, J., Phylogenetic correlations among chemical and physical plant defenses change with ontogeny. *New Phytol* **2015**, *206* (2), 796-806.
122. Kaisuke Yoneda, S. S., Hiroko Kusu, Seed biology of medicinal plants (XII). The degradations of alkaloids in the germination process of the seeds of *Datura stramonium* L. *JPN J Pharmacol* **1992**, *46* (4), 352-357.

123. Horn, P. J.; Silva, J. E.; Anderson, D.; Fuchs, J.; Borisjuk, L.; Nazarenus, T. J.; Shulaev, V.; Cahoon, E. B.; Chapman, K. D., Imaging heterogeneity of membrane and storage lipids in transgenic *Camelina sativa* seeds with altered fatty acid profiles. *Plant J* **2013**, *76* (1), 138-150.
124. Zaima, N.; Goto-Inoue, N.; Hayasaka, T.; Setou, M., Application of imaging mass spectrometry for the analysis of *Oryza sativa* rice. *Rapid Commun Mass Spectrom* **2010**, *24* (18), 2723-2729.
125. Horn, P. J.; Korte, A. R.; Neogi, P. B.; Love, E.; Fuchs, J.; Strupat, K.; Borisjuk, L.; Shulaev, V.; Lee, Y.-J.; Chapman, K. D., Spatial mapping of lipids at cellular resolution in embryos of cotton. *Plant Cell* **2012**, *24* (2), 622-636.
126. Yoshimura, Y.; Zaima, N.; Moriyama, T.; Kawamura, Y., Different localization patterns of anthocyanin species in the pericarp of black rice revealed by imaging mass spectrometry. *PLoS ONE* **2012**, *7* (2), e31285.
127. Burrell, M.; Earnshaw, C.; Clench, M., Imaging matrix assisted laser desorption ionization mass spectrometry: A technique to map plant metabolites within tissues at high spatial resolution. *J Exp Bot* **2007**, *58* (4), 757-763.
128. Gorzolka, K.; Bednarz, H.; Niehaus, K., Detection and localization of novel hordatine-like compounds and glycosylated derivatives of hordatines by imaging mass spectrometry of barley seeds. *Planta* **2014**, *239* (6), 1321-1335.
129. Peukert, M.; Matros, A.; Lattanzio, G.; Kaspar, S.; Abadía, J.; Mock, H.-P., Spatially resolved analysis of small molecules by matrix-assisted laser desorption/ionization mass spectrometric imaging (MALDI-MSI). *New Phytol* **2012**, *193* (3), 806-815.
130. Thunig, J.; Hansen, S. H.; Janfelt, C., Analysis of secondary plant metabolites by indirect desorption electrospray ionization imaging mass spectrometry. *Anal Chem* **2011**, *83* (9), 3256-3259.
131. Ifa, D. R.; Srimany, A.; Eberlin, L. S.; Naik, H. R.; Bhat, V.; Cooks, R. G.; Pradeep, T., Tissue imprint imaging by desorption electrospray ionization mass spectrometry. *Anal Methods-UK* **2011**, *3* (8), 1910-1912.
132. Ariseto, A. P.; Vicente, E.; Ueno, M. S.; Tfouni, S. A.; Toledo, M. C., Furan levels in coffee as influenced by species, roast degree, and brewing procedures. *J Agric Food Chem* **2011**, *59* (7), 3118-24.
133. Monien, B. H.; Engst, W.; Barknowitz, G.; Seidel, A.; Glatt, H., Mutagenicity of 5-hydroxymethylfurfural in V79 cells expressing human SULT1A1: Identification and mass spectrometric quantification of DNA adducts formed. *Chem Res Toxicol* **2012**, *25* (7), 1484-1492.
134. Zanin, R. C.; Corso, M. P.; Kitzberger, C. S. G.; Scholz, M. B. d. S.; Benassi, M. d. T., Good cup quality roasted coffees show wide variation in chlorogenic acids content. *LWT - Food Sci Technol* **2016**, *74*, 480-483.
135. IARC, Furan. In *Dry cleaning, some chlorinated solvents and other industrial chemicals*, World Health Organization: Lyon, France, 1995; Vol. 63, pp 393-407.
136. Neuwirth, C.; Mosesso, P.; Pepe, G.; Fiore, M.; Malfatti, M.; Turteltaub, K.; Dekant, W.; Mally, A., Furan carcinogenicity: DNA binding and genotoxicity of furan in rats *in vivo*. *Mol Nutr Food Res* **2012**, *56* (9), 1363-1374.

137. Peterson, L. A., Reactive metabolites in the biotransformation of molecules containing a furan ring. *Chem Res Toxicol* **2013**, *26* (1), 6-25.
138. Maga, J. A.; Katz, I., Furans in foods. *Crit Rev Food Sci* **1979**, *11* (4), 355-400.
139. Becalski, A.; Halldorson, T.; Hayward, S.; Roscoe, V., Furan, 2-methylfuran and 3-methylfuran in coffee on the Canadian market. *J Food Compos Anal* **2016**, *47*, 113-119.
140. Moon, J.-K.; Shibamoto, T., Role of roasting conditions in the profile of volatile flavor chemicals formed from coffee beans. *J Agric Food Chem* **2009**, *57* (13), 5823-5831.
141. Quarta, B.; Anese, M., Furfurals removal from roasted coffee powder by vacuum treatment. *Food Chem* **2012**, *130* (3), 610-614.
142. Sijia, W.; Enting, W.; Yuan, Y., Detection of furan levels in select Chinese foods by solid phase microextraction–gas chromatography/mass spectrometry method and dietary exposure estimation of furan in the Chinese population. *Food Chem Toxicol* **2014**, *64*, 34-40.
143. Capuano, E.; Fogliano, V., Acrylamide and 5-hydroxymethylfurfural (HMF): A review on metabolism, toxicity, occurrence in food and mitigation strategies. *LWT - Food Sci Technol* **2011**, *44* (4), 793-810.
144. Crews, C.; Castle, L., A review of the occurrence, formation and analysis of furan in heat-processed foods. *Trends Food Sci Tech* **2007**, *18* (7), 365-372.
145. Gökmen, V.; Açar, Ö. Ç.; Köksel, H.; Acar, J., Effects of dough formula and baking conditions on acrylamide and hydroxymethylfurfural formation in cookies. *Food Chem* **2007**, *104* (3), 1136-1142.
146. Gökmen, V.; Şenyuva, H. Z., Effects of some cations on the formation of acrylamide and furfurals in glucose–asparagine model system. *Eur Food Res Technol* **2007**, *225* (5), 815-820.
147. Kroh, L. W., Caramelisation in food and beverages. *Food Chem* **1994**, *51* (4), 373-379.
148. Roman-Leshkov, Y.; Chheda, J. N.; Dumesic, J. A., Phase modifiers promote efficient production of hydroxymethylfurfural from fructose. *Science (New York, N.Y.)* **2006**, *312* (5782), 1933-7.
149. Kato, H.; Hayase, F.; Shin, D. B.; Oimomi, M.; Baba, S., 3-Deoxyglucosone, an intermediate product of the Maillard reaction. *Prog Clin Biol Res* **1989**, *304*, 69-84.
150. Limacher, A.; Kerler, J.; Conde-Petit, B.; Blank, I., Formation of furan and methylfuran from ascorbic acid in model systems and food. *Food Addit Contam* **2007**, *24 Suppl 1*, 122-35.
151. Limacher, A.; Kerler, J.; Davidek, T.; Schmalzried, F.; Blank, I., Formation of furan and methylfuran by Maillard-type reactions in model systems and food. *J Agric Food Chem* **2008**, *56* (10), 3639-3647.
152. Perez Locas, C.; Yaylayan, V. A., Origin and mechanistic pathways of formation of the parent furan-A food toxicant. *J Agric Food Chem* **2004**, *52* (22), 6830-6836.
153. Owczarek-Fendor, A.; De Meulenaer, B.; Scholl, G.; Adams, A.; Van Lancker, F.; Eppe, G.; De Pauw, E.; Scippo, M.-L.; De Kimpe, N., Furan formation from lipids in starch-based model systems, as influenced by interactions with antioxidants and proteins. *J Agric Food Chem* **2011**, *59* (6), 2368-2376.
154. Owczarek-Fendor, A.; De Meulenaer, B.; Scholl, G.; Adams, A.; Van Lancker, F.; Yogendrarajah, P.; Uytterhoeven, V.; Eppe, G.; De Pauw, E.; Scippo, M.-L.; De Kimpe, N.,

- Importance of fat oxidation in starch-based emulsions in the generation of the process contaminant furan. *J Agric Food Chem* **2010**, *58* (17), 9579-9586.
155. Anese, M.; Bot, F.; Suman, M., Furan and 5-hydroxymethylfurfural removal from high- and low-moisture foods. *LWT - Food Sci Technol* **2014**, *56* (2), 529-532.
 156. Somorin, O., Caffeine distribution in *C. acuminata*, *T. cacao* and *C. arabica*. *J Food Sci* **1974**, *39* (5), 1055-1056.
 157. Zheng, X.-q.; Ashihara, H., Distribution, biosynthesis and function of purine and pyridine alkaloids in *Coffea arabica* seedlings. *Plant Sci* **2004**, *166* (3), 807-813.
 158. Dias, R. C.; Campanha, F. G.; Vieira, L. G.; Ferreira, L. P.; Pot, D.; Marraccini, P.; De Toledo Benassi, M., Evaluation of kahweol and cafestol in coffee tissues and roasted coffee by a new high-performance liquid chromatography methodology. *J Agric Food Chem* **2010**, *58* (1), 88-93.
 159. Conejero, G.; Noirot, M.; Talamond, P.; Verdeil, J. L., Spectral analysis combined with advanced linear unmixing allows for histolocalization of phenolics in leaves of coffee trees. *Front Plant Sci* **2014**, *5*, 39.
 160. Maeztu, L.; Sanz, C.; Andueza, S.; Paz De Peña, M.; Bello, J.; Cid, C., Characterization of espresso coffee aroma by static headspace GC-MS and sensory flavor profile. *J Agric Food Chem* **2001**, *49* (11), 5437-5444.
 161. Kuballa, T.; Stier, S.; Strichow, N., Furan concentrations in coffee and coffee beverages. *Deut Lebensm-Rundsch* **2005**, *101*, 229-235.
 162. Anese, M., Furan and other furanic compounds in coffee: Occurrence, mitigation strategies, and importance of processing. In *Processing and Impact on Active Components in Food*, Preedy, V., Ed. Academic Press: San Diego, 2015; pp 541-547.
 163. Lee, L. W.; Cheong, M. W.; Curran, P.; Yu, B.; Liu, S. Q., Modulation of coffee aroma via the fermentation of green coffee beans with *Rhizopus oligosporus*: II. Effects of different roast levels. *Food Chem* **2016**, *211*, 925-936.
 164. Lee, L. W.; Tay, G. Y.; Cheong, M. W.; Curran, P.; Yu, B.; Liu, S. Q., Modulation of the volatile and non-volatile profiles of coffee fermented with *Yarrowia lipolytica*: I. Green coffee. *LWT - Food Sci Technol* **2017**, *77*, 225-232.
 165. De Castro, R. D.; Marraccini, P., Cytology, biochemistry and molecular changes during coffee fruit development. *Braz J Plant Physiol* **2006**, *18*, 175-199.
 166. Becalski, A.; Seaman, S., Furan precursors in food: A model study and development of a simple headspace method for determination of furan. *Journal of AOAC International* **2005**, *88* (1), 102-6.
 167. Van Lancker, F.; Adams, A.; Owczarek-Fendor, A.; De Meulenaer, B.; De Kimpe, N., Mechanistic insights into furan formation in Maillard model systems. *J Agric Food Chem* **2011**, *59* (1), 229-35.
 168. *World Wildlife Crime Report: Trafficking in protected species*; United Nations Office on Drugs and Crime: 2016.
 169. *Convention on International Trade in Endangered Species* U.S. Fish and Wildlife Service: 2014.
 170. Dormontt, E. E.; Boner, M.; Braun, B.; Breulmann, G.; Degen, B.; Espinoza, E.; Gardner, S.; Guillery, P.; Hermanson, J. C.; Koch, G.; Lee, S. L.; Kanashiro, M.; Rimbawanto, A.; Thomas,

- D.; Wiedenhoeft, A. C.; Yin, Y.; Zahnen, J.; Lowe, A. J., Forensic timber identification: It's time to integrate disciplines to combat illegal logging. *Biol Conserv* **2015**, *191*, 790-798.
171. Lawrence, A. H.; Barbour, R. J.; Sutcliffe, R., Identification of wood species by ion mobility spectrometry. *Anal Chem* **1991**, *63* (13), 1217-1221.
172. Cabral, E. C.; Simas, R. C.; Santos, V. G.; Queiroga, C. L.; da Cunha, V. S.; de Sa, G. F.; Daroda, R. J.; Eberlin, M. N., Wood typification by Venturi easy ambient sonic spray ionization mass spectrometry: The case of the endangered Mahogany tree. *J Mass Spectrom* **2012**, *47* (1), 1-6.
173. Kite, G. C.; Green, P. W.; Veitch, N. C.; Groves, M. C.; Gasson, P. E.; Simmonds, M. S., Dalnigrin, a neoflavonoid marker for the identification of Brazilian rosewood (*Dalbergia nigra*) in CITES enforcement. *Phytochemistry* **2010**, *71* (10), 1122-31.
174. Flaete, P. O.; Haartveit, E. Y.; Vadla, K., Near infrared spectroscopy with multivariate statistical modelling as a tool for differentiation of wood from tree species with similar appearance. *NZ J Forestry Sci* **2006**, *36* (2-3), 382-392.
175. Yang, Z.; Liu, Y.; Pang, X.; Li, K., Preliminary investigation into the identification of wood species from different locations by near infrared spectroscopy. *Bioresources* **2015**, *10* (4), 13.
176. Tsumura, Y.; Kado, T.; Yoshida, K.; Abe, H.; Ohtani, M.; Taguchi, Y.; Fukue, Y.; Tani, N.; Ueno, S.; Yoshimura, K.; Kamiya, K.; Harada, K.; Takeuchi, Y.; Diway, B.; Finkeldey, R.; Na'iem, M.; Indrioko, S.; Ng, K. K. S.; Muhammad, N.; Lee, S. L., Molecular database for classifying *Shorea* species (Dipterocarpaceae) and techniques for checking the legitimacy of timber and wood products. *J Plant Res* **2011**, *124* (1), 35-48.
177. He, T.; Jiao, L.; Wiedenhoeft, A. C.; Yin, Y., Machine learning approaches outperform distance- and tree-based methods for DNA barcoding of *Pterocarpus* wood. *Planta* **2019**, *249* (5), 1617-1625.
178. Schroeder, H.; Cronn, R.; Yanbaev, Y.; Jennings, T.; Mader, M.; Degen, B.; Kersten, B., Development of molecular markers for determining continental origin of wood from White Oaks (*Quercus* L. sect. *Quercus*). *PLoS ONE* **2016**, *11* (6), e0158221.
179. Degen, B.; Ward, S. E.; Lemes, M. R.; Navarro, C.; Cavers, S.; Sebbenn, A. M., Verifying the geographic origin of mahogany (*Swietenia macrophylla* King) with DNA-fingerprints. *Forensic Sci Int* **2013**, *7* (1), 55-62.
180. Keppler, F.; Harper, D. B.; Kalin, R. M.; Meier-Augenstein, W.; Farmer, N.; Davis, S.; Schmidt, H.-L.; Brown, D. M.; Hamilton, J. T. G., Stable hydrogen isotope ratios of lignin methoxyl groups as a paleoclimate proxy and constraint of the geographical origin of wood. *New Phytol* **2007**, *176* (3), 600-609.
181. Kagawa, A.; Leavitt, S. W., Stable carbon isotopes of tree rings as a tool to pinpoint the geographic origin of timber. *J Wood Sci* **2010**, *56* (3), 175-183.
182. Fritts, H. C., Growth-rings of trees: Their correlation with climate. *Science (New York, N.Y.)* **1966**, *154* (3752), 973-979.
183. Pontara, V.; Bueno, M. L.; Garcia, L. E.; Oliveira-Filho, A. T.; Pennington, T. R.; Burslem, D. F. R. P.; Lemos-Filho, J. P., Fine-scale variation in topography and seasonality determine radial growth of an endangered tree in Brazilian Atlantic forest. *Plant Soil* **2016**, *403* (1), 115-128.

184. Imai, T.; Tanabe, K.; Kato, T.; Fukushima, K., Localization of ferruginol, a diterpene phenol, in *Cryptomeria japonica* heartwood by time-of-flight secondary ion mass spectrometry. *Planta* **2005**, *221* (4), 549-556.
185. Lunsford, K. A.; Peter, G. F.; Yost, R. A., Direct matrix-assisted laser desorption/ionization mass spectrometric imaging of cellulose and hemicellulose in populus tissue. *Anal Chem* **2011**, *83* (17), 6722-6730.
186. Saito, K.; Mitsutani, T.; Imai, T.; Matsushita, Y.; Fukushima, K., Discriminating the indistinguishable sapwood from heartwood in discolored ancient wood by direct molecular mapping of specific extractives using time-of-flight secondary ion mass spectrometry. *Anal Chem* **2008**, *80* (5), 1552-1557.
187. Saito, K.; Watanabe, Y.; Shirakawa, M.; Matsushita, Y.; Imai, T.; Koike, T.; Sano, Y.; Funada, R.; Fukazawa, K.; Fukushima, K., Direct mapping of morphological distribution of syringyl and guaiacyl lignin in the xylem of maple by time-of-flight secondary ion mass spectrometry. *Plant J* **2012**, *69* (3), 542-552.
188. Zhou, C.; Li, Q.; Chiang, V. L.; Lucia, L. A.; Griffis, D. P., Chemical and spatial differentiation of syringyl and guaiacyl lignins in poplar wood via time-of-flight secondary ion mass spectrometry. *Anal Chem* **2011**, *83* (18), 7020-7026.
189. Afendi, F. M.; Okada, T.; Yamazaki, M.; Hirai-Morita, A.; Nakamura, Y.; Nakamura, K.; Ikeda, S.; Takahashi, H.; Altaf-Ul-Amin, M.; Darusman, L. K.; Saito, K.; Kanaya, S., KNApSACK family databases: Integrated metabolite-plant species databases for multifaceted plant research. *Plant Cell Physiol* **2012**, *53* (2), e1.
190. Eyton, W. B.; Ollis, W. D.; Sutherland, I. O.; Gottlieb, O. R.; Taveira Magalhães, M.; Jackman, L. M., The neoflavanoid group of natural products—I: Dalbergiones—A new class of quinones. *Tetrahedron* **1965**, *21* (9), 2683-2696.
191. Ashakirin, S. N.; Tripathy, M.; Patil, U. K.; Majeed, A. B. A. In *Chemistry and bioactivity of cinnamaldehyde: A natural molecule of medicinal importance*, 2017.
192. Kuo, T.-H.; Huang, H.-C.; Hsu, C.-C., Mass spectrometry imaging guided molecular networking to expedite discovery and structural analysis of agarwood natural products. *Anal Chim Acta* **2019**.
193. United States Department of Justice, O. o. J. P., Latent Print Development. In *The Fingerprint Sourcebook*, CreateSpace Publishing: 2012; p 430.
194. Bailey, M. J.; Bradshaw, R.; Francese, S.; Salter, T. L.; Costa, C.; Ismail, M.; P. Webb, R.; Bosman, I.; Wolff, K.; de Puit, M., Rapid detection of cocaine, benzoylecgonine and methylecgonine in fingerprints using surface mass spectrometry. *Analyst* **2015**, *140* (18), 6254-6259.
195. Frick, A. A.; Chidlow, G.; Lewis, S. W.; van Bronswijk, W., Investigations into the initial composition of latent fingerprint lipids by gas chromatography–mass spectrometry. *Forensic Sci Int* **2015**, *254*, 133-147.
196. Girod, A.; Weyermann, C., Lipid composition of fingerprint residue and donor classification using GC/MS. *Forensic Sci Int* **2014**, *238*, 68-82.
197. Zhang, T.; Chen, X.; Yang, R.; Xu, Y., Detection of methamphetamine and its main metabolite in fingerprints by liquid chromatography–mass spectrometry. *Forensic Sci Int* **2015**, *248*, 10-14.

198. Francese, S.; Bradshaw, R.; Ferguson, L. S.; Wolstenholme, R.; Clench, M. R.; Bleay, S., Beyond the ridge pattern: Multi-informative analysis of latent fingermarks by MALDI mass spectrometry. *Analyst* **2013**, *138* (15), 4215-28.
199. Lim, A. Y.; Rowell, F.; Elumbaring-Salazar, C. G.; Loke, J.; Ma, J., Detection of drugs in latent fingermarks by mass spectrometric methods. *Anal. Methods-UK* **2013**, *5* (17), 4378-4385.
200. Musah, R. A.; Cody, R. B.; Dane, A. J.; Vuong, A. L.; Shepard, J. R. E., Direct analysis in real time mass spectrometry for analysis of sexual assault evidence. *Rapid Commun Mass Spectrom* **2012**, *26* (9), 1039-1046.
201. Rowell, F.; Seviour, J.; Lim, A. Y.; Elumbaring-Salazar, C. G.; Loke, J.; Ma, J., Detection of nitro-organic and peroxide explosives in latent fingermarks by DART- and SALDI-TOF-mass spectrometry. *Forensic Sci Int* **2012**, *221* (1-3), 84-91.
202. Day, J. S.; Edwards, H. G.; Dobrowski, S. A.; Voice, A. M., The detection of drugs of abuse in fingerprints using Raman spectroscopy I: latent fingerprints. *Spectrochim Acta A* **2004**, *60* (3), 563-8.
203. Tahtouh, M.; Kalman, J.; Roux, C.; Lennard, C.; Reedy, B., The detection and enhancement of latent fingermarks using infrared chemical imaging. *J Forensic Sci* **2005**, *50* (1), 64-72.
204. West, M. J.; Went, M. J., The spectroscopic detection of drugs of abuse in fingerprints after development with powders and recovery with adhesive lifters. *Spectrochim Acta A* **2009**, *71* (5), 1984-8.
205. Wei, Q.; Zhang, M.; Ogorevc, B.; Zhang, X., Recent advances in the chemical imaging of human fingermarks (a review). *Analyst* **2016**, *141* (22), 6172-6189.
206. Bailey, M. J.; Bright, N. J.; Croxton, R. S.; Francese, S.; Ferguson, L. S.; Hinder, S.; Jickells, S.; Jones, B. J.; Jones, B. N.; Kazarian, S. G.; Ojeda, J. J.; Webb, R. P.; Wolstenholme, R.; Bleay, S., Chemical characterization of latent fingerprints by matrix-assisted laser desorption ionization, time-of-flight secondary ion mass spectrometry, mega electron volt secondary mass spectrometry, gas chromatography/mass spectrometry, x-ray photoelectron spectroscopy, and attenuated total reflection fourier transform infrared spectroscopic imaging: An intercomparison. *Anal Chem* **2012**, *84* (20), 8514-8523.
207. Tripathi, A.; Emmons, E. D.; Wilcox, P. G.; Guicheteau, J. A.; Emge, D. K.; Christesen, S. D.; Fountain, A. W., 3rd, Semi-automated detection of trace explosives in fingerprints on strongly interfering surfaces with Raman chemical imaging. *Appl Spectrosc* **2011**, *65* (6), 611-9.
208. Attard-Montalto, N.; Ojeda, J. J.; Reynolds, A.; Ismail, M.; Bailey, M.; Doodkorte, L.; de Puit, M.; Jones, B. J., Determining the chronology of deposition of natural fingermarks and inks on paper using secondary ion mass spectrometry. *Analyst* **2014**, *139* (18), 4641-53.
209. Bailey, M. J.; Ismail, M.; Bleay, S.; Bright, N.; Levin Elad, M.; Cohen, Y.; Geller, B.; Everson, D.; Costa, C.; Webb, R. P.; Watts, J. F.; de Puit, M., Enhanced imaging of developed fingerprints using mass spectrometry imaging. *Analyst* **2013**, *138* (21), 6246-50.
210. Bailey, M. J.; Jones, B. N.; Hinder, S.; Watts, J.; Bleay, S.; Webb, R. P., Depth profiling of fingerprint and ink signals by SIMS and MeV SIMS. *Nucl Instrum Meth B* **2010**, *268* (11), 1929-1932.
211. Benton, M.; Rowell, F.; Sundar, L.; Jan, M., Direct detection of nicotine and cotinine in dusted latent fingermarks of smokers by using hydrophobic silica particles and MS. *Surf Interface Anal* **2010**, *42* (5), 378-385.

212. Bradshaw, R.; Bleay, S.; Wolstenholme, R.; Clench, M. R.; Francese, S., Towards the integration of matrix assisted laser desorption ionisation mass spectrometry imaging into the current fingerprint examination workflow. *Forensic Sci Int* **2013**, *232* (1-3), 111-24.
213. Bradshaw, R.; Denison, N.; Francese, S., Implementation of MALDI MS profiling and imaging methods for the analysis of real crime scene fingerprints. *Analyst* **2017**, *142* (9), 1581-1590.
214. Ifa, D. R.; Manicke, N. E.; Dill, A. L.; Cooks, R. G., Latent fingerprint chemical imaging by mass spectrometry. *Science (New York, N.Y.)* **2008**, *321* (5890), 805.
215. Kaplan-Sandquist, K.; LeBeau, M. A.; Miller, M. L., Chemical analysis of pharmaceuticals and explosives in fingerprints using matrix-assisted laser desorption ionization/time-of-flight mass spectrometry. *Forensic Sci Int* **2014**, *235*, 68-77.
216. Kaplan-Sandquist, K. A.; LeBeau, M. A.; Miller, M. L., Evaluation of four fingerprint development methods for touch chemistry using matrix-assisted laser desorption ionization/time-of-flight mass spectrometry. *J Forensic Sci* **2015**, *60* (3), 611-8.
217. Lauzon, N.; Dufresne, M.; Beaudoin, A.; Chaurand, P., Forensic analysis of latent fingerprints by silver-assisted LDI imaging MS on nonconductive surfaces. *J Mass Spectrom* **2017**, *52* (6), 397-404.
218. Moule, E. C.; Guinan, T. M.; Gustafsson, O. J. R.; Kobus, H.; Kirkbride, K. P.; Voelcker, N. H., Silver-assisted development and imaging of fingerprints on non-porous and porous surfaces. *Int J Mass Spectrom* **2017**, *422*, 27-31.
219. Nizioł, J.; Ruman, T., Surface-transfer mass spectrometry imaging on a monoisotopic silver nanoparticle enhanced target. *Anal Chem* **2013**, *85* (24), 12070-12076.
220. Sundar, L.; Rowell, F., Detection of drugs in lifted cyanoacrylate-developed latent fingerprints using two laser desorption/ionisation mass spectrometric methods. *Analyst* **2014**, *139* (3), 633-42.
221. Szyrkowska, M. I.; Czerski, K.; Rogowski, J.; Paryjczak, T.; Parczewski, A., ToF-SIMS application in the visualization and analysis of fingerprints after contact with amphetamine drugs. *Forensic Sci Int* **2009**, *184* (1-3), e24-6.
222. *The Challenges of New Psychoactive Substances*; Vienne, Austria, United Nations Office on Drugs and Crime: 2013; pp 89-90.
223. Bright, N. J.; Willson, T. R.; Driscoll, D. J.; Reddy, S. M.; Webb, R. P.; Bleay, S.; Ward, N. I.; Kirkby, K. J.; Bailey, M. J., Chemical changes exhibited by latent fingerprints after exposure to vacuum conditions. *Forensic Sci Int* **2013**, *230* (1-3), 81-6.
224. Abbott, P. J.; Jabour, Z. J., Vacuum technology considerations for mass metrology. *J Res Natl Inst Stan* **2011**, *116* (4), 689-702.
225. Comi, T. J.; Ryu, S. W.; Perry, R. H., Synchronized desorption electrospray ionization mass spectrometry imaging. *Anal Chem* **2016**, *88* (2), 1169-1175.
226. Mirabelli, M. F.; Chramow, A.; Cabral, E. C.; Ifa, D. R., Analysis of sexual assault evidence by desorption electrospray ionization mass spectrometry. *J Mass Spectrom* **2013**, *48* (7), 774-778.
227. Muramoto, S.; Forbes, T. P.; van Asten, A. C.; Gillen, G., Test sample for the spatially resolved quantification of illicit drugs on fingerprints using imaging mass spectrometry. *Anal Chem* **2015**, *87* (10), 5444-5450.

228. Takáts, Z.; Cotte-Rodriguez, I.; Talaty, N.; Chen, H.; Cooks, R. G., Direct, trace level detection of explosives on ambient surfaces by desorption electrospray ionization mass spectrometry. *Chem Commun* **2005**, (15), 1950-1952.
229. Keil, A.; Talaty, N.; Janfelt, C.; Noll, R. J.; Gao, L.; Ouyang, Z.; Cooks, R. G., Ambient mass spectrometry with a handheld mass spectrometer at high pressure. *Anal Chem* **2007**, *79* (20), 7734-7739.
230. Ifa, D. R.; Wiseman, J. M.; Song, Q.; Cooks, R. G., Development of capabilities for imaging mass spectrometry under ambient conditions with desorption electrospray ionization (DESI). *Int J Mass Spectrom* **2007**, *259* (1), 8-15.
231. Clemons, K.; Dake, J.; Sisco, E.; Verbeck, G. F. t., Trace analysis of energetic materials via direct analyte-probed nanoextraction coupled to direct analysis in real time mass spectrometry. *Forensic Sci Int* **2013**, *231* (1-3), 98-101.
232. Calcerrada, M.; García-Ruiz, C., Analysis of questioned documents: A review. *Anal Chim Acta* **2015**, *853*, 143-166.
233. Chlebda, D. K.; Majda, A.; Łojewski, T.; Łojewska, J., Hyperspectral imaging coupled with chemometric analysis for non-invasive differentiation of black pens. *Appl Phys A-Mater* **2016**, *122* (11), 957.
234. Qureshi, R.; Uzair, M.; Khurshid, K.; Yan, H., Hyperspectral document image processing: Applications, challenges and future prospects. *Pattern Recognit* **2019**, *90*, 12-22.
235. Reed, G.; Savage, K.; Edwards, D.; Nic Daeid, N., Hyperspectral imaging of gel pen inks: An emerging tool in document analysis. *Sci Justice* **2014**, *54* (1), 71-80.
236. N. M. Asri, M.; A. M. Noor, N.; N. S. M. Desa, W.; ee Ismail, D., Forensic analysis of gel pen inks using hyperspectral imaging coupled with chemometric procedures. *Arab J Forensic Sci* **2019**, *1* (9).
237. Khan, Z.; Shafait, F.; Mian, A., Automatic ink mismatch detection for forensic document analysis. *Pattern Recognit* **2015**, *48* (11), 3615-3626.
238. Brauns, E. B.; Dyer, R. B., Fourier transform hyperspectral visible imaging and the nondestructive analysis of potentially fraudulent documents. *Appl Spectrosc* **2006**, *60* (8), 833-840.
239. Amador, V. S.; Pereira, H. V.; Sena, M. M.; Augusti, R.; Piccin, E., Paper spray mass spectrometry for the forensic analysis of black ballpoint pen inks. *J Am Soc Mass Spectrom* **2017**, *28* (9), 1965-1976.
240. Almeida, C. M.; Sales, D. D.; Tosato, F.; dos Santos, N. A.; Allochio Filho, J. F.; Macrino, C. J.; Pinto, F. E.; Filgueiras, P. R.; Romão, W., Study of chemical profile and of lines crossing using blue and black ink pens by LDI (+) MS and LDI (+) imaging. *Microchem J* **2019**, *148*, 220-229.
241. Saini, K.; Rathore, R., Identification of volatile components of gel-pen inks through gas chromatography mass spectrometry. *Forensic Chem* **2018**, *11*, 98-102.
242. Junior, C. A. d. S.; Segur, P. A., Identification of dyes in pen ink by high resolution mass spectrometry: A laboratory experiment. *J Lab Chem Educ* **2017**, *5* (5), 108-115.
243. Akhmerova, D.; Krylova, A.; Stavrianidi, A.; Shpigun, O.; Rodin, I., Forensic identification of dyes in ballpoint pen inks using LC-ESI-MS. *Chromatographia* **2017**, *80* (11), 1701-1709.

244. Wilson, J. D.; LaPorte, G. M.; Cantu, A. A., Differentiation of black gel inks using optical and chemical techniques. *J Forensic Sci* **2004**, *49* (2), 364-70.
245. Jones, R. W.; Cody, R. B.; McClelland, J. F., Differentiating writing inks using direct analysis in real time mass spectrometry. *J Forensic Sci* **2006**, *51* (4), 915-8.
246. Jones, R. W.; McClelland, J. F., Analysis of writing inks on paper using direct analysis in real time mass spectrometry. *Forensic Sci Int* **2013**, *231* (1-3), 73-81.
247. Weyermann, C.; Bucher, L.; Majcherczyk, P.; Mazzella, W.; Roux, C.; Esseiva, P., Statistical discrimination of black gel pen inks analysed by laser desorption/ionization mass spectrometry. *Forensic Sci Int* **2012**, *217* (1), 127-133.
248. Williams, M. R.; Moody, C.; Arceneaux, L.-A.; Rinke, C.; White, K.; Sigman, M. E., Analysis of black writing ink by electrospray ionization mass spectrometry. *Forensic Sci Int* **2009**, *191* (1), 97-103.
249. Ifa, D. R.; Gumaelius, L. M.; Eberlin, L. S.; Manicke, N. E.; Cooks, R. G., Forensic analysis of inks by imaging desorption electrospray ionization (DESI) mass spectrometry. *Analyst* **2007**, *132* (5), 461-7.
250. Li, M.; Jia, B.; Ding, L.; Hong, F.; Ouyang, Y.; Chen, R.; Zhou, S.; Chen, H.; Fang, X., Document authentication at molecular levels using desorption atmospheric pressure chemical ionization mass spectrometry imaging. *J Mass Spectrom* **2013**, *48* (9), 1042-9.
251. Goacher, R. E.; DiFonzo, L. G.; Lesko, K. C., Challenges determining the correct deposition order of different intersecting black inks by time-of-flight secondary ion mass spectrometry. *Anal Chem* **2017**, *89* (1), 759-766.
252. Tang, H.-W.; Wong, M. Y.-M.; Chan, S. L.-F.; Che, C.-M.; Ng, K.-M., Molecular imaging of banknote and questioned document using solvent-free gold nanoparticle-assisted laser desorption/ionization imaging mass spectrometry. *Anal Chem* **2011**, *83* (1), 453-458.
253. Scherperel, G.; Reid, G. E.; Waddell Smith, R., Characterization of smokeless powders using nano-electrospray ionization mass spectrometry (nESI-MS). *Anal Bioanal Chem* **2009**, *394* (8), 2019-2028.
254. Abrego, Z.; Ugarte, A.; Unceta, N.; Fernandez-Isla, A.; Goicolea, M. A.; Barrio, R. J., Unambiguous characterization of gunshot residue particles using scanning laser ablation and inductively coupled plasma-mass spectrometry. *Anal Chem* **2012**, *84* (5), 2402-9.
255. Reis, E. L.; Sarkis, J. E.; Neto, O. N.; Rodrigues, C.; Kakazu, M. H.; Viebig, S., A new method for collection and identification of gunshot residues from the hands of shooters. *J Forensic Sci* **2003**, *48* (6), 1269-74.
256. Saverio Romolo, F.; Margot, P., Identification of gunshot residue: A critical review. *Forensic Sci Int* **2001**, *119* (2), 195-211.
257. Benito, S.; Abrego, Z.; Sánchez, A.; Unceta, N.; Goicolea, M. A.; Barrio, R. J., Characterization of organic gunshot residues in lead-free ammunition using a new sample collection device for liquid chromatography-quadrupole time-of-flight mass spectrometry. *Forensic Sci Int* **2015**, *246*, 79-85.
258. Costa, R. A.; Motta, L. C.; Destefani, C. A.; Rodrigues, R. R. T.; do Espírito Santo, K. S.; Aquije, G. M. F. V.; Boldrini, R.; Athayde, G. P. B.; Carneiro, M. T. W. D.; Romão, W., Gunshot residues (GSR) analysis of clean range ammunition using SEM/EDX, colorimetric test and ICP-MS: A comparative approach between the analytical techniques. *Microchem J* **2016**, *129*, 339-347.

259. Dalby, O.; Butler, D.; Birkett, J. W., Analysis of gunshot residue and associated materials--A review. *J Forensic Sci* **2010**, *55* (4), 924-43.
260. Gassner, A.-L.; Ribeiro, C.; Kobylinska, J.; Zeichner, A.; Weyermann, C., Organic gunshot residues: Observations about sampling and transfer mechanisms. *Forensic Sci Int* **2016**, *266*, 369-378.
261. Gassner, A.-L.; Weyermann, C., LC-MS method development and comparison of sampling materials for the analysis of organic gunshot residues. *Forensic Sci Int* **2016**, *264*, 47-55.
262. Kara, I.; Lisesivdin, S. B.; Kasap, M.; Er, E.; Uzek, U., The relationship between the surface morphology and chemical composition of gunshot residue particles. *J Forensic Sci* **2015**, *60* (4), 1030-3.
263. Ali, L.; Brown, K.; Castellano, H.; Wetzel, S. J., A study of the presence of gunshot residue in Pittsburgh police stations using SEM/EDS and LC-MS/MS. *J Forensic Sci* **2016**, *61* (4), 928-938.
264. Perez, J. J.; Watson, D. A.; Levis, R. J., The classification of gunshot residue using laser electrospray mass spectrometry and offline multivariate statistical analysis. *Anal Chem* **2016**.

Appendix

Table of Contents

Appendix 1	Mass measurement data for the ions featured in the <i>Datura leichhardtii</i> seed.	156
Appendix 2	MALDI mass spectrum of aqueous extract of a <i>D. leichhardtii</i> seed with PEG 200 as a calibrant.	157
Appendix 3	Product-ion spectra for tropinone.	158
Appendix 4	Product-ion spectra for tropine.	159
Appendix 5	Product-ion spectra for arginine.	160
Appendix 6	Product-ion spectra for atropine.	161
Appendix 7	Product ion spectra for scopolamine.	162
Appendix 8	Color-overlaid ion images of furan and 5-hydroxymethylfurfural in a roasted coffee bean.	163

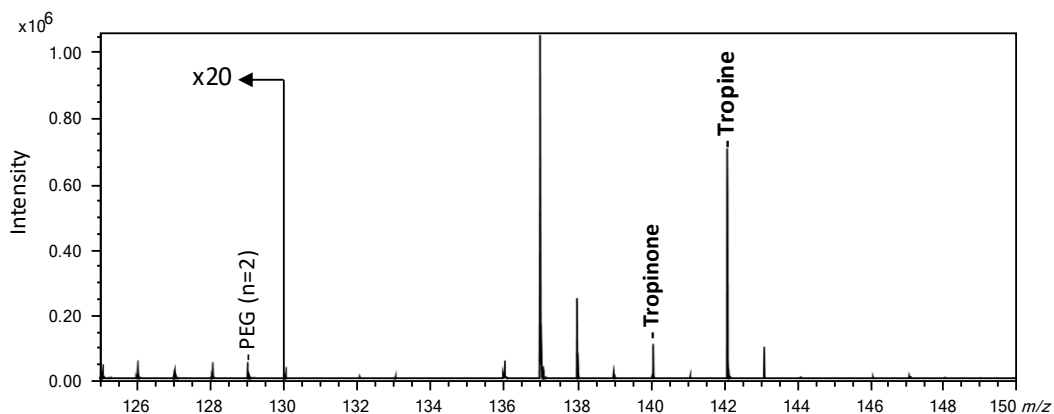
Appendix 1. Mass measurement data for the ions featured in the *Datura leichhardtii* seed.

Compound*	Composition	Observed Mass	Calculated Mass	Difference (mmu)
Unknown identity peak	-	124.1124	-	-
Unknown identity peak	-	131.0465	-	-
Tropinone	C ₈ H ₁₃ NO + H ⁺	140.1079	140.1075	0.4
Tropine	C ₈ H ₁₅ NO + H ⁺	142.1197	142.1232	3.5
Unknown identity peak	-	163.0742	-	-
Unknown identity peak	-	174.1124	-	-
Arginine	C ₆ H ₁₄ N ₄ O ₂ + H ⁺	175.1217	175.1195	2.2
Unknown identity peak	-	179.0695	-	-
Unknown identity peak	-	197.0820	-	-
Atropine	C ₁₇ H ₂₃ NO ₃ + H ⁺	290.1744	290.1756	1.2
Littorine [§]	C ₁₇ H ₂₃ NO ₃ + H ⁺	290.1744	290.1756	1.2
Scopolamine	C ₁₇ H ₂₁ NO ₄ + H ⁺	304.1552	304.1549	0.3
Unknown identity peak [‡]	-	381.3340	-	-

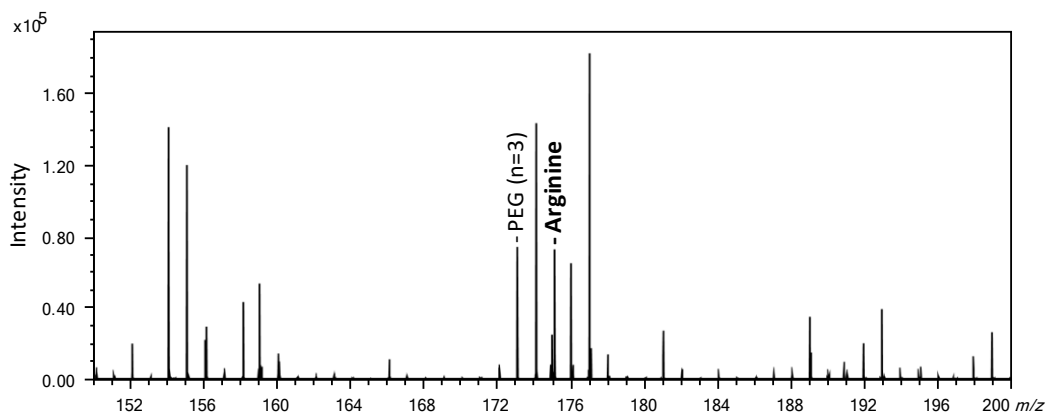
*Unless otherwise stated, peaks of unknown identity that are listed are those with of abundance $\geq 9.2\%$ relative to the base peak. [§]Assignment is tentative. [‡]Spatial distribution of this mass was confined to the embryo and half of the seed coat.

Appendix 2. MALDI mass spectra of an aqueous extract of a *D. leichhardtii* seed with PEG 200 as a calibrant. Peaks corresponding to tropinone, tropine, arginine, scopolamine and atropine are shown. Panels A, B, and C show the indicated mass ranges.

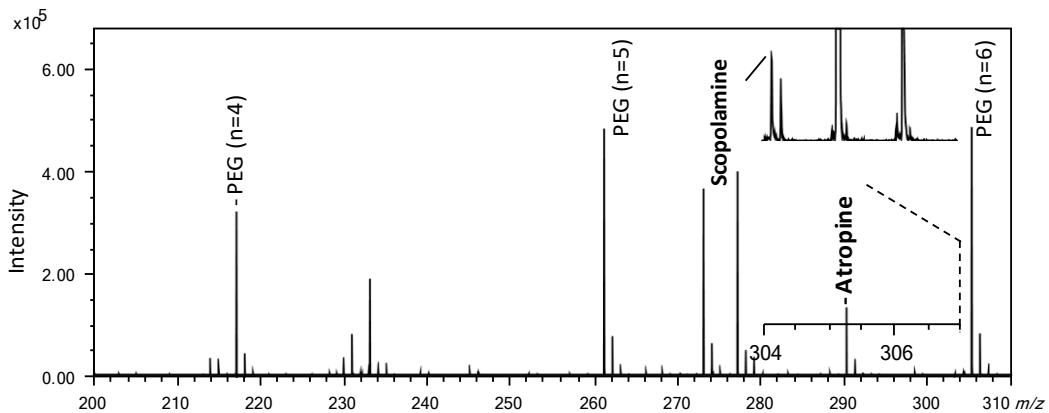
Panel A



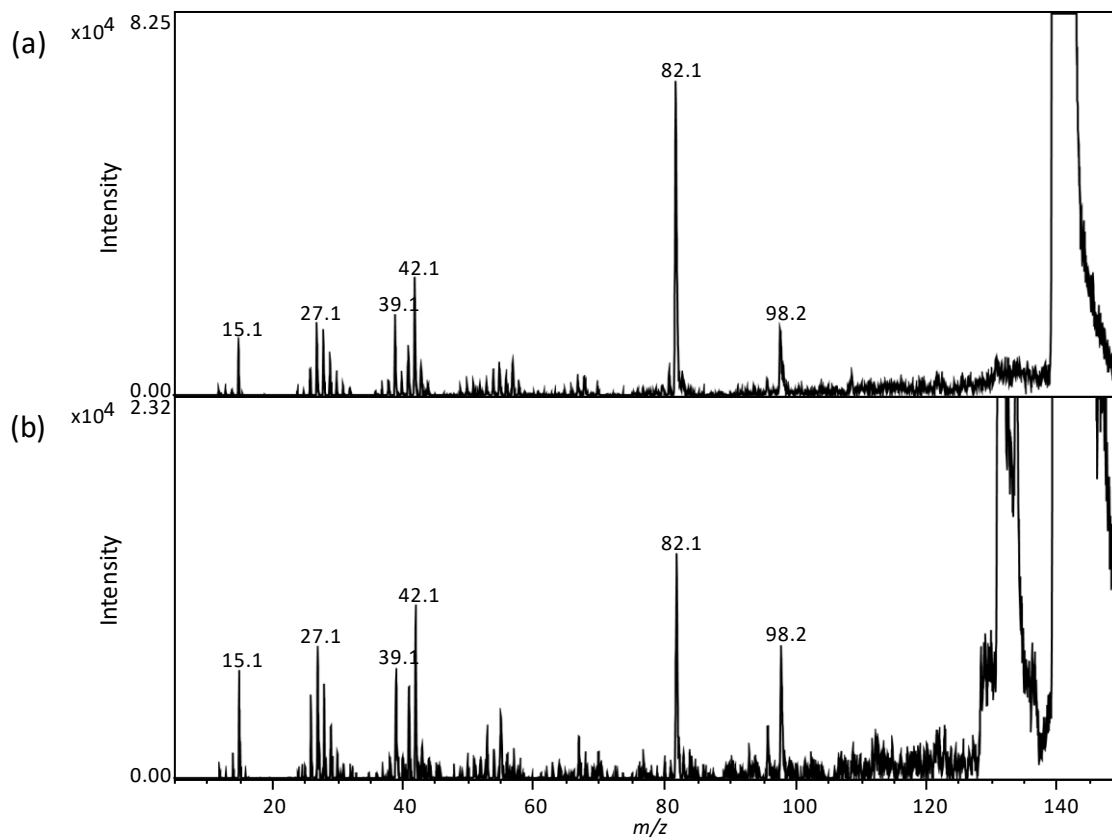
Panel B



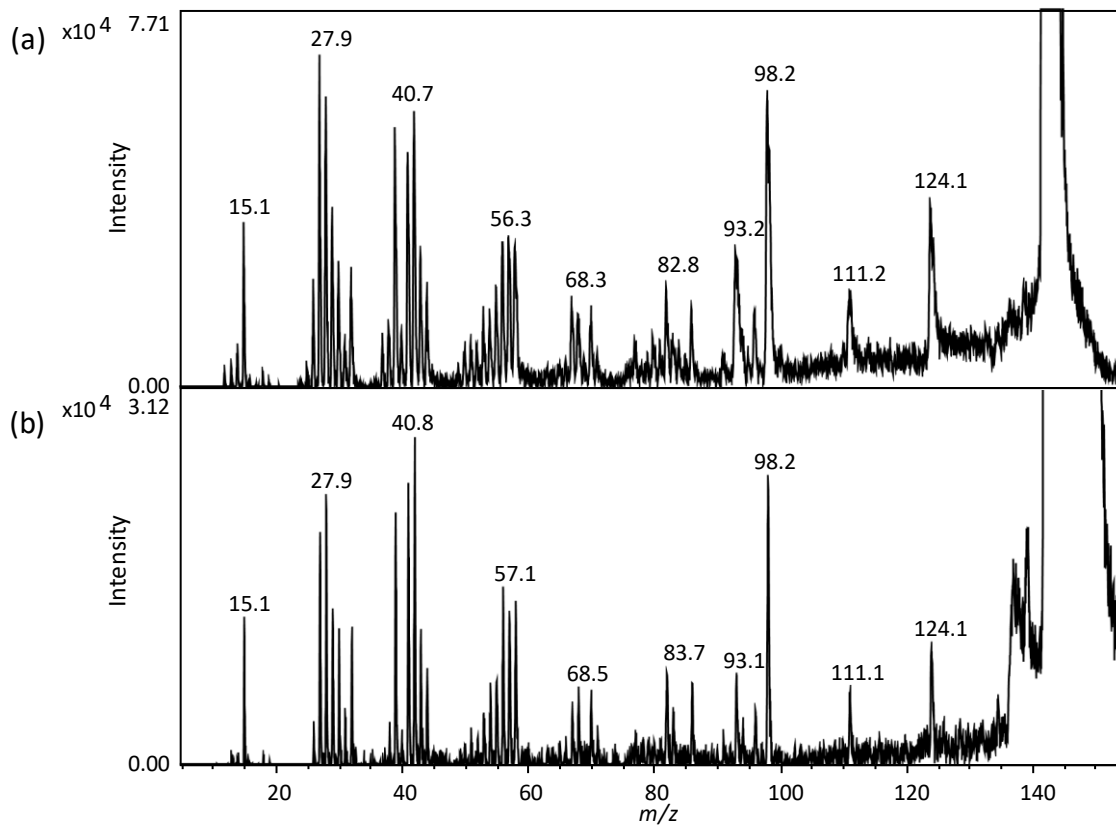
Panel C



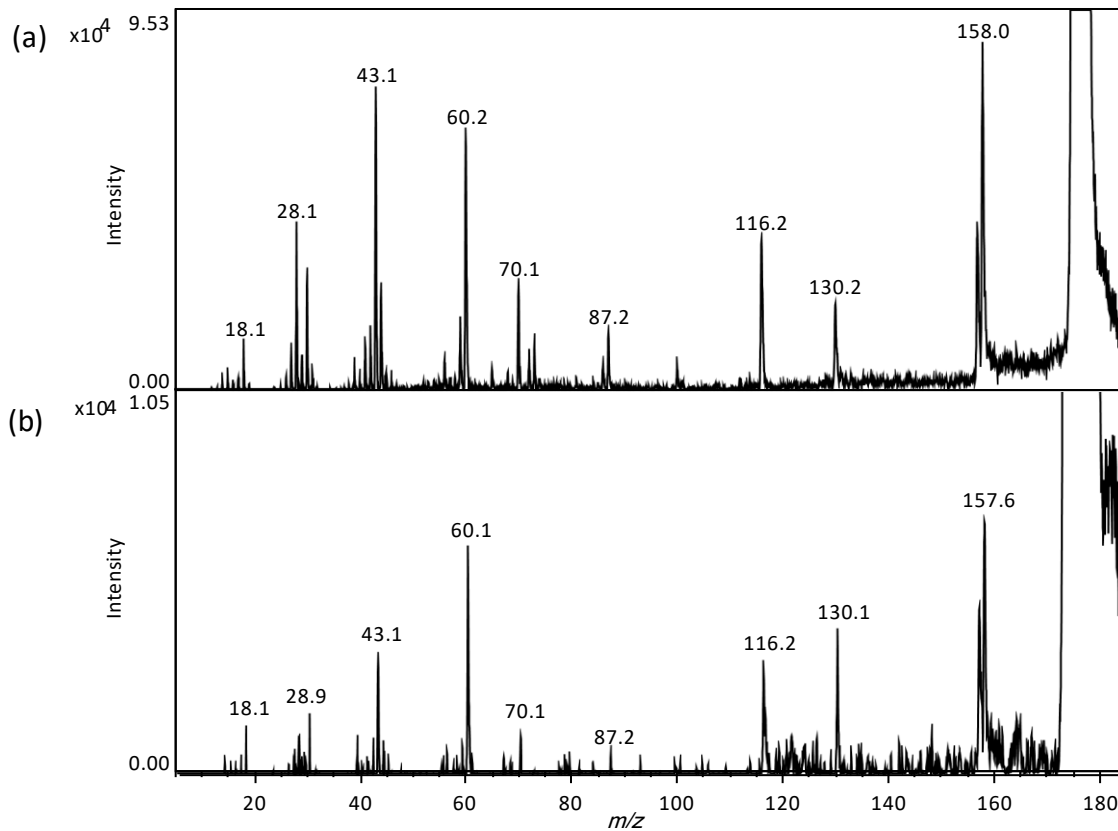
Appendix 3. Product-ion spectra for tropinone (m/z 140.1) authentic standard solution (a) and aqueous seed extract (b).



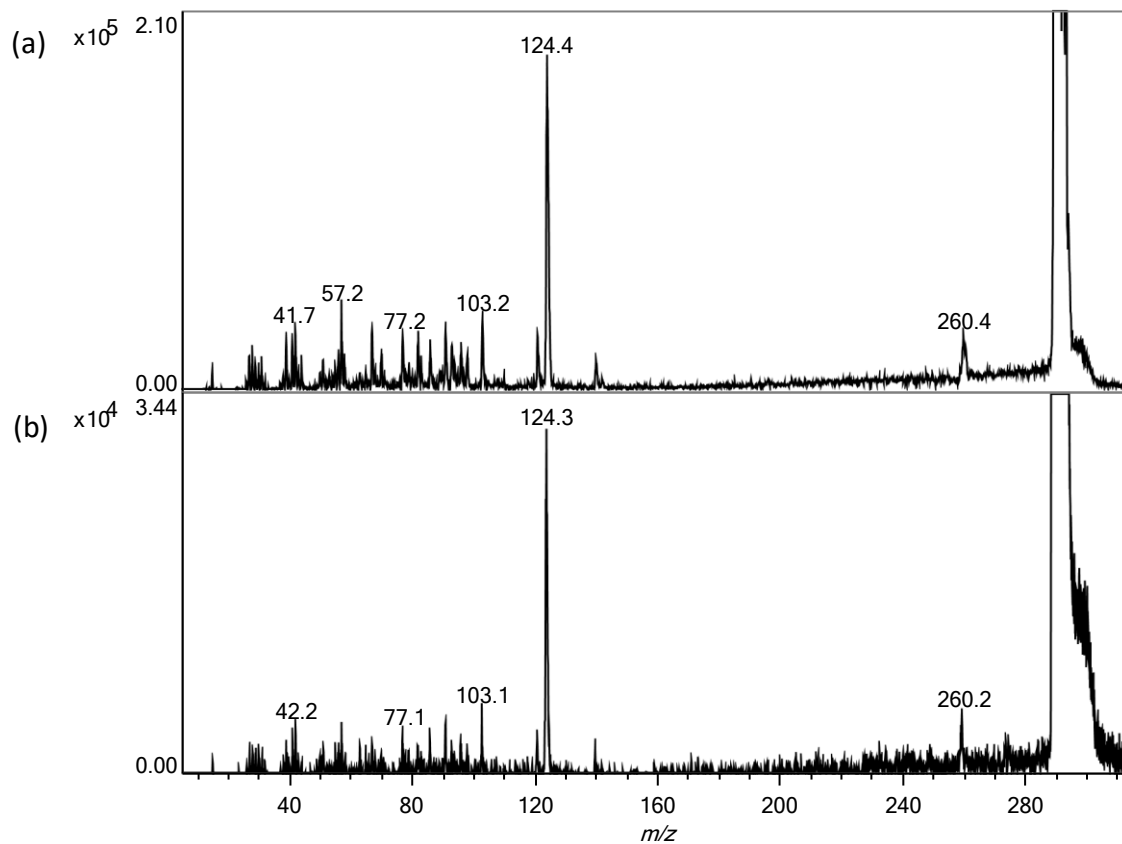
Appendix 4. Product-ion spectra for tropine (m/z 142.1) authentic standard solution (a) and aqueous seed extract (b).



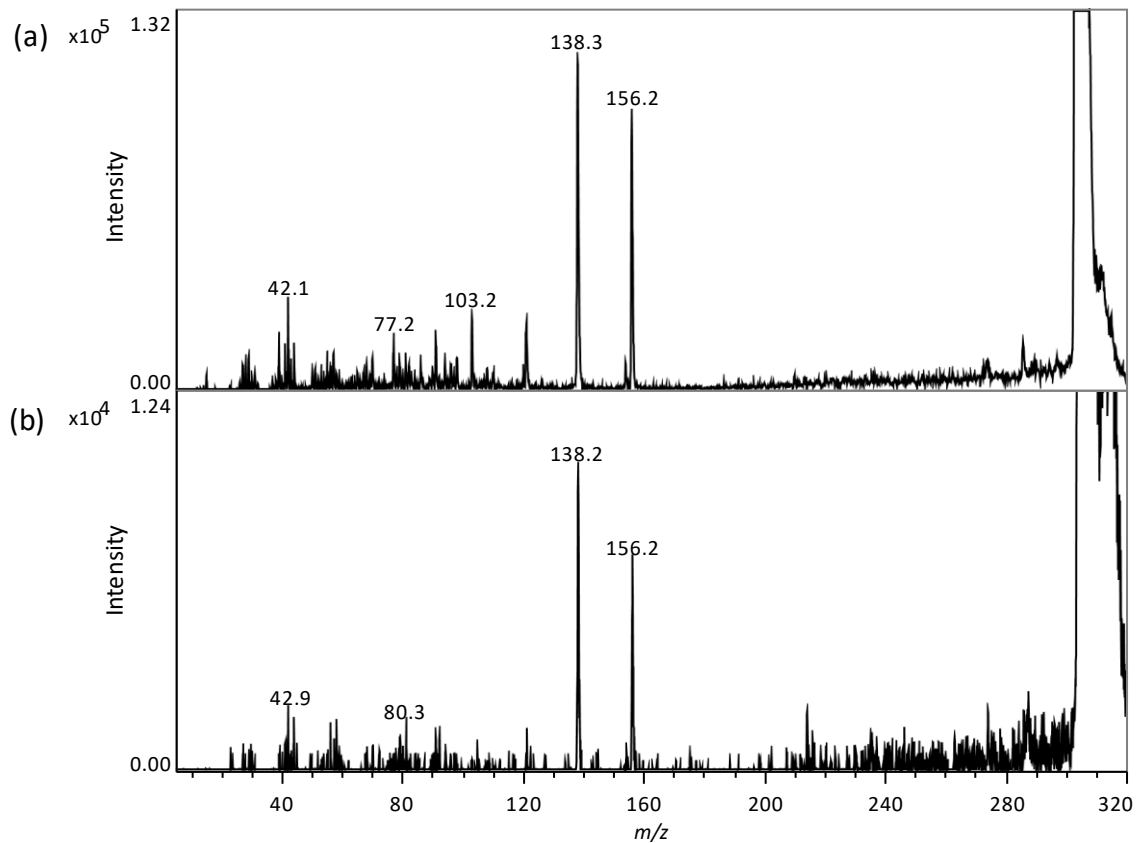
Appendix 5. Product-ion spectra for arginine (m/z 175.1) authentic standard solution (a) and aqueous seed extract (b).



Appendix 6. Product-ion spectra for atropine (m/z 290.2) authentic standard solution (a) and aqueous seed extract (b).



Appendix 7. Product-ion spectra for scopolamine (m/z 304.2) authentic standard solution (a) and aqueous seed extract (b).



Appendix 8. The color-overlaid ion images of furan (m/z 69.0340) and 5-hydroxymethylfurfural (m/z 127.0395) in a roasted coffee bean. The color scale from black to yellow within each panel is indicative of zero or low intensity to a high intensity of the indicated ion.

